EPFL

Thèse n° 8651

In situ photopolymerizable hydrogels for intracranial aneurysms treatment

Présentée le 9 juillet 2021

Faculté des sciences et techniques de l'ingénieur
Laboratoire de biomécanique en orthopédie
Programme doctoral en biotechnologie et génie biologique

pour l'obtention du grade de Docteur ès Sciences

par

Oriane POUPART

Acceptée sur proposition du jury

Prof. N. Stergiopulos, président du jury
Prof. D. Pioletti, Prof. C. Moser, directeurs de thèse
Dr O. Jordan, rapporteur
Prof. S. Lerouge, rapporteuse
Dr P.-E. Bourban, rapporteur

École polytechnique fédérale de Lausanne

2021

Acknowledgements

First and foremost, I would like to express my deepest gratitude to my thesis director Prof. Dominique Pioletti for giving me the opportunity to conduct my thesis in his laboratory. I am thankful for his valuable guidance and constructive comments over the past four years. I also thank him for always creating a pleasant work and group atmosphere. I would like to thank my thesis co-director Prof. Christophe Moser for prodiving valuable advice during my PEXs.

I would like to thank my thesis committee, Prof. Nikolaos Stergiopulos, Dr. Pierre-Etienne Bourban, Dr. Olivier Jordan and Prof. Sophie Lerouge, who have dedicated their time to review and evaluate my thesis.

I highly acknowledge all the collaborators involved in this research project who significantly contributed to my PhD thesis. I would like to express my special thanks to Dr. Pascal Mosimann for making this work possible and for sharing his precious knowledge of the interventional neuroradiology world. I am very grateful for his tremendous contribution and countless brilliant ideas. My special thanks are extended to Dr. Andreas Schmocker for the fruitful discussions and his constant enthusiasm on this work. I would like to thank Riccardo Conti and Prof. Hansjörg Grützmacher for their valuable chemical expertise and the synthesis of polymers and photoinitiators. I would also like to thank Dr. Katja Nuss and the team of Vetsuisse Faculty in Zurich for performing the *in vivo* studies. I also thank Lucio Pancaldi for helping me with the aneurysm models fabrication and for sharing the 3D printer. Many thanks to the Swiss National Science Foundation for the financial support.

I would like to warmly thank all the former and current members of the Laboratory of Biomechanical Orthopedics (LBO) for the friendly and supportive atmosphere. It was a pleasure to work and spend great moments together. Very special thanks go to Sandra Jaccoud for helping and advising me with numerous cell experiments, to Yasmine Boulaanache for sharing the office and a lot of discussions with me, to Céline Wyss for her countless advice, to Josiane Smith-Clerc for doing the TP with me and to Virginie Kokocinski for her help with the administrative work and her constant positive energy. I will always be grateful for their tremendous support and friendliness. Many thanks also to Alexandre Terrier, Tanja Hausherr, Jens Antons, Naser Nasrollahzadeh, Peyman Karami, Yanheng Guo, Theofanis Stampoultzis, Ece Uslu, Vijay Rana, Claire Delabarde, Ulrike Kettenberger, Arne Vogel, William Bovy, Adeliya Latypova, Valérie Malfroy, Raphaël Obrist, Killian Cosendey, Ehsan Sarshari, Matthieu Boubat and Pezhman Eghbalishamsabadi. I would also like to express my gratitude to Pierre-Arnaud Aeberhard, with whom I shared many unforgettable moments during the first year of my PhD thesis.
Many thanks to Sabrina Martone who helped me with the administrative part of my thesis and the members of the two neighbor laboratories, LHTC and MICROBS, for the nice atmosphere.

I would like to thank all students I have supervised during my thesis and who contributed to my work: Magalie Matray, Auriane Marret, Camille Daganaud, Victor Thorendal, Jean-Pierre Pohli, Pascal Boucq and Emma Roussel.

A huge thanks to my friends in Lausanne for all the shared happy moments and their precious support: Matina Pagoulatou, Camille Spinelli, Brunhild Corfu, Janody Pougala, Raquel Parreira and Florian Formica. I would also like to warmly thank my closest friends who were not physically in Lausanne but were always there for me: Delphine Cirette, Pierre Salah, Jérémie Chrétien, Paul De Nonancourt, Manon Riccetti and Laurane Charpentier.

I would like to thank my wonderful partner, Martin Touron, for sharing the ups and downs of this journey with me and for filling my life with so much joy and love.

Finally, this thesis would not have been possible without my family. I would like to express my eternal gratitude to my sisters, Marine and Clémentine, my nephew Charles and my niece Léa, and especially my parents, Bernadette and Romain, for always supporting and encouraging me in every decision I have made. I am so grateful for their education and their unconditional love. Thank you for everything!

Lausanne, April 2021

Abstract

Intracranial aneurysm is a cerebrovascular disease, characterized by an artery dilation in the brain. An aneurysm is prone to rupture, which causes a life-threatening subarachnoid hemorrhage. The major drawbacks of the current treatments, open surgical clipping and endovascular therapy, are the invasiveness of the surgery and the high recurrence and retreatment rates, respectively. *In situ* forming injectable hydrogels have emerged as a promising approach to overcome the current drawbacks. Ideally, the embolic agent should (1) permanently and completely occlude the aneurysm, (2) be implanted via a minimally invasive surgery, (3) be safe for the patient, and (4) promote the endothelialization at the aneurysm neck. In this thesis, *in situ* photopolymerizable hydrogels based on poly(ethylene glycol) dimethacrylate (PEGDMA) were developed for the treatment of intracranial aneurysms. The thesis was divided into four main studies, addressing the above-mentioned requirements.

First, PEGDMA hydrogels were developed and characterized according to polymer molecular weight and concentration. Denser covalently cross-linked hydrogel networks were obtained by decreasing the molecular weight and increasing the polymer concentration. It was demonstrated that PEGDMA hydrogels of 6 kDa molecular weight at a concentration of 15 wt% meet the physical and mechanical requirements of aneurysm embolic agent. More specifically, their compressive elastic modulus and compliance cover the range of native aneurysm tissue and their minimal swelling behavior avoids protrusion in the parent artery and limits stresses applied on the aneurysm wall. The fatigue-resistance of the hydrogels under pulsatile flow-induced loadings was subsequently evaluated within *in vitro* models fabricated by casting polydimethylsiloxane (PDMS) around 3D printed water-soluble sacrificial molds. The hydrogels withstood the 5.5 million cycles, corresponding to an implantation of two months *in vivo*, without protrusion or migration into the parent artery and maintained their weight and elastic modulus. However, slight roughness of 2 to 10 μm in depth due to erosion was noticed at the hydrogel surfaces compared to 2 μm for non-mechanically loaded hydrogels.

In the second part, the *in vitro* proof-of-concept of photopolymerizable hydrogels implementation into intracranial aneurysms models using the same microcatheters as in clinical practice was validated. The PEGDMA precursors exhibited a low viscosity allowing their injectability through 430 μm microcatheters. The addition of iodinated contrast agent as solvent enabled the precursors to be visible under fluoroscopy during the injection and directly after photopolymerization. Furthermore, the precursors polymerized in a controlled manner within less than 8 minutes by visible light illumination using a customized light-conducting microcatheter. The hydrogel precursors are, therefore, appropriate to ensure the minimal invasiveness of the surgical technique.

In the third part, the biocompatibility of the precursors was assessed *in vitro* and in an *in vivo* systemic toxicity study in rats. The obtained results revealed that the PEGDMA precursors did not trigger any acute or delayed toxicity and did not induce thrombus formation or inflammation. Additionally, the polymerized hydrogels did not affect the endothelial cells survival after one week of contact and did not induce any cell adhesion.

Finally, the biofunctionalization of PEGDMA hydrogels with gelatin methacrylate (GelMA) was proposed as a strategy to promote the *in situ* endothelialization. The incorporation of GelMA into PEGDMA network significantly improved the endothelial cell migration, adhesion and spreading on the hydrogel surfaces and a cellular network was formed after one week of culture. The adherent cells on the hybrid hydrogels were then exposed to laminar flow in a microfluidic channel and withstood the shear stresses. Moreover, the biofunctionalization did not affect the mechanical properties and fatigue-resistance while the swelling characteristics were reduced and the viscosity and photopolymerization time were increased.

The overall results showed that the photopolymerizable PEGDMA-based hydrogels possess the appropriate properties to be a promising candidate for intracranial aneurysms treatment. *In vivo* safety and efficacy studies are required to confirm these promising results.

Keywords: intracranial aneurysms, hydrogels, poly(ethylene glycol) dimethacrylate, photopolymerization, minimally invasive implantation, elastic modulus, fatigue, swelling, endothelialization.

Résumé

Un anévrisme intracrânien est une maladie cérébrovasculaire caractérisée par une dilatation d'une artère du cerveau. Un anévrisme peut se rompre, provoquant une hémorragie sous-arachnoïdienne potentiellement mortelle. Les traitements actuels, à savoir chirurgicaux (clip) et endovasculaires (coil), présentent chacun des inconvénients spécifiques; pour les premiers le caractère invasif et pour les seconds les taux élevés de récurrence et de retraitement. Les hydrogels injectables se solidifiant *in situ* se sont révélés être une approche prometteuse pour pallier ces inconvénients. Idéalement, l'agent embolique devrait (1) occlure complètement et définitivement l'anévrisme, (2) être implanté de manière mini-invasive, (3) être sans danger pour le patient, et (4) promouvoir l'endothélialisation du collet de l'anévrisme. Dans cette thèse, des hydrogels photopolymérisables *in situ* basés sur le poly(éthylène glycol) diméthacrylate (PEGDMA) ont été développés pour le traitement des anévrismes intracrâniens. Cette thèse est divisée en quatre études répondant aux exigences mentionnées ci-dessus.

Tout d'abord, les hydrogels PEGDMA ont été développés et caractérisés en fonction du poids moléculaire et de la concentration du polymère. Des réseaux réticulés de manière covalente ont été obtenus en diminuant le poids moléculaire et en augmentant la concentration de polymère. Il a été démontré que les hydrogels PEGDMA avec un poids moléculaire de 6 kDa et une concentration de 15 wt% répondent aux exigences physiques et mécaniques d'un agent embolique. Plus précisément, leur module élastique de compression et leur compliance couvrent ceux du tissu natif et leur comportement de gonflement minimal empêche la protrusion dans l'artère et limite les contraintes appliquées sur la paroi de l'anévrisme. La résistance à la fatigue des hydrogels sous chargements pulsatiles induits par flux a ensuite été évaluée dans des modèles *in vitro* fabriqués en coulant du polydiméthylsiloxane (PDMS) autour de moules sacrificiels hydrosolubles imprimés en 3D. Les hydrogels ont résisté aux 5.5 millions de cycles, correspondant à une implantation de deux mois *in vivo*, sans protrusion ni migration dans l'artère et ont conservé leur poids et leur module élastique. Toutefois, une légère rugosité de 2 à 10 μm de profondeur due à l'érosion a été observée aux surfaces de l'hydrogel comparé à 2 μm pour les hydrogels non chargés mécaniquement.

Par la suite, la preuve de concept de l'implantation des hydrogels photopolymérisables a été validée *in vitro* dans des modèles d'anévrismes intracrâniens en utilisant les mêmes microcathéters qu'en clinique. Les précurseurs PEGDMA présentent une faible viscosité permettant leur injectabilité dans des microcathéters de 430 μm de diamètre interne. L'ajout d'un agent de contraste iodé en tant que solvant a permis aux précurseurs d'être visibles sous fluoroscopie pendant l'injection et directement après la photopolymérisation. De plus, les précurseurs ont polymérisé de manière contrôlée en moins de 8 minutes par illumination de lumière visible par

le biais d'un microcathéter conducteur de lumière. Les précurseurs d'hydrogels sont donc appropriés pour garantir le caractère mini-invasif de la technique chirurgicale.

Puis, la biocompatibilité des précurseurs a été évaluée *in vitro* et dans une étude *in vivo* de toxicité systémique chez le rat. Les résultats obtenus ont révélé que les précurseurs PEGDMA n'ont pas déclenché de toxicité aiguë ou retardée et n'ont pas induit de formation de caillots ou d'inflammation. De plus, les hydrogels polymérisés n'ont pas affecté la survie des cellules endothéliales après une semaine de contact et n'ont induit aucune adhésion cellulaire.

Enfin, la biofonctionnalisation des hydrogels PEGDMA avec de la gélatine méthacrylée (GelMA) a été proposée pour promouvoir l'endothélialisation *in situ*. L'incorporation de GelMA dans le réseau PEGDMA a considérablement amélioré la migration, l'adhésion et l'étalement des cellules endothéliales sur les surfaces de l'hydrogel et un réseau cellulaire s'est formé après une semaine de culture. Les cellules adhérentes sur les hydrogels hybrides ont été ensuite exposées à un flux laminaire dans un canal microfluidique et ont supporté les contraintes de cisaillement. De plus, la biofonctionnalisation n'a pas influencé les propriétés mécaniques ni la résistance à la fatigue des hydrogels tandis que le comportement de gonflement a diminué et la viscosité ainsi que le temps de photopolymérisation ont augmenté.

Les résultats globaux ont montré que les hydrogels photopolymérisables basés sur le PEGDMA possèdent les propriétés appropriées pour être un candidat prometteur pour le traitement des anévrismes intracrâniens. Des études *in vivo* d'innocuité et d'efficacité sont nécessaires pour confirmer ces résultats prometteurs.

Mots-clés: anévrismes intracrâniens, hydrogels, poly(éthylène glycol) diméthacrylate, photopolymérisation, implantation mini-invasive, module élastique, fatigue, gonflement, endothélialisation.

Contents

List of Figures

List of Tables

List of Abbreviations

DMSO	Dimethyl sulfoxide
EC	Endothelial cell
ECM	Extra cellular matrix
EPC	Endothelial progenitor cell
GAG	Glycosaminoglycan
GelMA	Methacrylated gelatin
HUVEC	Human umbilical vein endothelial cell
IA	Intracranial aneurysm
ICA	Internal carotid artery
IEL	Internal elastic lamina
LAP	Lithium phenyl(2,4,6-trimethylbenzoyl) phosphinate
MMP	Matrix metalloproteinase
MR	Magnetic resonance
PBS	Phosphate-buffered saline
PDMS	Polydimethylsiloxane
PEG	Polyethylene glycol
PEGDMA	Polyethylene glycol dimethacrylate
PEG-BAPO	Polyethylene glycol substituted bis(acyl)-phosphane oxides
PI	Photoinitiator
PVA	Polyvinyl acetate
RGD	Arginine-Glycine-Aspartic acid
RT	Room temperature
SAH	Subarachnoid hemorrhage
SMC	Smooth muscle cell
SMP	Shape-memory polymer
UV	Ultra-Violet
VEGF	Vascular endothelial growth factor

Chapter 1

State of the Art

1.1 Intracranial aneurysms

An intracranial aneurysm (IA) is a cerebrovascular disease and a substantial health care burden. The overall prevalence of having one or multiple IAs has been estimated to 2-4% worldwide [1]. IA is an abnormal and weak dilation of part of the arterial wall resulting in a bulging on the artery in the brain, typically at the bifurcations of arteries in the circle of Willis. The circle of Willis, represented in Figure 1.1, is the arterial anastomotic ring that supplies blood to the brain and connects the left internal carotid artery (ICA), right ICA, and vertebrobasilar circulation by communicating arteries [2]. The anterior communicating artery is the most frequent IA location (35%), followed by the ICA (30%, including the carotid artery, the posterior communicating artery and the ophthalmic artery) and the middle cerebral artery (22%) [3]. IAs are classified by type and size. The three main types of IAs are saccular (counting for 90% of the IAs), fusiform and dissecting aneurysms. The size of aneurysms ranges from small ones (under 10 mm, representing 90% of the IAs) up to giant ones (up to 50 mm). Smoking (2.2 to 3.1x increase), alcohol consumption (2x rise) and hypertension (2.5x rise) are the most significant risk factors for the formation of an aneurysm [4]. Moreover, elderly patients, women and patients with aneurysm family history are more prone to develop an aneurysm [1].

Unruptured aneurysms often remain asymptomatic, which makes their detection difficult before rupture. Over the past decades, the diagnosis has been improved due to the greater availability and sensitivity of imaging techniques, such as magnetic resonance imaging (MRI) or computed tomography (CT). The most feared complication of an IA is rupture, leading to bleeding into the subarachnoid space, named a subarachnoid hemorrhage (SAH). The incidence of ruptured aneurysms is low, approximately 0.5% per year. However, mortality due to SAH is between 40 and 50% and severe morbidity between 10 and 20% [5]. 85% of the SAH cases are caused by aneurysm rupture [6].

The pathogenesis of the formation, growth, and rupture of IAs has been widely investigated during the past few decades but remains incompletely understood and controversially debated. Nevertheless, the interactions between the wall's mechanobiology, the hemodynamic forces and the inflammatory responses seem to be critical factors [7]–[13]. It is crucial to understand the mechanisms leading to the development and rupture of aneurysms to optimize the treatments.

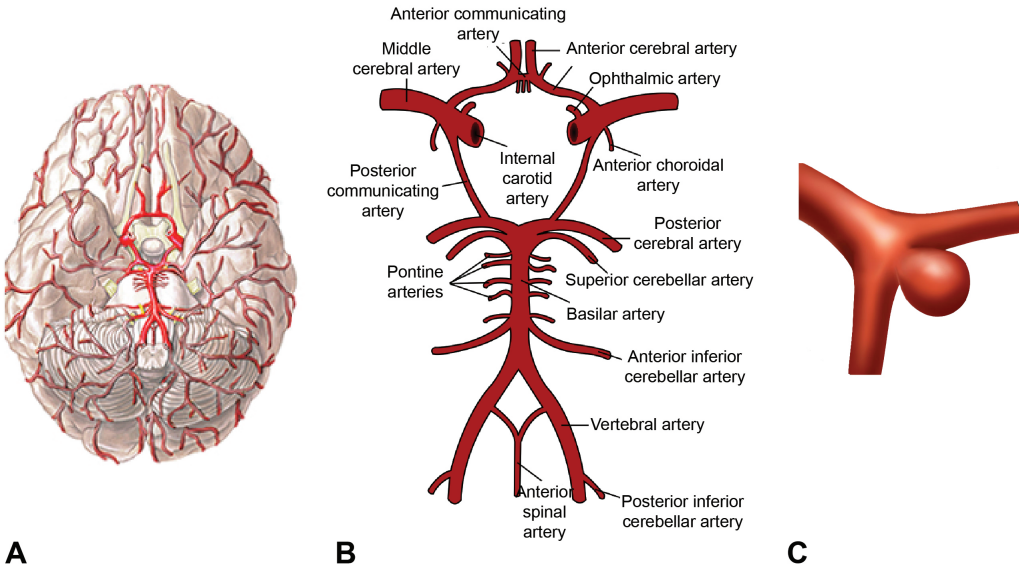

FIGURE 1.1: (A) Bottom view of the brain [14]. (B) Circle of Willis: the arterial anastomotic ring that supplies blood to the brain. (C) Representation of a saccular aneurysm (Adapted with permission from [15]).

1.1.1 Mechanobiology of the arterial wall

Cerebral arteries are composed of three layers: the tunica intima, the tunica media and the tunica adventitia, as illustrated in Figure 1.2. The intima consists of a single layer of endothelial cells (ECs) lining the vessel lumen surrounding by a basement membrane underlying loose connective tissue. The tunica intima is separated from the tunica media by the internal elastic lamina (IEL), a layer of elastic fibers. The tunica media is composed of layers of smooth muscle cells (SMCs) embedded in an extracellular matrix (ECM) rich in elastin and collagen fibers and glycosaminoglycans (GAGs). The adventitia is made up of a collagen-rich ECM, fibroblasts, vasa vasorium and perivascular nerves [16], [17].

The ECM components in the tunica media and the internal elastic lamina are considered as the main contributors to the structural vessel integrity and viscoelasticity and mostly determine the arterial mechanical properties. More particularly, smooth muscle cells play an essential role in the contractility of the vascular wall. The elastic fibers give elasticity and collagen fibers provide tensile strength and stiffness [11]. The load-bearing characteristic of the arteries is dominated by the elastin fibers (elastic modulus of 0.2 to 0.6 MPa) under physiological pressures and low strains (lower than 50%) and by the collagen fibers (elastic modulus of 2 to 6 MPa) for higher strains [17], [18]. GAGs are highly hydrated making them gelatinous ground substances and allow to resist compressive stresses and the tissue to diffuse nutrients [19]. Besides, the vascular cell content (ECs, SMCs and fibroblasts) is responsible for collagen regulation which is primordial for arterial wall integrity and recovery [20].

Intracranial arteries have the same structural composition as extracranial arteries. However, they present some differences. They are muscular-type arteries characterized by a well-developed internal elastic lamina, a lack of elastin fibers and smooth muscle cells in the tunica media, no external elastic lamina and a thinner adventitia [21]. These differences make the intracranial arteries more vulnerable to aneurysm formation and rupture than other arteries [7].

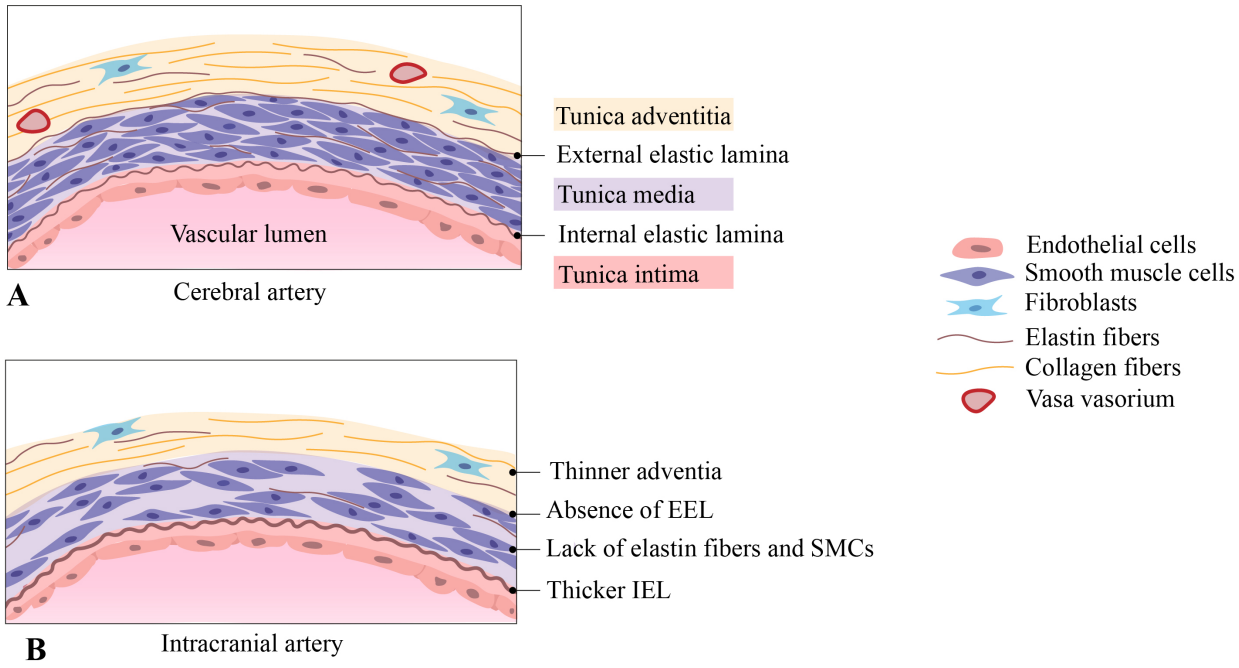

FIGURE 1.2: Structural composition of (A) a cerebral artery and (B) an intracranial artery. Intracranial arteries are characterized by a thicker internal elastic lamina, a lack of elastin fibers and smooth muscle cells in the tunica media, no external elastic lamina and a thinner adventitia.

1.1.2 Hemodynamics

Cerebral arteries are continuously subjected to hemodynamic stresses due to blood flow's pulsatile nature [22]. Cyclic circumferential stresses σ_θ are generated by the arterial wall distention by transmural pressure. The mean stresses can be calculated by Laplace's relation (1.1) and are around 100-150 kPa. Shear stresses τ_w are flow-induced tangential frictional forces acting on the vessel wall. Wall shear stresses can be calculated by Poiseuille's formula (1.2) and range from 1 to 5 Pa. Residual stresses σ_r are also exerted to the arterial wall. The different forces are illustrated in Figure 1.3.

$$\sigma_\theta = \frac{aP}{h} \tag{1.1}$$

$$\tau_w = \frac{4\mu Q}{\pi a^3} \tag{1.2}$$

where P is the transmural pressure, h is the deformed wall thickness, a is the deformed luminal radius, μ is the blood viscosity and Q is the volumetric flow rate.

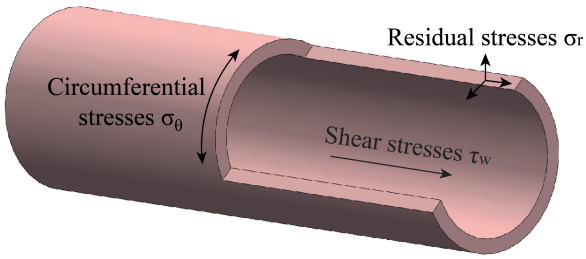

FIGURE 1.3: Hemodynamic stresses induced on cerebral arteries: circumferential stresses, shear stresses and residual stresses.

1.1.3 Pathogenesis of intracranial aneurysms

The aneurysm formation is initiated by a disruption of the hemostatic balance, triggered by high wall shear stresses [23], [24], environmental factors (such as smoking or hypertension) [4] or genetic factors [25], [26]. This causes dysfunction and phenotypical modulations of ECs and SMCs to pro-inflammatory phenotype [27], [28], promoting inflammation and ECM breakdown. The infiltration into the tunica media of inflammatory cells such as macrophages and mast cells [29]–[31] releases matrix metalloproteinases (MMPs) [32] and pro-inflammatory cytoxines, respectively. The inflammatory cascade leads to arterial wall morphological changes and remodeling [33] including degeneration of internal elastic lamina, degradation of ECM proteins [34], thinning of the tunica media and apoptosis of SMCs, resulting in aneurysm formation. Figure 1.4 illustrates the different steps of the IA formation. The interconnections between arterial wall structural composition, hemodynamics and inflammation are also associated with the progression and rupture of an aneurysm.

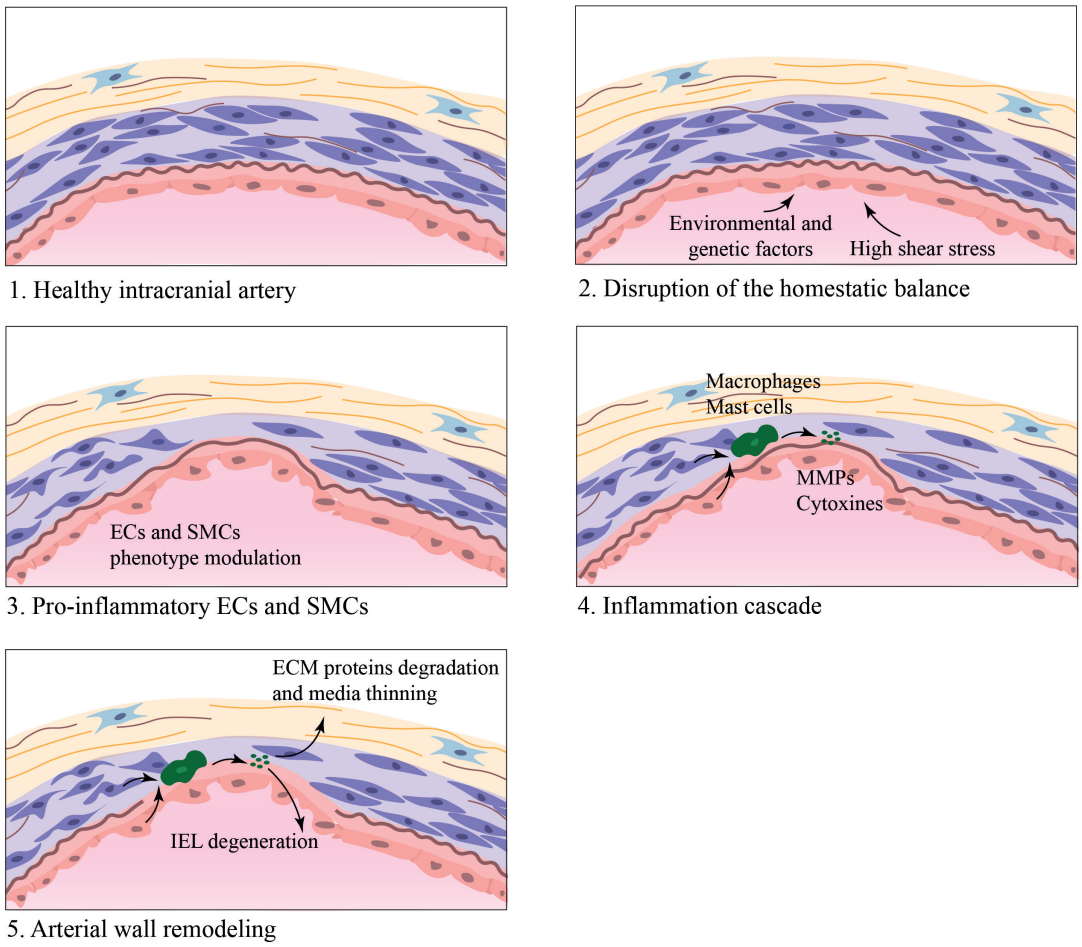

1. Healthy intracranial artery
2. Disruption of the homestatic balance
3. Pro-inflammatory ECs and SMCs
4. Inflammation cascade
5. Arterial wall remodeling

FIGURE 1.4: Pathogenesis of intracranial aneurysms involving environmental and genetic factors, the mechanobiology of the wall, the hemodynamic forces and the inflammatory responses.

1.2 Current treatments of intracranial aneurysms

The patient's knowledge of having an IA is an essential source of stress and anxiety due to the risk of rupture. Therefore, disease management needs to be optimal. Conventional treatments for IAs are open surgical clipping or endovascular management.

1.2.1 Open surgical clipping

Open surgical clipping is an invasive surgery performed under general anesthesia. It consists of a craniotomy, removal of a part of the skull to expose the brain, followed by the placement of a metal clip across the aneurysm neck, as represented in Figure 1.5.A. The metal clip aims to seal off the aneurysm from the blood flow permanently.

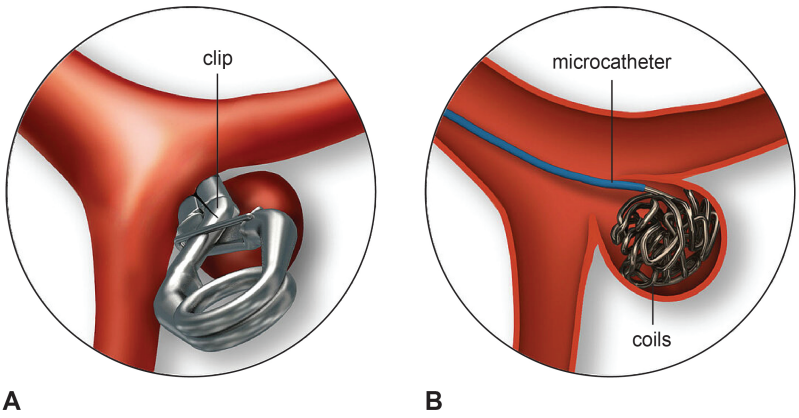

FIGURE 1.5: (A) Surgical clipping: placement of a metal clip across the aneurysm neck. (B) Endovascular coiling: packing of detachable coils into the aneurysmal sac through the microcatheter (Adapted with permission from [15]).

1.2.2 Endovascular therapy

From the early 1990s, endovascular techniques have been increasingly developed and used due to the minimal invasiveness of the procedure and nowadays have been considered the gold-standard in IA treatment. A microcatheter is navigated from the femoral artery to the aneurysm and detachable coils are deployed and packed into the aneurysmal sac, as illustrated in Figure 1.5.B. The coils induce thrombosis in order to isolate the aneurysm from the blood flow. The procedure is performed under fluoroscopy guidance. Extensive studies such as Internal Subarachnoid Trial (ISAT) [35], [36] or Barrow Ruptured Aneurysm Trial [37]–[40] have demonstrated better outcomes, in terms of mortality and morbidity, for coiling-treated patients compared to clipping. However, the recanalization is more frequent for coiling-treated aneurysms due to the compaction of coils, causing the need for re-treatment. The long-term aneurysm stability after coiling embolization is strongly correlated to the volume occlusion [41], [42]. Coils usually fill less than 35% of the total aneurysmal volume [43], which leaves room for coils compaction and thrombus formation within the aneurysm and explains the high recanalization rate.

Assisted coiling

Adjunctive devices such as balloon or stent are used to improve the coiling technique, in particular for wide-necked aneurysms [44]. Balloon or stent-assisted coiling refers to the inflation of a balloon or the deployment of a stent across the neck of the aneurysm to block it during coils placement. The goal of adjunctive devices is to prevent the coils prolapse into the parent artery [45]. In the Analysis of Treatment by Endovascular Approach of Nonruptured Aneurysms (ATENA) study, the mortality, morbidity and complications rates did not differ for coiling only and balloon-assisted coiling [46]. Similarly, no significant differences regarding the complications, the clinical outcomes and the mortality rate were found for stent-assisted coiling. However, meta-analysis and systematic reviews have found that the occlusion rate is lower in stent-assisted coiling compared to simple coiling, the progressive thrombosis rate is

higher and the recurrence rate is lower [47]–[49]. Moreover, stent-treated patients have to undergo antiplatelet therapy.

Flow diverters
Flow diverters are high porous stent-like endovascular devices, mostly used for complex IAs, such as giant, large, wide-necked and fusiform aneurysms [50], [51]. Their high porosity structure is designed to reduce both inflow and outflow within the aneurysm and favor the blood flow along the parent vessel. Thus, intrasaccular thrombosis is promoted and neointimal growth is induced at the aneurysm neck, resulting in the parent artery remodeling. For large and giant aneurysms, flow diverters have demonstrated a higher occlusion rate and less recurrence compared to conventional stents. The morbidity rate was similar for both techniques [52]. Like for stents, long-term antiplatelet therapy is required.

Flow disruptors
Intrasaccular flow disruptors are self-expanding braided mesh devices, aiming to modify the blood flow at the aneurysm neck, inducing fast intrasaccular thrombosis [53]. Examples are Woven EndoBridge (WEB, Microvention), Medina and Artisse (Medtronic). One main advantage is that flow disruptors do not require antiplatelet therapy. The safety and effectiveness of the technique have been validated [54], [55], in particular for wide-neck bifurcations aneurysms [56] but might be limited for the irregular shape of IAs.

Bioactive coiling
Hydrogel-coated coils are detachable metal coils covered with a hydrogel polymer, such as AZUR (Terumo Medical Corporation) or HydroCoil (Microvention). Due to the expansion of the hydrogel by four times in size in the presence of blood, the aneurysm occlusion rate is increased [57]. Studies have shown that hydrogel coiling treatment had lower recurrence rate and higher occlusion rate than standard coils and similar adverse events and morbidity rates [58]–[61].
Bioactive polymer coils were also developed by coating of bioabsorbable polyglycolic/polylactic acid (PGLA) copolymers, such as Matrix (Boston Scientific Neurovascular), or incorporation of polyglycolic acid (PGA) polymer, such as Cerecyte (Cardiva Medical Inc.). These polymers modified-coils aim to accelerate thrombus formation and fibrous tissue deposition at the aneurysm neck, demonstrated *in vivo* [62], [63]. Nevertheless, recurrence, recanalization and retreatment outcomes were similar between bioactive and platinum coils [64], [65].

Liquid embolic agents
Liquid embolic agents have also been developed [66] and two types are currently commercially available. One is acrylic glues, composed of n-butyl-2-cyanoacrylate (n-BCA), which polymerize within seconds in contact with an anionic environment like blood [67], such as Trufill (DePuySynthes) and Histoacryl (Braun). The other is solvent-based agents composed of a copolymer of ethylene-vinyl alcohol dissolved in dimethyl sulfoxide (DMSO) [68]. When exposed to blood, the solvent dissipates and the polymer precipitates within minutes. Such liquid embolic agents are Onyx-500HD (ev3 Neurovascular) and PHIL (MicroVention). These liquid

embolic agents aim to augment the volume occlusion rate, due to their liquid state allowing filling any forms and sizes of aneurysms. However, the main limitations are their self-solidifying properties in contact with blood, the risk of leakage and downstream migration that may cause arterial occlusion and ischemic stroke. Also, the microcatheter can be trapped into the solid state agent [69]. Moreover, the DMSO solvent can cause vasospam and angionecrosis if injected too fast or in high volume [70].

The different treatments, with their advantages and drawbacks, are summarized in Table 1.1.

Treatment	Advantages	Drawbacks
Open surgical clipping	Low recurrence and high occlusion rates	High invasiveness and poor outcomes
Simple coiling therapy	Low invasiveness	High recurrence rate and low occlusion rate
Balloon-assisted coiling	Low invasiveness	High recurrence rate and low occlusion rate
Stent-assisted coiling	Low invasiveness and low recurrence rate	Lower occlusion rate and antiplatelet therapy
Flow diverters	Low invasiveness, high occlusion and low recurrence rates	Antiplatelet therapy
Flow disruptors	Low invasiveness	Unadapted for irregular-shaped aneurysms
Hydrogel-coated coiling	Low invasiveness, low recurrence and high occlusion rates	Similar adverse events and morbidity rates than coils
Bioactive polymer coiling	Accelerate fibrous tissue deposition	Similar recurrence, recanalization and retreatment rates than coils
Liquid embolic agents	Low invasiveness and fill all aneurysms	No control of the solidification and solvent toxicity

TABLE 1.1: Advantages and drawbacks of the different treatments for cerebral aneurysms.

1.3 Requirements for the ideal embolic material for intracranial aneurysm embolization

All the current IA treatments aim to occlude the aneurysm to reduce the blood flow into the aneurysm sac and isolate the aneurysm from the parent vessel by neointima formation at its neck. However, there is still no ideal treatment on the market. Not only developing such a novel and ideal embolic material is challenging, but also defining precise requirements since no clear consensus exists yet. The requirements are established in accordance with the literature and surgeons guidelines and divided into mechanical and physical, implantation and biological aspects.

1.3.1 Mechanical and physical requirements

The embolic agent must match the mechanical properties of the IAs due to the continuous interactions between the embolic agent and the blood. The embolic agent must withstand the hemodynamic forces exerted by the blood flow without failure or permanent deformation, implying the embolic agent to have sufficient mechanical strength and elasticity [71]–[74]. The embolic agent's compliance should also match the compliance of the cerebrovasculature to ensure normal physiological flow [75], [76]. The embolic agent's geometry should be consistent with the intracranial aneurysm shape [76] to minimize the disturbances and instabilities of the flow dynamics responsible for aneurysm growth and rupture [77]. Furthermore, the forces exerted by the embolic agent on the aneurysm wall should be minimal to prevent rupture. The embolic agent should completely occlude the aneurysm sac and be stable, meaning no migration or fragmentation, since the mechanical stability at the aneurysm neck seems to be a pivotal approach to improve the embolic agent performance [78]. Finally, all these characteristics should be maintained over time due to the permanent implantation of the embolic agent. Therefore, the fatigue resistance of the embolic agent is indispensable.

1.3.2 Implantation requirements

Nowadays, minimally invasive approaches are preferred due to better outcomes, smaller scars, shorter postoperative hospital stay, lower cost and fewer complications [79]. The embolic agent should hence be easily delivered through microcatheters, preferably 430 μm inner diameter microcatheters, corresponding to those used in 95% of endovascular cases.
In the case of balloon-assisted techniques, despite that a balloon can remain inflated and block the flow in the parent artery for as long as 18 consecutive minutes [80], the solidification of the embolic agent should remain as short as possible, 10 minutes at most, ideally a few seconds, to reduce the risk of ischemic stroke and vessel injury. The embolic agent solidification also needs to be totally controllable.
Finally, the radiopacity of the embolic agent is a crucial consideration for monitoring its real-time implantation, since endovascular therapy is performed under fluoroscopic imaging [81]. Ideally, few or any artifacts should be left by the embolic agent during the follow-up imaging.

1.3.3 Biological requirements

Like all medical devices, the embolic material must be safe for the patient, implying to be biocompatible, non-toxic and sterilizable. The embolic agent should not promote thrombus formation since intrasaccular aneurysm thrombosis can be unorganized and unstable and hence cause ischemic strokes due to the thrombus protrusion in the parent artery lumen or dislodgement of the intrasaccular thrombus [82]. Moreover, the antiplatelet medication should be avoided. Inflammation plays a role in the aneurysm pathogenesis [29], thus the embolic agent should not trigger inflammatory effects. Ideally, the embolic agent should promote neointima tissue growth across the aneurysm neck, leading to the complete exclusion of the aneurysm from the parent vessel. This process, called *in situ* endothelialization, has emerged as a promising solution for aneurysm healing [83].

1.4 Emerging approaches

In response to the shortcomings of current treatments, the development of novel preclinical embolic agents has received a great deal of attention [84], [85]. Many researchers have focused on biomaterials for vascular embolization; however, only a handful of embolic agents were specifically designed for IAs. The following section presents the emerging approaches for IAs embolization, including shape-memory polymer foams and *in situ* forming hydrogels.

1.4.1 Shape-memory polymer foams

Shape-memory polymer (SMP) foams have emerged as an embolization device alternative over the past two decades [86]–[88]. SMP foams can change their shape in response to an external stimulus. For aneurysm embolization, the SMP foam is deformed from its initial shape to a temporary compressed shape to be delivered through a catheter and expanded to fill the aneurysm volume upon blood contact. Polyurethane-based SMP foams present suitable characteristics for aneurysm occlusion. The foams can expand ten times their crimped diameter within a few minutes, without applying excessive radial forces, even when the foam is 50% oversized [89], [90]. This expansion enables significant packing density into the aneurysm [91]. The incorporation of tungsten particles allows the foam to be radiopaque [92] and the tunable porous structure of the foam permits cellular infiltration and neointima formation [86]. *In vivo* studies in porcine aneurysm model have demonstrated the foam's biocompatibility and minimal inflammatory response [92], [93]. Furthermore, rapid and superior healing by forming a complete endothelial layer across the aneurysm neck was observed for foam-treated aneurysms compared to coils [94].
Nonetheless, since SMP foams are not delivered in the liquid phase but in a compact form, they are limited by the need of pre-forming them to comply with the patient-specific aneurysm dimensions.

1.4.2 *In situ* forming hydrogels

During the past two decades, *in situ* gelling systems have also raised interest as IA embolic agents, due to their ability to be injected in liquid phase filling any shape and size of aneurysm and to solidify *in situ* via various stimuli, such as temperature, pH, ionic strength, chemical reaction or light irradiation. Hydrogels also present the advantage of being composed of high water content and not organic and potentially toxic solvents compared to current clinical embolic agents. *In situ* forming hydrogels for aneurysm embolization include:

- alginate-based ionic cross-linked systems [95]–[98];
- poly(N-isopropylacrylamide) and poly(ethylene glycol) (PNIPAM-PEG) [99] and chitosan-based [100], [101] thermosensitive gels;
- PEG and poly(urethane sulfide sulfamethazine) (PEG-PUSSM) pH-triggered gels [102];
- poly(propylene glycol) diacrylate and pentaerythritol tetrakis(3-mercaptopropionate) (PPODA-QT) chemically cross-linked systems [103]–[106];

- poly(NIPAAm-co-HEMA-acrylate) with poly(NIPAAm-co-cysteamine)) (NHA-NC) and poly(NIPAAm-co-cysteamine-vinylsulfone) with poly(NIPAAm-co-cysteamine) (NCVS-NC) dual chemically and physically cross-linked gels [107];
- poly(ethylene glycol) diacrylate (PEGDA) [97] and gelatin with polyamine [108] photoactivated hydrogels.

Although these *in situ* gelling systems present promising outcomes *in vitro* and *in vivo* compared to current treatments, none of them have been approved for clinical applications up to date. Moreover, hydrogels present several limitations. For systems triggered by factors based on the difference between *in vitro* and *in vivo* such as temperature, pH and ionic strength, the hydrogels may prematurely solidify along the microcatheter or later dilute in the aneurysm causing adverse consequences. Photoactivated hydrogels require a specific optical device for *in situ* illumination.

1.5 Hydrogels

1.5.1 Biomedical hydrogels

Hydrogels are three-dimensional hydrophilic polymer networks, which can absorb and retain large amounts of water or biological fluids [109]. Due to their high water content and similarity in structure to the ECM of biological tissues, hydrogels have gained considerable interest as suitable materials for biomedical applications, such as drug delivery [110]–[112], cell encapsulation [113], [114] and tissue engineering [115]–[117]. A wide variety of hydrogels have been developed from natural or/and synthetic polymers, cross-linked by physical or/and chemical interactions. The advantages and drawbacks of the hydrogels according to their type and cross-linking are summarized in Table 1.2.

Historically, hydrogels were pre-formed outside the patient and implanted using invasive surgeries. However, in the late 90s, advances in chemistry and materials science allow developing injectable and *in situ* forming hydrogels [110]. The hydrogel precursor is injected through a minimally invasive manner and solidify *in situ* by a stimulus such as temperature, pH, chemical reaction or light irradiation.

Classification	Description	Advantages	Drawbacks
Natural	Derived from proteins polymers (such as collagen and elastin) and polysaccharides polymers (such as alginate, heparin, chitosan and hyaluronic acid)	Biocompatibility, low cytotoxicity, bioactivity, biodegradability, similarity to physiological environment	Low mechanical properties, expensive, ill-defined, batch-to-batch variation, difficult to tune properties
Synthetic	Derived from synthetic polymers (such as PHEMA, PVA, PEG, poloxamers and PAAm)	Strong mechanical properties, easy to produce, highly reproducible, well-defined, ease of tuning properties	Bio-inert, potential toxicity, side reactions
Physical	Cross-linked by physical interactions such as ionic interactions, hydrogen bonding, hydrophobic interactions, entanglements bonding and crystallization	No reactive groups required for 3D network cross-linking	Weak interactions, low mechanical properties, reversible network, difficult to tune properties
Chemical	Cross-linked through covalent chemical bonds	Strong interactions, improved mechanical properties, irreversible and stable network	

TABLE 1.2: Classification of the hydrogels according to their type (natural or synthetic) and cross-linking (physical or chemical) and their advantages and drawbacks [118]–[120].

1.5.2 Photopolymerization

Photopolymerization is a process, initiated by photo-irradiation, of the formation of covalently cross-linked hydrogels. Photopolymerization presents many advantages: minimal heat release, high reaction rates at ambient or physiological conditions and spatial and temporal control over polymerization [121], [122]. Contrary to other stimuli, the photo-irradiation is easily controlled by switching on and off the light, enabling the user to define a specific location and time for the irradiation [123]. Therefore, photopolymerizable hydrogels are an attractive material to treat IAs. The hydrogel precursor can be injected through a microcatheter conducting the light and be cured *in situ* once the surgeon estimates that the precursor completely fills the aneurysm.

Multifunctional monomers and pre-polymers functionalized with photo-reactive groups are used to form photopolymerizable hydrogels [124]. Pre-polymers are preferred over monomers

because of a more homogeneous network [125] and a greater biocompatibility. The photoreactive groups conjugated to the polymer backbone or termini are typically acrylate or methacrylate, due to the high reactivity of their double-bonded carbon C=C. The polymerization is generally initiated by a photoinitiator (PI), which absorbs photons at a specific wavelength and forms radicals. The radicals react with the unsaturated groups and induce propagation and chain growth. The main steps of the free radical photopolymerization mechanism are shown in Figure 1.6.

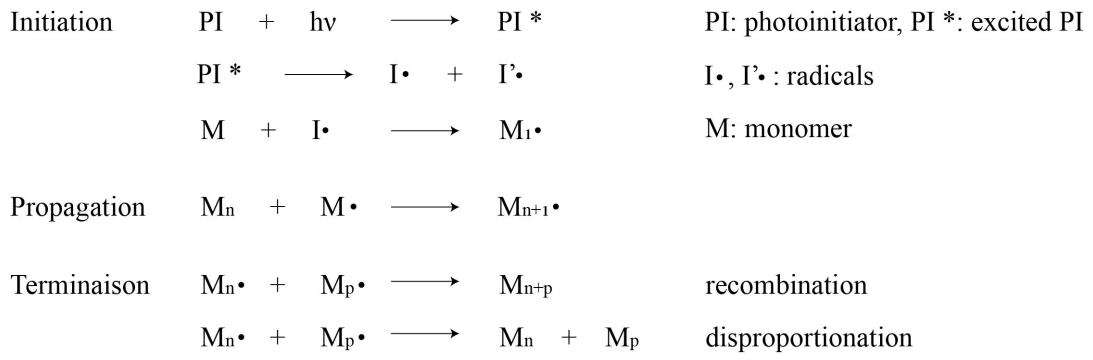

FIGURE 1.6: Mechanism of free radical photopolymerization.

Water-solubility, non-cytotoxicity and efficient absorbance within the visible region are required for the photoinitiators used for biomedical hydrogels. Irgacure 2959 (2-hydroxy-1-(4-(2-hydroxyethoxy)phenyl)-2-methylpropan-1-one) is the most widely used water-soluble photoinitiator for biomedical applications. However, Irgacure 2959 has a limited water solubility and low efficiency in the UV-A spectral range (315-400 nm). Visible-light sensitive photoinitiators present several advantages over UV including less cytotoxicity and greater depth of polymerization [126]. Consequently, water-soluble photoinitiators sensitive to visible light have been recently developed [127], such as lithium acylphosphinate (LAP) [128], VA-086 [129], bisacylphosphine oxide (BAPO) [130], [131], monoacylphosphine oxide (MAPO) [132] and eosin [133]. Their chemical structures are represented in Figure 1.7.

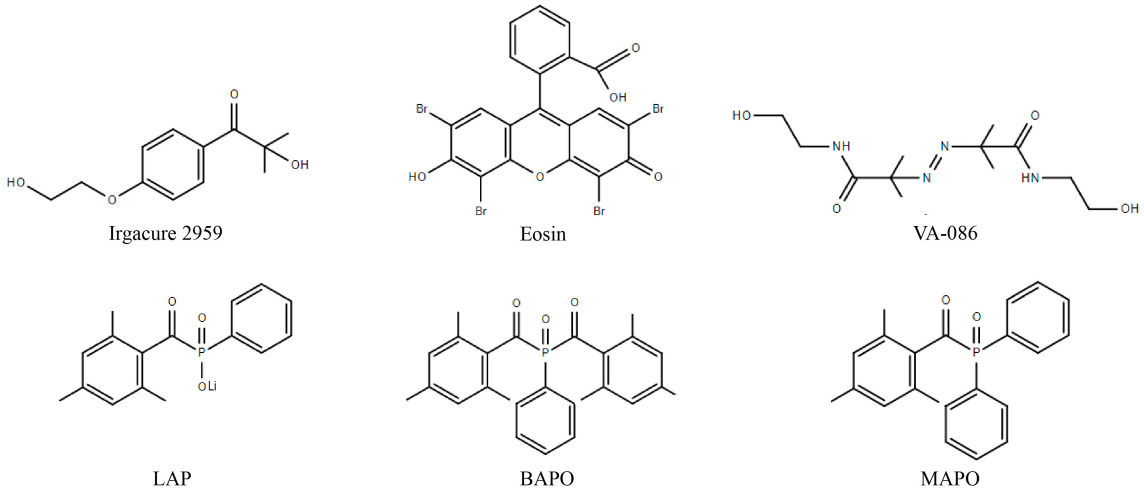

FIGURE 1.7: Chemical structures of photoinitiators used for biomedical hydrogels.

1.5.3 Photopolymerizable PEG-based hydrogels

Poly(ethylene glycol) (PEG), one of the synthetic polymers approved by the FDA for different specific clinical applications, has been extensively investigated due to its hydrophilicity, biocompatibility, non-immunogenicity and ease of chemical modification to tailor its properties. A wide range of PEG-based hydrogels has been developed, including PEG acrylamide, vinyl sulfone, maleimide, acrylate or methacrylate. Among the different cross-linking methods to form PEG hydrogels, chemical cross-linking is generally selected due to the formation of more stable hydrogels. Photopolymerization is the most common mechanism of covalently cross-linked PEG hydrogels, in particular PEG diacrylate (PEGDA) and dimethacrylate (PEGDMA). Their mechanical properties are relatively good and, most importantly, can be easily tuned by varying the monomer concentration, molecular weight and water content [134].

However, the bioinert nature of PEG hydrogels remains one of its main drawbacks. Consequently, the introduction of bioactivity into PEG hydrogels has been widely investigated to promote the regeneration of native tissues [135]. More specifically, the strategies to enhance *in situ* endothelialization focused on the adhesion, differentiation and proliferation of ECs and endothelial progenitor cells (EPCs) on the embolic agents [83], [136]–[138]. To that end, several approaches inspired by mimicking the ECM were developed for PEG-based hydrogels, including the incorporation of:

- Cell adhesive proteins such as fibronectin [139], collagen [140], [141] or gelatin [142], [143];
- Cell adhesive peptides derived from ECM proteins, such as RGD [144], [145], YIGSR or REDV [146] peptides;
- GAGs such as heparin [147]–[149] or hyaluronic acid [150], [151];
- Growth factors such as vascular endothelial growth factor (VEGF) [152] or basic fibroblast growth factor (bFGF) [153];
- Others molecules such as aptamers [154] or magnetic molecules [155].

1.5.4 Required properties and related characterization methods

Photopolymerizable hydrogels for IA treatment must fulfill all the requirements detailed in Paragraph 1.3. These requirements specified for each property by their threshold value are summarized in Figure 1.8 and their characterization methods have been listed in Table 1.3. Although the required properties were divided into mechanical and physical, implantation and biological aspects, it is important to point out the interrelation between most of these properties.

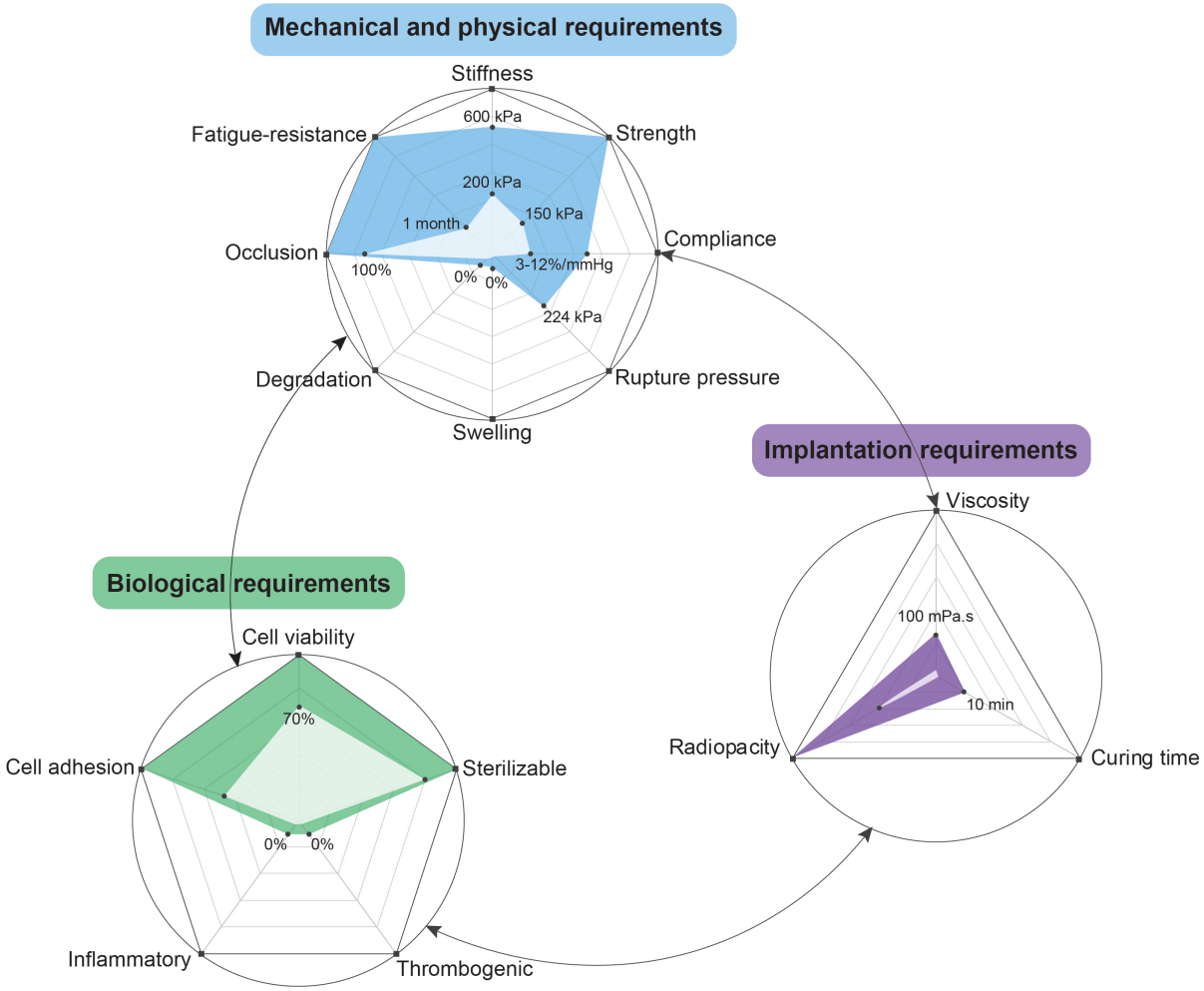

FIGURE 1.8: Target properties of photopolymerizable hydrogels for the treatment of intracranial aneurysms

Properties	Specifications	Characterization methods
Have elasticity similar to those of IAs	Young modulus E = 0.2-0.6 MPa [17]	Compression test [95], [98], [108]
Withstand the hemodynamic stresses	Compressive strength σ > 100-150 kPa, rupture strain ϵ > 10-15% [22]	Compression test [95], [98], [108], burst pressure test [156], [157]
Have compliance similar to those of IAs	Compliance C = 3-12%/mmHg [158]	Strains measurements in burst test by extensometer [76] and Doppler ultrasound [159], [160]
Exert minimal forces on the IA wall	Rupture pressure P < 224 kPa [161]	Stresses measurements in burst test using tracking markers and computational test [89]
Have a consistent geometry with the IA shape	Volume swelling ratio SR $\approx$ 0%	Weight analysis [97], [101], [104], [107], Dimensions changes [98]
Be stable over time	Degradation rate $\approx$ 0%	Weight loss over time *in vitro* [107] and *in vivo* [101], [102]
Occlude completely the aneurysm	Occlusion volume $\approx$ 100%	Embolization in *in vitro* models [97], [107], [108] and *in vivo* [96], [99], [102], [105]–[107]
Be resistant to fatigue	Non-significantly different Young moduli over time $E_0 \approx E_{months}$	Compression test over time [104], cyclic uniaxial tensile loading [162]
Be injectable through 430 μm microcatheters	Precursor viscosity μ < 100 mPa.s [163]	Rheology [95], [98], [100]–[103], [107], injectability through microcatheters with syringe pump [95], [98]
Cure fast and controllably	Photopolymerization time t < 10 min [80]	Tube inversion [102], stir bar [97], rheology [101], [103], [104]
Be radiopaque	Visible under fluoroscopy	Fluoroscopy observation *in vitro* [101] and *in vivo* [96], [99], [101], [102], [105]
Be biocompatible	Cell viability > 70% [164]	Live/Dead assay [102], [107], MTT assay [107], *in vivo* testing and histology [95], [96]
Be sterilizable	Same material properties before and after sterilization	Chemical structure, mechanical integrity, and biocompatibility evaluation [165]
Be non-thrombogenic	Activated partial thromboplastin time APTT > 100 s, Prothrombin time PT > 37 s, Fibrinogen < 1 g/L [166], [167]	Platelet, hematology, complement system, coagulation and thrombosis assays [164], [168]
Be non-inflammatory	Absence of inflammatory cells	*In vivo* testing and histology [96], [101]
Induce endothelialization	Cell adhesion, spreading and proliferation	Cell adhesion assay, *in vivo* testing and histology [101], [105], [106]

TABLE 1.3: Required properties for photopolymerizable hydrogels used for the treatment of intracranial aneurysms and their related specifications and characterization methods.

Chapter 2

Scope of the thesis

2.1 Motivation

The intracranial aneurysm rupture causes a life-threatening subarachnoid hemorrhage. The major drawbacks of the current treatments, open surgical clipping and endovascular therapy, are the invasiveness of the surgery and the high recurrence and retreatment rates, respectively. It would be fundamental to have a minimally invasive and long-term durable treatment. *In situ* forming injectable hydrogels have emerged as a promising approach to overcome the current drawbacks since their precursor can be injected in liquid form and solidify *in situ*. In particular, photopolymerizable hydrogels are beneficial for their spatio-temporal control over polymerization. The ideal embolic agent should satisfy demanding requirements, as following: (1) permanently and completely occlude the aneurysm, (2) be implanted via a minimally invasive surgery, (3) be safe for the patients, and (4) promote the endothelialization at the aneurysm neck.

2.2 Objectives

The present thesis aims at developing *in situ* photopolymerizable hydrogels for the treatment of intracranial aneurysms. To achieve that, the four following aims, each of which is a subject of a chapter, are addressed:

1. Develop fatigue-resistant hydrogels with mechanical properties matching those of the native aneurysm tissue and with minimal swelling behavior *(Chapter 3)*.

2. Validate the proof-of-concept of a photopolymerizable hydrogel implementation into an *in vitro* aneurysm model under fluoroscopy *(Chapter 4)*.

3. Evaluate the biocompatibility and thrombogenicity of the precursor and hydrogel *(Chapter 5)*.

4. Promote *in situ* endothelialization potential of the hydrogels by biofunctionalization *(Chapter 6)*.

The four specific aims of this thesis are summarized in Figure 2.1.

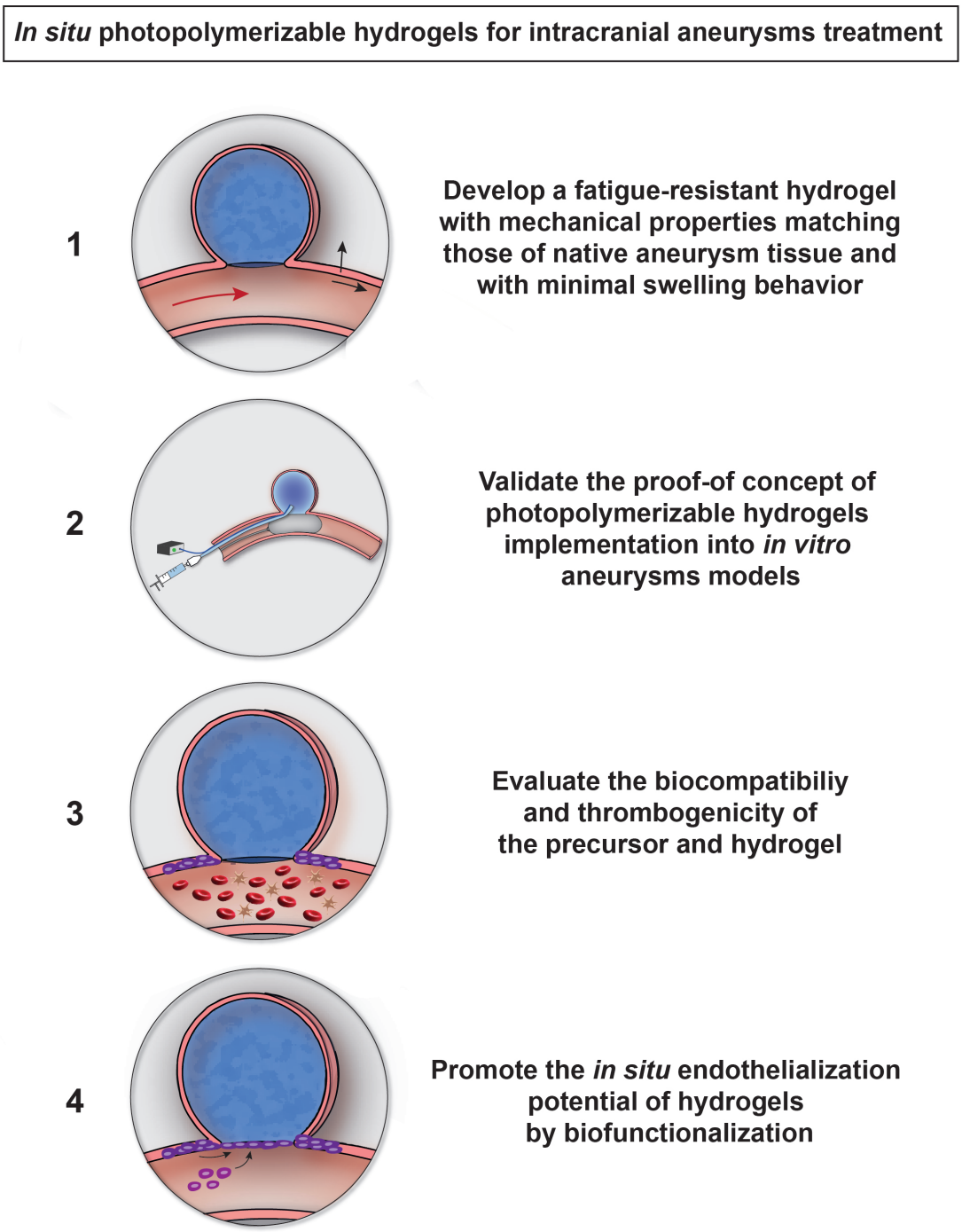

FIGURE 2.1: Overall objective and specific aims of the present thesis.

Chapter 3

Pulsatile flow-induced fatigue-resistant photopolymerizable hydrogels for the treatment of intracranial aneurysms

This chapter is based on the following publication: O. Poupart, R. Conti, A. Schmocker, L. Pancaldi, C. Moser, K.M. Nuss, M.S. Sakar, T. Dobrocky, H. Grützmacher, P.J. Mosimann, and D.P. Pioletti, "Pulsatile Flow-Induced Fatigue-Resistant Photopolymerizable Hydrogels for the Treatment of Intracranial Aneurysms," Frontiers in Bioengineering and Biotechnology, vol. 8, no. January, pp. 1–12, 2021 [169].

3.1 Abstract

An alternative intracranial aneurysm embolic agent is emerging in the form of hydrogels due to their ability to be injected in liquid phase and solidify *in situ*. Hydrogels have the ability to fill an aneurysm sac more completely compared to solid implants such as those used in coil embolization. In this work, we investigate the potential of poly(ethylene glycol) dimethacrylate (PEGDMA) hydrogels as embolic agent due to their favorable and tunable mechanical properties. The long-term integrity and stability of such hydrogels need to be evaluated to avoid implant compaction and aneurysm recurrence over time. To that end, molecular weight and polymer content of the hydrogels were tuned to match the elastic modulus and compliance of aneurysmal tissue while minimizing the swelling volume and pressure. The hydrogel precursor was injected and photopolymerized in an *in vitro* aneurysm model, designed by casting polydimethylsiloxane (PDMS) around 3D printed water-soluble sacrificial molds. The strains applied by the hydrogels on the aneurysm wall, measured by digital image correlation (DIC), significantly diminished compared to aneurysm models without hydrogel. The hydrogels were then exposed to a fatigue test under physiological pulsatile flow, inducing a combination of circumferential and shear stresses. The hydrogel withstood 5.5 million cycles and no significant weight loss of the implant was observed nor did the polymerized hydrogel protrude or migrate into the parent artery. Slight surface erosion defects of 2 to 10 μm in depth were observed after loading compared to 2 μm maximum for non-loaded hydrogels. According to these results, our fine-tuned photopolymerized hydrogel is expected to withstand the physiological conditions of an *in vivo* implant study.

Keywords: Pulsatile fluid flow-induced loading, intracranial aneurysms, polyethylene glycol dimethacrylate, hydrogels, fatigue, erosion

3.2 Introduction

An intracranial aneurysm is an outpouching of a cerebral artery which may be present in approximately 4% of the population [3]. Aneurysm rupture is associated with a high rate of mortality and severe morbidity, thereby requires effective treatment [5]. Endovascular therapy, essentially coil embolization, may be performed acutely after an aneurysm rupture or electively to prevent bleeding. The treatment goal is the complete and permanent occlusion of the aneurysm while maintaining patency of the parent artery. Despite tight packing, usually less than 35% of the total aneurysmal volume is filled with coils [43]. This low packing density leaves room for thrombus remodeling and coil compaction, which may consequently lead to aneurysm recanalization and thus make the aneurysm prone to (re)rupture. Long-term stability is strongly correlated with the embolization volume ratio [41], [170]. In addition, certain aneurysm morphologies (i.e. broad-necked aneurysms) may require advanced endovascular techniques like balloon-assisted, or stent-assisted coiling, and flow-diversion. However, compared to simple coiling, these techniques are associated with longer procedure times, higher peri-interventional risks, increased cost and require experienced operator skills.

To overcome the limitations of the current endovascular techniques, the optimal embolic agent should (1) completely fill the aneurysm, (2) demonstrate long-term stability, (3) not protrude or migrate into the parent vessel and (4) match the mechanical properties of the aneurysmal wall and surrounding tissues (Figure 3.1.B) [71].

In the past decade, various alternative embolic agents with improved packing density including hydrogel-coated coils [58], shape memory polymer foams [92], [94] and *in situ* forming hydrogels have been reported [97]–[99], [105], [107], [108]. Photopolymerizable hydrogels provide better spatial and temporal curing control compared to hydrogels responsive to chemical, temperature or pH stimuli [171] and allow to fill any shapes *in situ*. Photopolymerizable poly(ethylene glycol) dimethacrylate (PEGDMA) hydrogels have been studied for a wide range of tissue engineering applications [172], however their use for intracranial aneurysm embolization is limited [97]. In this work, we investigate whether photopolymerized PEGDMA-based hydrogels may be a potential candidate as a long-term embolic agent for intracranial aneurysms. Mechanical characterization and fatigue resistance tests of the photopolymerized hydrogel are required to demonstrate long-term integrity and stability before proceeding to *in vivo* testing.

The swelling pressure and volume ratio of the hydrogels are critical factors. Since aneurysm rupture can occur when wall stresses exceed tissue strength, hydrogel swelling and expansion must be sufficient to fill the cavity but as minimal as possible to avoid exerting excessive pressure against the aneurysm wall or protruding into the parent artery to avoid thromboembolic complications (Figure 3.1.C). On the other hand, premature hydrogel degradation, deformation or shrinkage may favor aneurysm recurrence [173], underlying the importance for the polymer

to withstand the continuous dynamic biomechanical load related to pulsatile blood flow [72]. Ideally, the compliance, mechanical strength and elasticity of the hydrogel should match those of the parent artery [75], [76]. In other words, preservation of the photopolymerized hydrogel's original shape, weight and mechanical properties is crucial to ensure long-term results [174].

In this study, molecular weight and polymer content of PEGDMA hydrogels were adjusted to fulfill the requirements of aneurysm embolic agents. Their swelling and mechanical properties were tested in static conditions and their fatigue resistance was evaluated within an *in vitro* aneurysm model dynamically stimulated by a pulsatile flow.

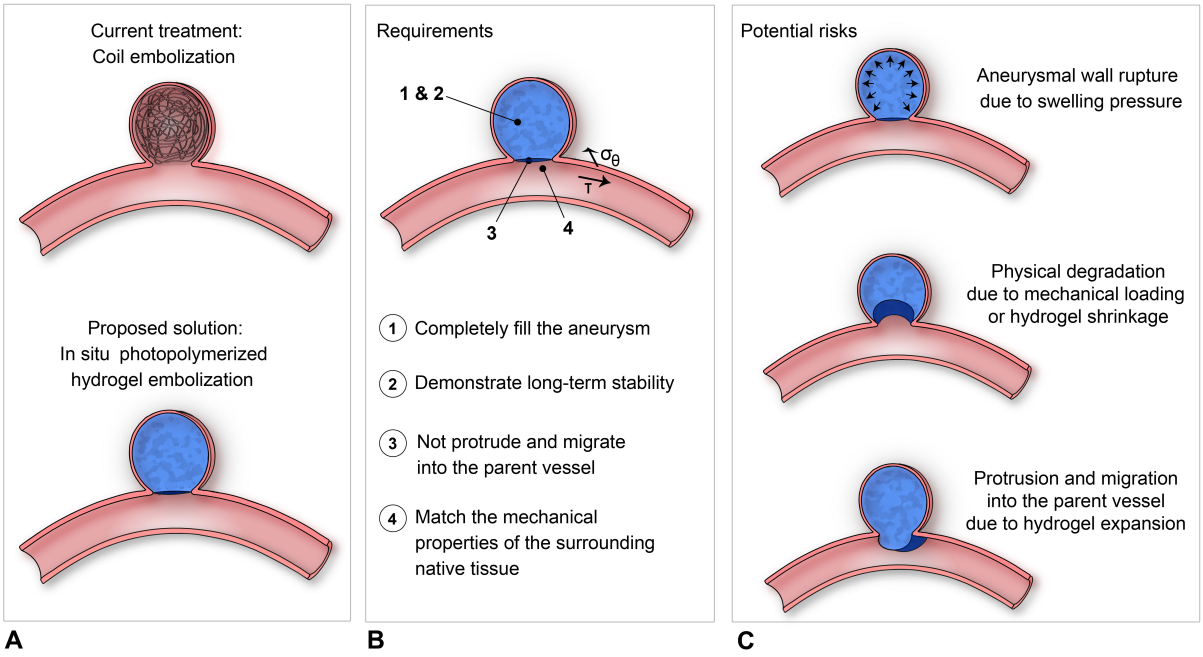

FIGURE 3.1: (A) Proposed solution of using *in situ* photopolymerized hydrogel for intracranial aneurysm embolization instead of coil embolization. (B) Requirements and (C) Potential risks of such a solution.

3.3 Materials and methods

3.3.1 Sample preparation

Materials

PEGDMA 2 and 6 kDa were synthesized from poly(ethylene glycol) (PEG, M_n = 2000 and 6000 g/mol) purchased from Sigma Aldrich (Merck, Switzerland) according to a previously reported procedure with subtle modifications [175]. The ^{1}H-NMR spectrum revealed a degree of methacrylation beyond 90%. PEGDMA 20 kDa was purchased from Polysciences (Germany).

The light-sensitive and water-soluble photoinitiator, known as poly(ethylene glycol) substituted bis(acyl)phosphane oxides (PEG-BAPO), was synthesized by phospha-Michael addition, as previously reported [131].
The iodine-based contrast medium Accupaque (350 mg/ml, GE Healthcare, Chicago, IL, United States) was provided by the Bern University Hospital and the intravenous fat emulsion Intralipid 20% was purchased from Sigma Aldrich (Merck, Switzerland).

Hydrogel synthesis and preparation

PEGDMA (10, 15 or 20 wt%) with the molecular weights of 2, 6 or 20 kDa and PEG-BAPO (0.1 wt%) were dissolved in equivalent weight concentrations of phosphate buffered saline (PBS) and Accupaque. The hydrogel precursors were homogenized by Vortex and degassed using a vacuum pump. Then, the precursors were sterilized through a 0.22 μm syringe-filter (Rotilabo, Car Roth, GmbH). Finally, intralipids (5 wt%) were added to the precursors. Hydrogels were termed PEGDMAak-b, where a represents the molecular weight, k = kDa and b the concentration of PEGDMA polymer. All samples were illuminated for 10 min at a wavelength of 405 nm and an intensity of 15 mW/cm^2.

3.3.2 Material characterization

Swelling ratios

Hydrogel precursor samples were photopolymerized either in cylindrical molds before being extracted or within intracranial aneurysm models and kept inside them. The samples were immersed in PBS at 37°C and 5% CO_2, resulting in either a free swelling or constrained swelling with the exposure to the PBS solvent only at the aneurysm neck. The swelling study was performed during one month and the weight and volume swelling ratios, SR_w and SR_{vol}, at the time point t were determined using the following formulas:

$$\text{SRw } [\%] = 100(w_t\text{-}w_0)/w_0$$
$$\text{SRvol } [\%] = 100(V_t\text{-}V_0)/V_0$$

where w_0, V_0, w_t and V_t correspond to the weight and volume of the samples after synthesis and the weight and volume of the swollen samples after an immersion of a duration t, respectively. Volumes are calculated with Archimedes' principle by immersing the samples in extra pure hexane (99+%, Fisher Chemical) for free swelling and in pure ethanol for constrained swelling to avoid the PDMS swelling in hexane.

Swelling pressure

The pressure exerted by the swollen hydrogels was measured using a confined compression setup [176]. After synthesis, 0.1 N pre-load was applied on the sample to ensure proper confinement. The chamber was filled with PBS to enable the swelling of the samples and the load was monitored while keeping the displacement constant during 48h to reach the equilibrium swelling. The swelling pressure was defined as the maximum pressure reached during the test.

Mechanical testing

Mechanical properties of the hydrogels were evaluated using an Instron E3000 linear mechanical testing machine (Norwood, MA, USA) equipped with a 250 N load cell.
Hydrogel samples were compressed to 50% applied strain at a constant speed of 0.1 mm/s. Load and displacement were recorded and the elastic modulus E was calculated by linear regression of the true stress-strain curve between the strains of 10% to 20%. Samples were immersed in PBS and placed in the incubator at 37°C and 5% CO2. After different immersion time points, the same compression test was repeated.
As-prepared hydrogels (after synthesis) were also compressed to 80% applied strain. Failure stress and strain were defined as the maximum stress and strain, respectively, before hydrogel breaking. The compliance of the hydrogels was determined and defined as the strains applied under pressures between 10.5 and 16 kPa, corresponding to the physiological systolic blood pressure (80-120 mmHg).

3.3.3 Implantation of the hydrogel in an *in vitro* intracranial aneurysm model

Design of *in vitro* intracranial aneurysm model

The *in vitro* intracranial aneurysm model was designed by casting polydimethylsiloxane (PDMS) around 3D printed water-soluble sacrificial molds. Specifically, molds were first produced from polyvinyl alcohol (PVA, Digitec, Ultimaker Natural PVA filament, 2.85 mm) using a 3D printer (Ultimaker 3, Netherlands). A thin layer of water was applied on the PVA molds to smooth the surface. Secondly, polydimethylsiloxane (PDMS, Dow Corning, Sylgard 184) with a 10:1 mixture of base to cross-linker was prepared and degassed in a vacuum chamber before being casted into the assembled PVA molds. The assembly was squeezed with a vise grip at room temperature for 24h and then placed at 60°C for 1h to achieve complete PDMS curing. Finally, the assembly was placed in an ultrasonic water bath at 65°C for 3 days to enable the PVA molds to dissolve. Figure 3.2 shows the different fabrication steps and an example of *in vitro* intracranial aneurysm model.
The elastic modulus of the models was determined by a traction assay using tensile molds in Teflon designed according to ASTM D412 [177]. In addition, the wall thickness of the aneurysm and the parent vessel was measured at 4 different locations for each model using a caliper with a measurement accuracy of 0.02 mm.

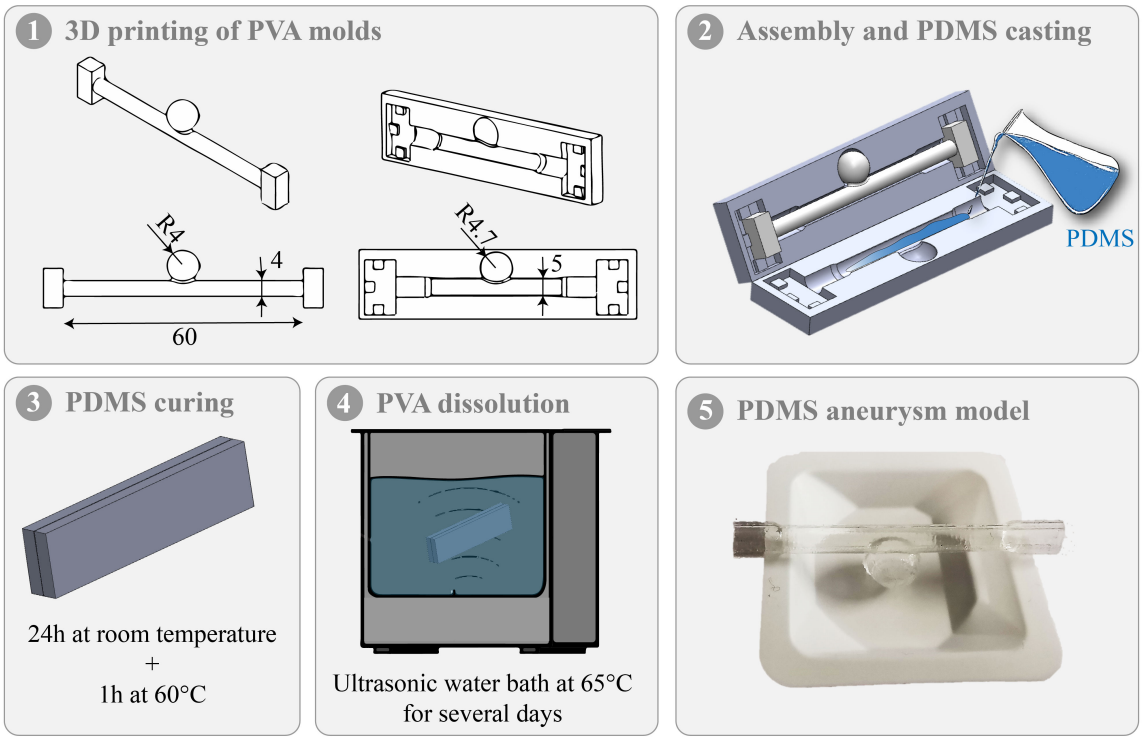

FIGURE 3.2: Different steps of the *in vitro* intracranial aneurysm model fabrication by casting PDMS around 3D printed water-soluble sacrificial PVA molds.

Implantation and pulsatile fluid flow-induced loading

To test the performance of the hydrogel, the hydrogel precursor was photopolymerized for 10 min in the aneurysm model using an optical glass fiber (105 μm, 0.22 NA, 1.5 m, ThorLabs, Newton, NJ, United States), proximally connected to an illumination module composed of 405 nm, 200 mW light power laser diodes [178]. The intensity at the tip of the fiber was 15 mW/cm^2. The aneurysm model was connected to an *in vitro* flow system which was filled with a mixture of glycerol and water in a 1:1.78 ratio with 0.134% PicroSirius Red dye to mimic the light-absorbing properties of human blood. A peristaltic pump (Masterflex, ColeParmer, Vernon Hills, IL, United States) was used to generate a pulsatile flow and set to 220 ml/min to simulate human internal carotid artery flow rate [179]. The intracranial arterial pressure (91.2 $\pm$ 9.6 mmHg [180]) was induced by a vertical 1.2 m liquid column.

Aneurysm wall strains assessment by digital image correlation

The strains applied by the hydrogels on the wall of the *in vitro* intracranial aneurysms models were measured by digital image correlation (DIC) technique by using VIC-3D system (Correlated Solutions, Inc. Irmo, SC, USA). The *in vitro* models were sprayed randomly with graphite (GRAPHIT 33, Kontakt Chemie) to make a speckle pattern with random distribution and high contrast. The hydrogels were exposed to at least 10 cycles of loadings induced by the pulsatile flow. The analysis of the displacements fields and the Von Mises strains was performed on 10

loading cycles and the average and maximal strains for each cycle was calculated. Maximal strains were calculated as the 99^{th} quantile value of one cycle.

Fatigue test and characterization after long-term loading

The hydrogels were dynamically loaded at 2.3 Hz by the pulsatile fluid flow system for one month, corresponding to 5.5 million cycles in total. After the cyclic loadings, the aneurysm model was dismantled to collect the hydrogel sample. To evaluate the performance of the hydrogel, (i) the sample was weighed, (ii) the surface profile of the hydrogels examined under 3D laser scanning microscopy (VK-X200 Keyence with a 50x lens) and (iii) cylindrical samples, obtained by a 5 mm diameter punch, were compressed using the mechanical test as described above. The results were compared to the hydrogel in the as-prepared state (after synthesis) and to the hydrogel in the swollen state (after one month of swelling).

3.3.4 Statistical analysis

Each experiment was performed in triplicate or more and the statistical data analysis was performed with MATLAB (Mathworks, Natick, MA, United States). All data are expressed as mean $\pm$ standard deviation. One-way analysis of variance (ANOVA) was used for comparison. $P < 0.05$ was considered as a significant result (denoted as *) and $p > 0.05$ non-significant (denoted ns). $p < 0.01$ was denoted as ** and $p < 0.001$ as ***.

3.4 Results

3.4.1 Effect of PEGDMA molecular weight

PEGDMA hydrogels with different polymer molecular weights (2, 6 and 20 kDa) and a concentration of 10% expressed a different volume swelling ratio and elastic modulus.
The swelling ratio increased with the PEGDMA molecular weight and remained stable over the course of the experiment of 28 days (Figure 3.3.A). In free conditions, PEGDMA2k-10 samples showed a slightly decreased volume (-12 $\pm$ 2%), while PEGDMA6k-10 and PEGDMA20k-10 samples manifested slightly (13 $\pm$ 1%) or extremely (151 $\pm$ 6%) increased volume swelling, respectively. The swelling ratio was significantly reduced within the constrained aneurysm model compared to free samples (e.g. 58% vs. 151% for PEGDMA20k-10, respectively), due to the limited medium absorption into the network of the hydrogel. This swelling behavior has led to a slight shrinkage of the hydrogel at the neck (PEGDMA2k-10), a moderate (PEGDMA6k-10) or excessive (PEGDMA20k-10) protrusion of the hydrogel into the parent artery. This observation was confirmed when loading the hydrogel under fluid flow, as shown in Figure 3.3.C.
PEGDMA6k-10 hydrogels demonstrated a higher elastic modulus compared to hydrogels with a lower or higher molecular weight (Figure 3.3.B). PEGDMA20k-10 hydrogels withstood the maximal applied strain of 80% without failure whereas PEGDMA 2k and 6k failed under compression at a stress of 108 $\pm$ 19 kPa and 179 $\pm$ 15 kPa and an applied strain of 54 $\pm$ 4% and 65 $\pm$ 1%, respectively.

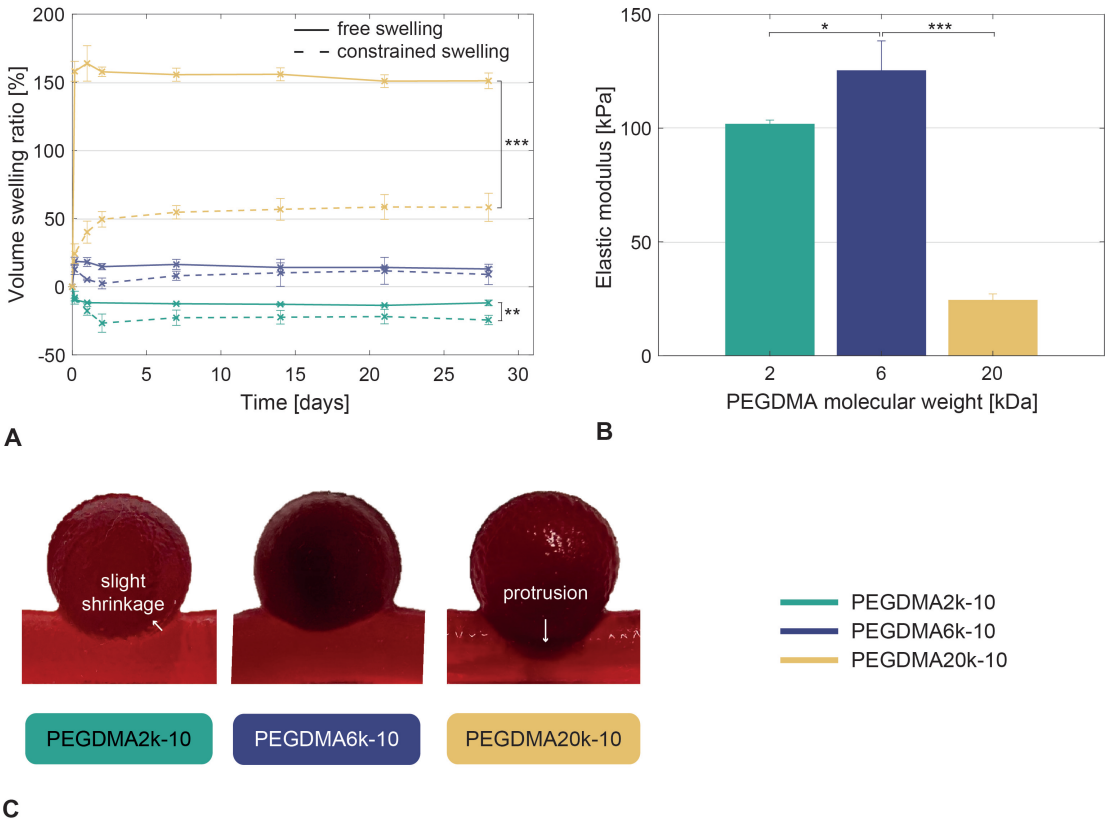

FIGURE 3.3: (A) Volume swelling ratio in free and constrained (within the aneurysm model) conditions, revealing a significant increase of the volume swelling ratio when increasing PEGDMA molecular weight. Statistically significant differences are only displayed between the free and constrained swelling conditions. (B) Compressive elastic modulus of the hydrogels demonstrating higher elastic modulus for PEGDMA6k-10 compared to 2 to 20 kDa hydrogels. (C) Direct visualization of the hydrogels within the intracranial aneurysm model after one week of fluid flow-induced loading showing slight shrinkage of the PEGDMA2k-10 hydrogel at the neck and excessive protrusion of the PEGDMA20k-10 hydrogel.

3.4.2 Effect of PEGDMA polymer content

The swelling ratio increased with the polymer content (Figure 3.4.A), particularly in free conditions. PEGDMA6k-20 hydrogels reached a maximal swelling pressure of 365 $\pm$ 31 kPa, a three-fold increase compared to hydrogels of equal molecular weight but with a polymer content of 10-15 wt% where a pressure inferior to 100 kPa was measured (Figure 3.4.B). Increasing the polymer content increases the mechanical properties of the hydrogels (Figure 3.4.C). The compressive elastic modulus was 125 $\pm$ 13, 280 $\pm$ 33 and 507 $\pm$ 7 kPa for 10, 15 and 20% of PEGDMA6k, respectively. The failure stress also increased while the applied strain at rupture did not vary: PEGDMA6k at 10, 15 and 20% failed under compression at a stress of 179 $\pm$ 15 kPa, 480 $\pm$ 127 kPa and 507 $\pm$ 125 kDa and an applied strain of 65 $\pm$ 1%, 72 $\pm$ 7% and 64 $\pm$ 2% respectively. Compliance, under physiological pressures, was 7.37 $\pm$ 1.07, 7.25 $\pm$ 1.18 and 4.12 $\pm$ 0.60 % for 10, 15 and 20% polymer content, respectively (Figure 3.4.D).

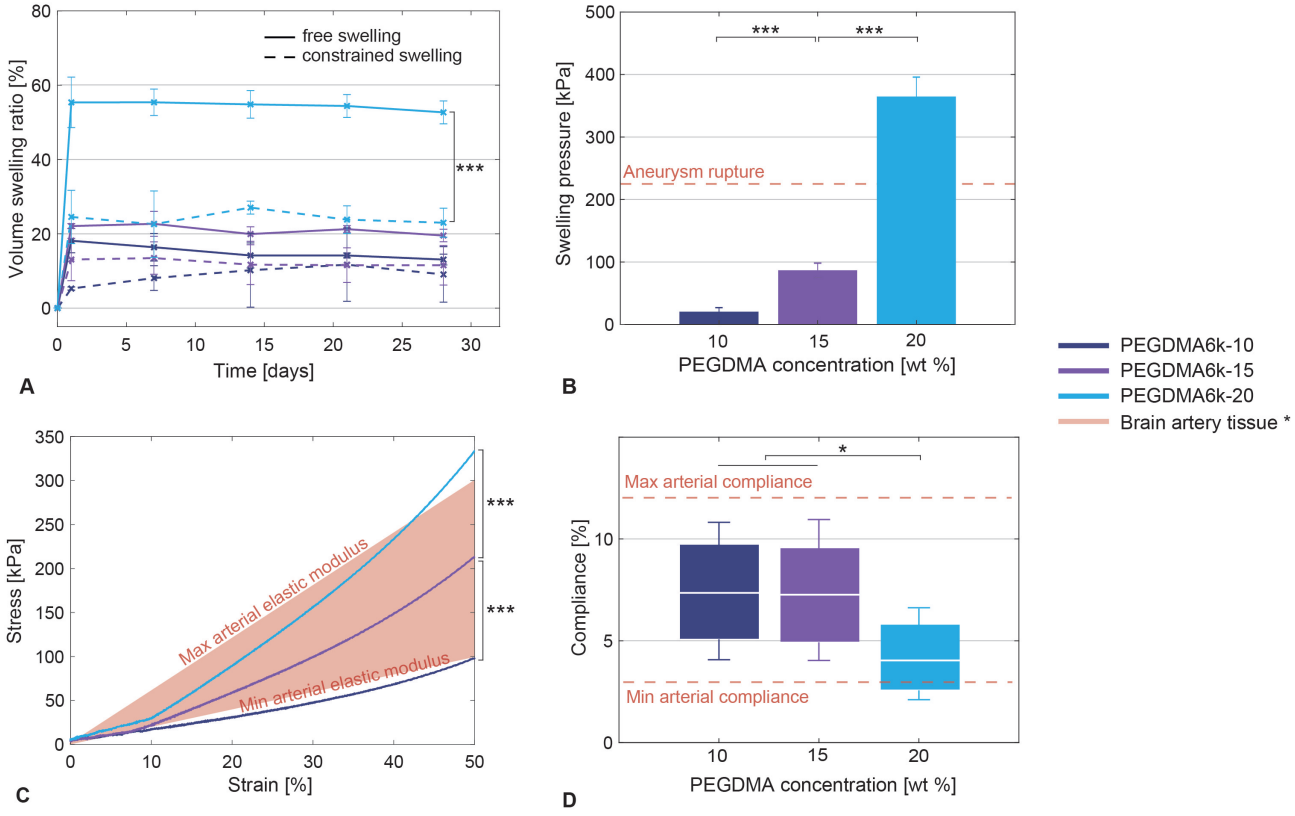

FIGURE 3.4: (A) Volume swelling ratio in free and constrained (within the aneurysm model) swelling conditions, showing a significant increase of the volume swelling ratio when increasing PEGDMA concentration. Statistically significant differences are only displayed between the free and constrained swelling conditions. (B) Maximal pressure induced by the swollen hydrogels increases when increasing the polymer content. (C) Strain-stress curve of the compression test, revealing a significant increase of the elastic modulus with the polymer content. (D) Compliance of the hydrogels under physiological pressures (80-120 mmHg). Box plots depicted mean (white line) and values at 80 and 120 mmHg (bottom and top of the box). PEGDMA6k-10 and PEGDMA6k-15 hydrogels have a significant higher compliance than PEGDMA6k-20 hydrogels.
* parent artery tissue data from literature [17], [158], [161]

3.4.3 *In vitro* aneurysm models characterization

The mean vessel diameter and wall thickness of the *in vitro* models designed was 4.14 ± 0.069 mm and 330 ± 56 μm, respectively. The mean aneurysm diameter and wall thickness of the aneurysm was 8.45 ± 0.189 mm and 374 ± 64 μm, respectively. These values and those reported in humans are provided in Table 3.1 for comparison. In addition, the tensile elastic modulus was measured to be 0.662 ± 0.068 MPa, which is similar to human brain aneurysms, determined to range from 0.2 to 0.6 MPa under strains lower than 50% [31]. The expansion and contraction of the *in vitro* model was observed under pulsatile flow.

		PDMS model	From the literature
Parent vessel	Wall thickness [μm]	330 ± 56	460 ± 60 [181]
	Diameter [mm]	4.14 ± 0.069	4.66 ± 0.78 [182]
Aneurysm	Wall thickness [μm]	374 ± 64	70 to 530 [183]
	Diameter [mm]	8.45 ± 0.189	3 to 10 [184]

TABLE 3.1: Dimensions in our PDMS models compared to human values reported in the literature.

3.4.4 Evaluation of aneurysm wall strains after hydrogel implantation

In this work, the central region of the wall aneurysm model was considered for the strains measurement by DIC, as shown in Figure 3.5.A. The mean and maximum strain per cycle on the aneurysm wall are presented in Figures 3.5.B and 3.5.C, respectively. The implantation of the hydrogels significantly decreased the strains applied on the aneurysm wall. Moreover, increasing the polymer content and therefore the stiffness of the hydrogels also decreased the mean and maximum strain per cycle on the aneurysm wall. A two to four-fold decrease was calculated compared to the untreated aneurysm model (without hydrogel) ($p < 10^{-12}$).

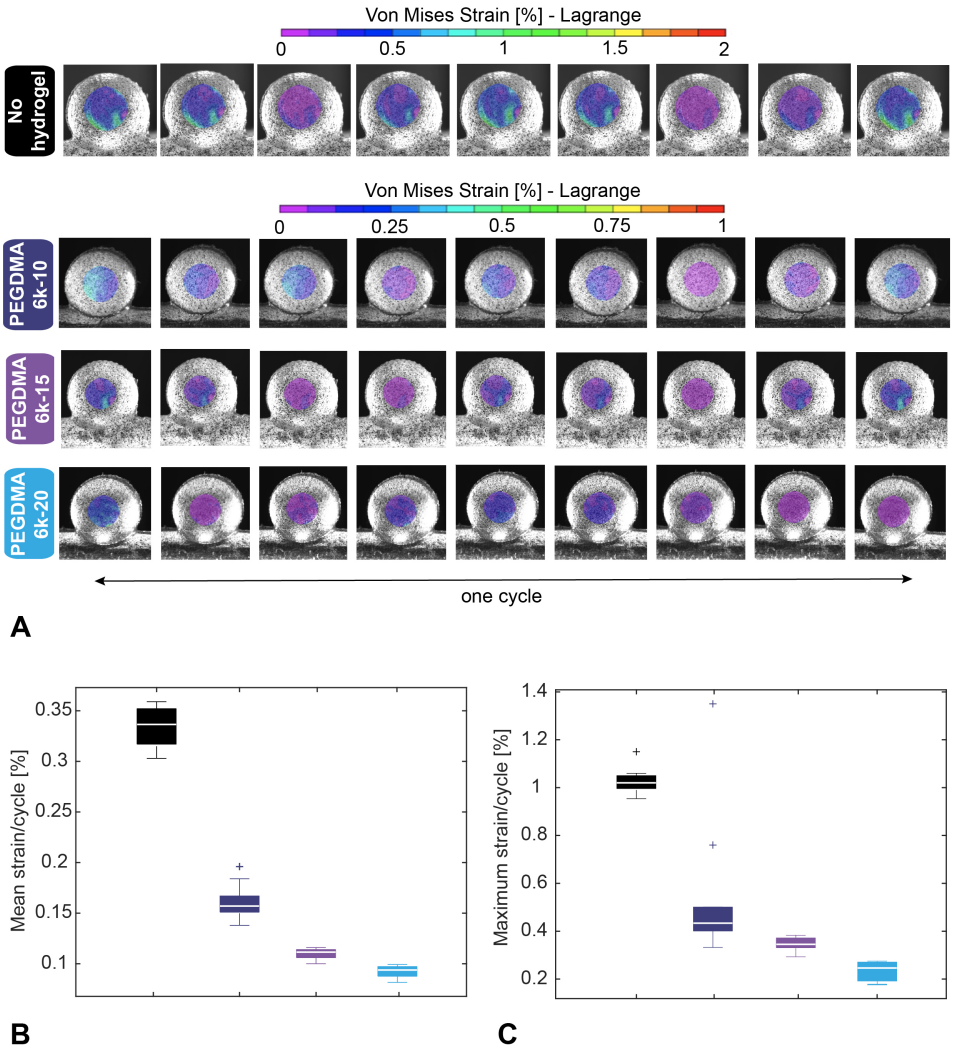

FIGURE 3.5: (A) DIC imaging showing the Von Mises strains fields for the duration of one loading cycle. Scale bars are 0-2% with a 0.125 increment between colors for the model without hydrogel (control) and 0-1% with a 0.0625 increment between colors for the models with PEGDMA6k hydrogels. (B) Mean strain and (C) Maximum strain per cycle calculated on 10 cycles, showing a significant decrease when the hydrogels are implanted into the *in vitro* aneurysm model compared to an empty aneurysm model.

3.4.5 Fatigue-resistance after pulsatile fluid flow-induced loading

Figure 3.6.A demonstrates the PEGDMA6k hydrogels with 10 and 15% content over one month of loading induced by blood substitute pulsatile fluid flow. The different hydrogels completely occluded the aneurysm sac without protruding or migrating excessively into the parent artery. No geometric distortion or signs of macroscopic damage was apparent.
The weight and elastic modulus variations of the hydrogels after the flow-induced loading are presented in Figures 3.6.B and 3.6.C. After 5.5 million cycles, there was no significant weight difference between the hydrogel in the as-prepared state and the loaded hydrogel for both polymer contents. However, the weight of swollen hydrogels was significantly lower (p=0.0399

and 0.0376 for 10 and 15% polymer concentration, respectively) than after one month of loading. Moreover, a slight decrease in the elastic modulus after cyclic loading was noticed, i.e. approximately 5% for PEGDMA6k-10 and 10% for PEGDMA6k-15, although this remained non-significant compared to the as-prepared hydrogels (p=0.394 and 0.2111 for 10 and 15% polymer concentration, respectively). The profile of the hydrogels surface that was in contact with the blood substitute is shown in Figure 3.7.A. As-prepared and swollen hydrogels presented a smooth surface with minor defects of maximum 2 μm in depth, whereas loaded hydrogels demonstrated unorganized and heterogeneous roughness, with defects ranging from 2 to 10 μm in depth, as shown in Figure 3.7.B.

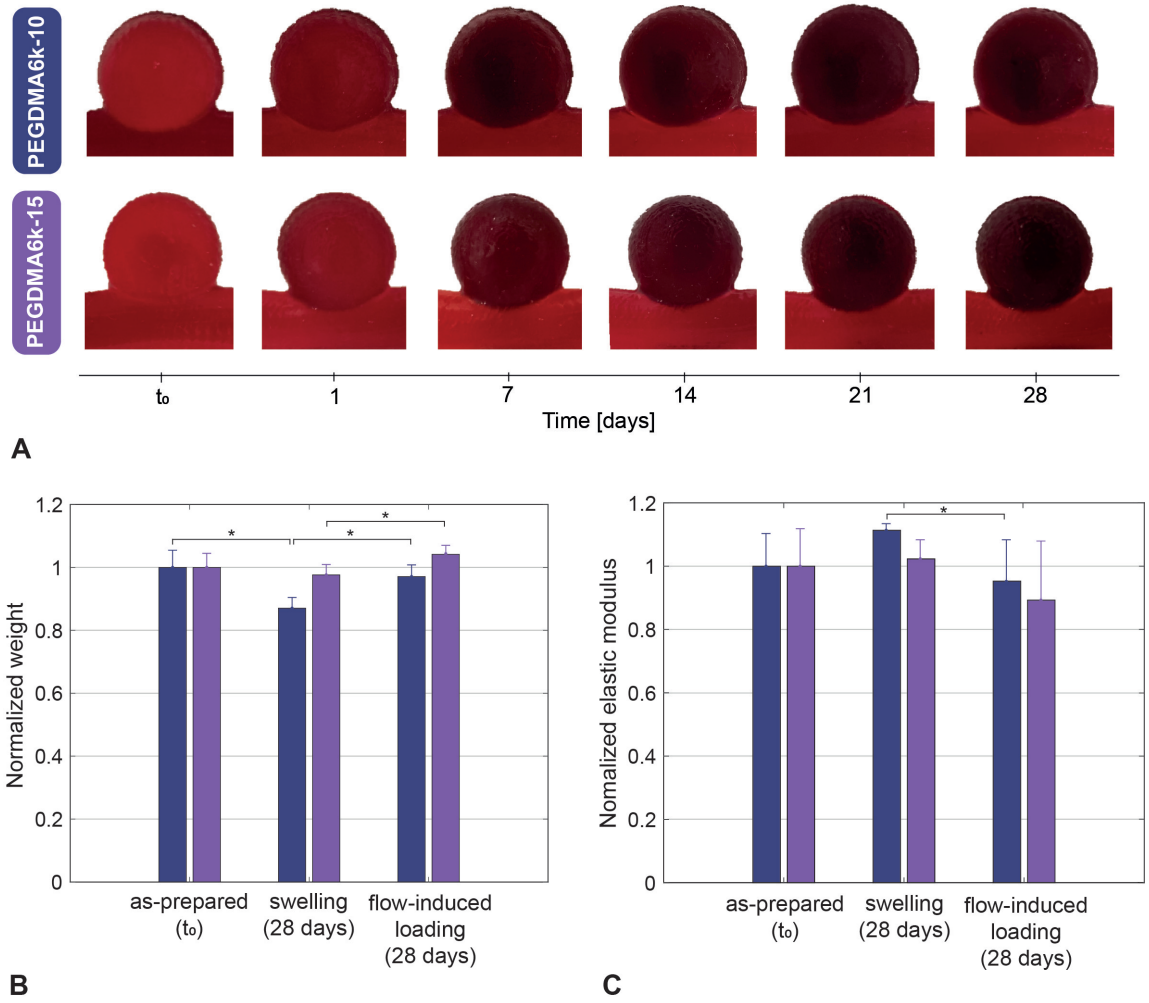

FIGURE 3.6: (A) Direct visualization of the hydrogels within the intracranial aneurysm model during one month of pulsatile fluid flow-induced loading showing complete occlusion without protrusion, migration, geometric distortion nor signs of macroscopic damage. (B) Weight and (C) Mechanical property variations, normalized to the as-prepared state of the hydrogel, after one month of swelling and one month of fluid flow-induced loading (n=3).

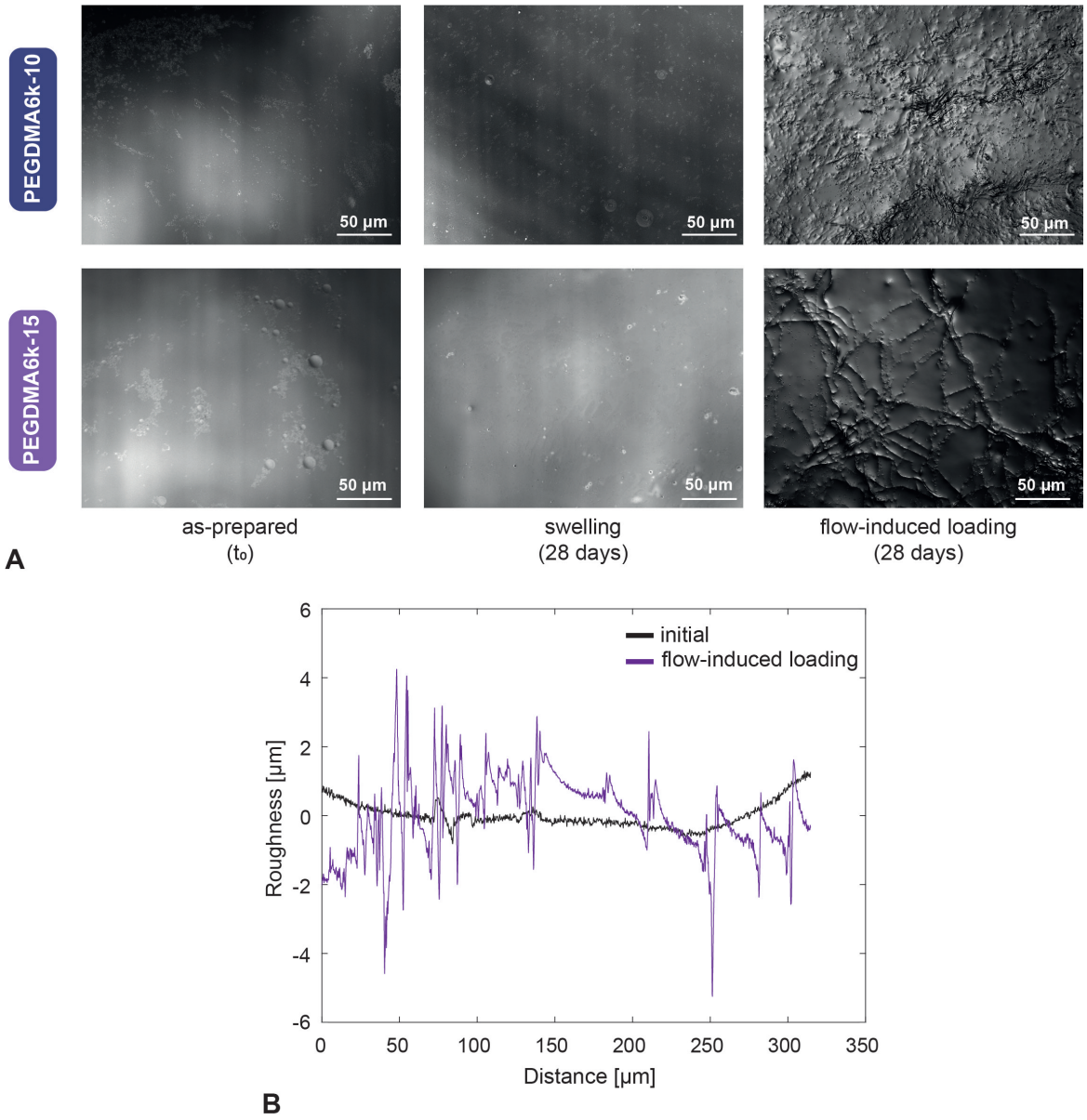

FIGURE 3.7: (A) Magnified microscopic view showing the surface profile of hydrogels in the as-prepared state (left), after one month of swelling (middle) and one month of fluid flow-induced loading (right). (B) Roughness profile of PEGDMA6k-15 hydrogel in the as-prepared state and after one-month of fluid flow induced loading, the latter revealing defects in the range of 2 to 10 μm in depth.

3.5 Discussion

To our knowledge, the present study is the first to assess the fatigue-resistance under physiological pulsatile flow of photopolymerizable hydrogels for intracranial aneurysm embolization. PEGDMA hydrogels, according to their polymer molecular weights (2, 6 and 20 kDa) and concentrations (10-20%), were selectively fine-tuned to fulfill the requirements of intracranial aneurysm embolic agent. The main finding of our work is that PEGDMA hydrogels of 6 kDa molecular weight at a concentration of 15% seem to be appropriate to withstand the continuous interactions with the blood flow. In fact, under pulsatile flow within an *in vitro* aneurysm model during one month, these hydrogels exhibited (1) a complete occlusion, (2) an integrity and stability due to the preservation of their shape, weight and mechanical properties, despite slight surface erosions, (3) a minimal swelling volume avoiding protrusion in the parent artery and a low swelling pressure limiting stresses applied on the aneurysm wall, and (4) an elastic modulus and compliance covering the range of native aneurysm tissue.

3.5.1 Hydrogel swelling and mechanical characterization

Molecular weight of polymers is known to affect the mechanical properties of hydrogels [185]. The present study is consistent with and supplements PEGDMA hydrogels characterization reported in literature [186], [187]. An increase in polymer molecular weight decreases the cross-linking density of the hydrogel network, favoring the water diffusion through the long chains of polymer. This leads to an increase in the volume swelling ratio and a decrease in the elastic modulus. The elastic modulus of PEGDMA2k-10 hydrogels, however, was unexpectedly lower compared to PEGDMA6k-10 hydrogels. For all hydrogels, the photoinitiator PEG-BAPO concentration was fixed at 0.1 wt% for biocompatibility purposes, meaning the same amount of formed radicals. The hydrogel network is formed by a free radical polymerization of the methacrylate functional groups. PEGDMA2k-10 hydrogels have a higher number of methacrylate groups due to their shorter chain length. Consequently, the ratio between the produced radicals and the methacrylate groups is lower with PEGDMA2k-10 compared to PEGDMA6k-10. Moreover, the mobility and diffusivity of the pendant double bonds are more restricted for short chain length [188]. This might limit further crosslinking and favor the termination reactions over chain propagation. We believe that both differences in the radicals-to-methacrylate groups ratio and kinetics of the photopolymerization can explain the lower elastic modulus for PEGDMA2k compared to PEGDMA6k. Low polymer molecular weight (2 kDa) adds brittleness to the hydrogel, as revealed by mechanical failure at stresses lower than the 100-150 kPa threshold of circumferential stresses driven by the blood pressure [22].

The swelling and mechanical properties are also influenced by the concentration of polymers [185]. At similar molecular weight (6 kDa), increasing the polymer content increases both the elastic modulus and the volume swelling ratio, which is in line with previous reports [175], [185], [189], [190]. Hydrogels with a high polymer content have a denser covalently crosslinked network in the as-prepared state, entailing a lower mesh size and more squeezed polymer chains. The swelling equilibrium is reached when the osmotic driving forces are balanced with

the elastic retraction forces. When increasing the polymer concentration, the osmotic pressure also increases [191] and drives solvent molecules into the hydrogel network. Due to their same molecular weight, the hydrogels reached the same swelling equilibrium and same mesh size in their swollen steady state. This implies that the hydrogels with high polymer content absorb more water and swell more to give the network more freedom to expand. PEGDMA hydrogels of 6 kDa molecular weight at a concentration of 10 to 20% far withstood physiologic blood pressures of 10.5-16 kPa (80-120 mmHg) and circumferential stresses of 100-150 kPa. Up to 50% strain, the load-bearing characteristic of arteries is dominated by elastin fibers, which results in the elastic modulus ranging from 200 to 600 kPa [17]. The compressive elastic modulus of the hydrogels, ranging from 125 to 507 kPa, thereby covers the range of the native tissue, except slightly lower for a concentration of 10%. Close mechanical properties for the hydrogel and the native tissue ensure stresses caused by blood flow to be gradually transfer to the tissue and to minimize the blood flow disturbances [71]. The compliance match of the hydrogels and the native tissue (3-12%/100 mmHg under physiological pressures [158]) suggests also that the blood flow at the interface between the hydrogel and the surrounding tissue should not be disturbed [75], [76].
The swelling pressure results indicate that the PEGDMA6k-20 hydrogels, due to their increased volume swelling of 25%, apply a pressure significantly higher than the critical rupture pressure of human cerebral arteries of 224 $\pm$ 60 kPa [161]. This would imply that PEGDMA6k-20 hydrogels would not be suitable for aneurysm embolization. It is worth mentioning that these results are in contrast to the results obtained by Hwang et al., where an expansion of 150 to 200% of a shape memory foam did not induce critical circumferential stresses [89]. It should also be noted that in our swelling pressure test the hydrogels were fully confined, corresponding to the worst-case scenario. The swelling pressure might therefore be lower in semi-confined conditions such as within an aneurysm. Furthermore, the hydrogels reached their swelling equilibrium after 24h of swelling, involving that the pressurization rate is very low compared to the one used for the determination of human cerebral arteries rupture pressure [161]. Thus, the aneurysm tissue could possibly bear this gradual pressure.

Finally, we need to acknowledge that the *in vitro* characterization was performed under fairly idealized conditions. However, this aimed to identify the hydrogels which fulfill the mechanical requirements in static conditions and exclude those inducing potential risks such as protrusion for PEGDMA20k-10 or excessive pressures for PEGDMA6k-20. The appropriate hydrogels were then exposed to a fatigue test within aneurysm models to characterize them in more realistic conditions.

3.5.2 *In vitro* intracranial aneurysm models

Silicone aneurysms models are commonly used to test new devices [192], because they exhibit better transparency, resistance and navigability compared to others materials such as flexible resins like TangoPlus or VeroClear [193]. The technique developed herein has been used to fabricate intracranial aneurysm models in previous studies. However, several layers of PDMS

were dip-coated or painted on the sacrificial mold [194], [195], making the technique time-consuming and not reproducible. Moreover, in the previously mentioned studies, the thickness of the wall was not stated or too thick (600-800 μm). Replicas manufactured by Elastrat company (Geneva, Switzerland) are based on this technique. Although the models mimic the shape and curvature of the human vasculature, the models are very expensive ($\approx$ \$1000/model), thick and stiff. The advantage of our model is the one-step casting method, the thin aneurysmal wall obtained mimicking that of real tissue, as well as similar dimensional and mechanical properties compared to native tissue not to mention a very affordable manufacturing price ($\approx$ \$10/model).

In addition, the use of PVA as sacrificial mold has two main benefits. PVA is a water-soluble polymer at 65°C, thereby no toxic solvent is required for the dissolution of the sacrificial mold. Moreover, the biocompatibility of our model is not affected by the potentially infiltrated and non-dissolved PVA into the PDMS model due to the biocompatibility of PVA polymer. Comparatively, numerous studies have used acrylonitrile butadiene styrene (ABS) for the sacrificial mold which dissolves in xylene [196] or acetone [197].

Although the geometry of the *in vitro* aneurysm model used in our experiments is too simple and linear to simulate complex microcatheter navigation or deployment of devices, its mechanical properties are much closer to human tissue characteristics and thereby better suited for the long-term assessment of intrasaccular hydrogel implants. Moreover, the technique of casting PDMS around PVA sacrificial molds could be adapted to replicate more tortuous geometries as in the human vasculature.

3.5.3 Aneurysm wall strain decrease with hydrogels implantation

In this study, the DIC technique was used to measure the displacements and strains fields because it is more suitable for small displacements and it is a contactless technique, contrary to others strain measurement techniques such as interferometric or strain gauges [198]. A few studies have used the DIC technique to understand the mechanical behavior of the aneurysms [199], [200]. Nonetheless, the aneurysm wall strains and stresses are mostly assessed by numerical simulations, where a significant reduction of the aneurysm wall strains and stresses was observed when coils are inserted [201]. In the same way, the present study showed that the implantation of hydrogels into an aneurysm substantially reduces the displacements and strains applied on the aneurysm wall. Hydrogels with close elastic modulus to the one of the aneurysm model (PEGDMA6k-20) showed lower displacements and strains than PEGDMA6k-10 hydrogels. This hence confirms the importance of the match between mechanical properties of the hydrogels and the aneurysm tissue, as specified previously. The reduction of aneurysm wall strains by the hydrogel implantation could diminish the aneurysm rupture risk.

A limitation of our work is that only the central region of the aneurysm was considered. Others aneurysmal regions such as the neck and the dome would be of interest to investigate. Moreover, the swelling process was not included in this study, as the strains field was measured directly after photopolymerization. As mentioned previously, the hydrogels applied a certain pressure

due to the swelling process. The swelling impact on the aneurysm wall strains could also be examined by DIC technique.

3.5.4 Fatigue resistance of hydrogels

The present study evaluated the *in vitro* fatigue resistance of the hydrogels by assessing the mechanical loss, residual mass and surface profile after mechanical loading. The hydrogels were subjected to a loading induced by pulsatile fluid flow for one month. This duration was determined according to the time needed for neoendothelial cells to grow over coils which generally occurs 4 weeks following implantation [202]. Long-term fatigue of hydrogels is often studied under prolonged static or cyclic uniaxial loading [203]. It is important to highlight that, in this work, the load-bearing ability of the hydrogels was tested under more realistic loading conditions, combining pulsatile circumferential stretch and fluid shear stresses. Indeed, similar circulating systems were used in previous *in vitro* studies to reproduce realistic blood flow and therefore closely simulate circumferential and wall shear stresses [204]–[206].

The results after 5.5 million cycles of pulsatile flow loading pointed that the hydrogels have a great integrity and stability owing to the preservation of their shape, weight and elastic modulus. However, mechanical loading has induced roughness and erosion of the hydrogel surface that was in contact with the fluid. The weight of the loaded hydrogels was not significantly different from the as-prepared hydrogels but higher than the one-month swollen hydrogels. We hypothesize that it might be due to an alternating of swelling and erosion cycles. In fact, when the hydrogel has reached its swelling equilibrium weight, the hydrogel surface erodes, which decreases the hydrogel weight and enables to start again the swelling process [207]. Surface erosion, forming roughness defects and micro-cracks of several microns, induces a small increase in porosity [208]. This change of the surface microstructure enhances the permeability and water absorption of the hydrogels [209], [210], which might explain the increase of weight swelling ratio after loading and hence after erosion. A further analysis of the erosion phenomena could confirm these results.

Erosion of a material is generally characterized by the residual mass and mechanical properties loss [208], [211] but the surface profile has not been studied. Our findings suggest that mass and mechanical loss are not sufficient to conclude regarding the erosion phenomena. Thus, an important implication of our findings is that the characterization of the surface might be of primary interest for the fatigue resistance evaluation.

A question associated with the erosion is its impact on the long-term efficiency of hydrogels as embolic agents. Even so roughness defects of loaded hydrogels are relatively low (less than 10 μm), the risk of hydrogel fragments moving downstream and thus the risk of stroke should not be underestimated. Another concern is that the erosion might be faster in blood. Indeed, one limitation is that the fatigue study we performed was in a fluid composed of PBS and glycerin without degradation enzymes. Nevertheless, the erosion process could also be advantageous to

increase the hydrogel pores size and thus cell penetration [212], which could foster the endothelialization of the hydrogel surface along the aneurysm neck.

A limitation of our work is that the fatigue resistance was studied only for a short duration (one month at 2.3 Hz corresponding to an implantation of 2 months *in vivo*) compared to years of implantation of an embolic agent in an aneurysm. However, an endothelial layer generally forms at the implant surface within one month of implantation, acting as a physical barrier to prevent direct contact between the blood and the implant [202]. In case of cell adhesive properties, the hydrogels might hence be protected at its surface by the endothelial layer. Nonetheless, these properties should be further studied to determine whether the exclusion of the aneurysm from the parent artery by endothelialization will reduce the risks caused by fatigue loading.

Furthermore, we need to acknowledge that although the hydrogels remained within the aneurysm model, the adhesion of the hydrogel to the endothelial tissue cannot be elucidated in the context of the present study and needs to be further investigated in order to avoid migration of the hydrogel into the artery. For this, an *in vivo* study in an elastase-aneurysm model in rabbits will examine the tissue adhesion as well as clinical safety and long-term efficiency of the photopolymerizable hydrogels as embolic agent.

3.6 Conclusion

Photopolymerizable PEGDMA hydrogels of 6 kDa molecular weight at a concentration of 15% demonstrated mechanical properties and compliance consistent with the native aneurysm tissue while presenting a minimal swelling volume and pressure. The hydrogels considerably reduced the displacements and strains on the aneurysm wall compared to untreated aneurysm models. The hydrogels were able to withstand 5.5 million cycles of pulsatile flow loading in an *in vitro* aneurysm model without a significant change in shape, mechanical properties or weight loss, despite slight surface erosion. This might enable neoendothelial cells to proliferate and lead to permanent sealing at the neck. *In vivo* studies are required to confirm these results and evaluate the long-term integrity and stability of such hydrogels, as well as their tissue adhesion properties in true physiological conditions.

3.7 Acknowledgements

We would like to thank Céline Samira Wyss for her assistance with the surface characterization and Emma Roussel for her work on DIC.

Chapter 4

In vitro implementation of photopolymerizable hydrogels as a potential treatment of intracranial aneurysms

This chapter is based on the following publication: O. Poupart, A. Schmocker, R. Conti, C. Moser, K.M. Nuss, H. Grützmacher, P.J. Mosimann, and D.P. Pioletti, "In vitro Implementation of Photopolymerizable Hydrogels as a Potential Treatment of Intracranial Aneurysms," Frontiers in Bioengineering and Biotechnology, vol. 8, no. April, pp. 1–13, 2020 [178].

4.1 Abstract

Intracranial aneurysms are increasingly being treated with endovascular therapy, namely coil embolization. Despite being minimally invasive, partial occlusion and recurrence are more frequent compared to open surgical clipping. Therefore, an alternative treatment is needed, ideally combining minimal invasiveness and long-term efficiency. Herein, we propose such an alternative treatment based on an injectable, radiopaque and photopolymerizable poly(ethylene glycol) dimethacrylate (PEGDMA) hydrogel. The rheological measurements demonstrated a viscosity of 6.53 $\pm$ 2.77 mPa.s and 16.83 $\pm$ 4.07 mPa.s for 10 and 15% PEGDMA, allowing the hydrogel precursors to be injected through 430 μm inner diameter microcatheters. Photorheology revealed fast hydrogel solidification in less than 8 minutes due to the use of a new visible photoinitiator. The addition of an iodinated contrast agent in the precursor contributed to the visibility of the precursor injection under fluoroscopy. Using a customized light-conducting microcatheter and illumination module, the hydrogel was implanted in an *in vitro* silicone aneurysm model with tortuous anatomy. Specifically, *in situ* fast and controllable injection and photopolymerization of the developed hydrogels is shown to be feasible in this work. Photopolymerizable hydrogels are expected to be promising candidates for future intracranial aneurysm treatments.

Keywords: intracranial aneurysms (IA), injectable hydrogels, *in situ* photopolymerization, light-conducting microcatheter, poly(ethylene glycol) dimethacrylate

4.2 Introduction

Intracranial aneurysms are saccular dilatations or outpouchings of brain arteries that are prone to rupture, causing death or severe morbidity in over half of the patients [213]. While minimally invasive endovascular therapy has many advantages and is increasingly being performed, the risk of IA recurrence remains higher compared to surgical clipping [36], [214], [215]. Adjunctive devices such as flow diverting stents may decrease this risk by promoting endothelial growth at the neck of the IA [216] but currently require dual anti-platelet medication to avoid parent artery thrombosis, thereby increasing the risk of bleeding. Device compaction [217], inflammation [218] and intra-saccular clot remodeling [219] appear to play a decisive role in healing and recurrence. Therefore, a liquid agent capable of (i) selectively filling the entire aneurysm, (ii) reversing the chronic inflammatory wall changes, (iii) preventing thrombosis, and (iv) attracting endothelial cells could eliminate the current drawbacks of endovascular therapy.

Using liquid embolic agents to treat aneurysms is not a new concept [66]. They allow the whole volume of aneurysms of any shape or size to be filled. The main limitation lies in their self-solidifying properties once in contact with blood, risk of spillage and downstream migration that may cause arterial occlusion and ischemic stroke. The risk of microcatheter entrapment within the solid agent, particularly with fast polymerizing substances such as acrylic glues, is also significant [69]. While non-adhesive ethyl-vinyl-alcohol (EVOH) copolymer agents precipitate over several minutes [68], the dimethyl sulfoxide (DMSO) solvent they contain can induce vasospasm and angionecrosis depending on the concentration and volume injected [70], [220], which is especially harmful if left to stagnate in such a restricted space as an aneurysm. Moreover, leakage and solidification in the parent artery remains a serious potential complication, even with balloon assistance.

Injectable *in situ* forming hydrogels have raised considerable interest for biomedical applications [221]–[223], including as potential novel embolic agents for aneurysms or transcatheter embolization. The liquid precursors of these hydrogel-based embolic agents have been triggered to solidify *in situ* by different stimuli, such as temperature [99], [224], [225], pH [102], chemical reaction [107], [226], [227] or light irradiation [97], [108]. Compared to the others stimuli, light-induced photopolymerization allows better spatial and temporal control of the curing [171], [228]. This control is essential to avoid any premature gelation or later dilution that could occur with temperature-sensitive, pH-sensitive and chemically-crosslinked types. To our knowledge, only a few studies have developed photopolymerizable hydrogels for IA treatment. Ishikawa et al. [108] have reported *ex situ* photopolymerization of hydrogels in an aneurysm model whereas Barnett et al. [97] described *in situ* photopolymerization of hydrogels in a saccular aneurysm model using 2.8 French-microcatheter (700 μm inner diameter).

To demonstrate the feasibility of *in vitro* implementation of photopolymerizable hydrogels, many requirements need to be taken into consideration. First, it has to exhibit low viscosity to be injectable through a microcatheter with an inner diameter of 430 μm, such as those used

for coil delivery in current clinical practice. Second, the hydrogel needs to be radiopaque to be visible under fluoroscopy. Furthermore, despite evidence that a balloon can remain inflated and block the flow in the parent artery for as long as 18 consecutive minutes [80], photopolymerization time should remain as short as possible, 10 minutes at most, ideally a few seconds, to diminish the risk of ischemic stroke and vessel injury. Finally, use of light in the visible spectrum to induce photopolymerization should be preferred over ultraviolet emission to avoid possible damage to encapsulated cells, host tissues or DNA [229], [230] and allow deeper light penetration within a highly absorbing medium such as blood.

Photopolymerizable polyethylene glycol dimethacrylate (PEGDMA) hydrogels have been widely used for tissue engineering [172]. Indeed, PEGDMA hydrogels present many advantages such as tunable mechanical properties, ease of chemical conjugation and biocompatibility. Herein, we describe the use of a radiopaque photopolymerizable hydrogel obtained from PEGDMA mixed with clinically approved iodinated contrast medium and a next-generation visible light-sensitive and water-soluble photoinitiator, known as poly(ethylene glycol) substituted bis(acyl)-phosphane oxides (PEG-BAPO) [131]. To address the challenge of inserting a photoactivable hydrogel into an intracranial aneurysm, we also present the development of a light-conducting microcatheter (inner lumen of 430 μm) combined with an illumination module to guide visible light to the aneurysm. We hereby report a proof-of-concept study to treat intracranial aneurysms with photopolymerizable hydrogels under fluoroscopy in a realistic flow model (Figure 4.1).

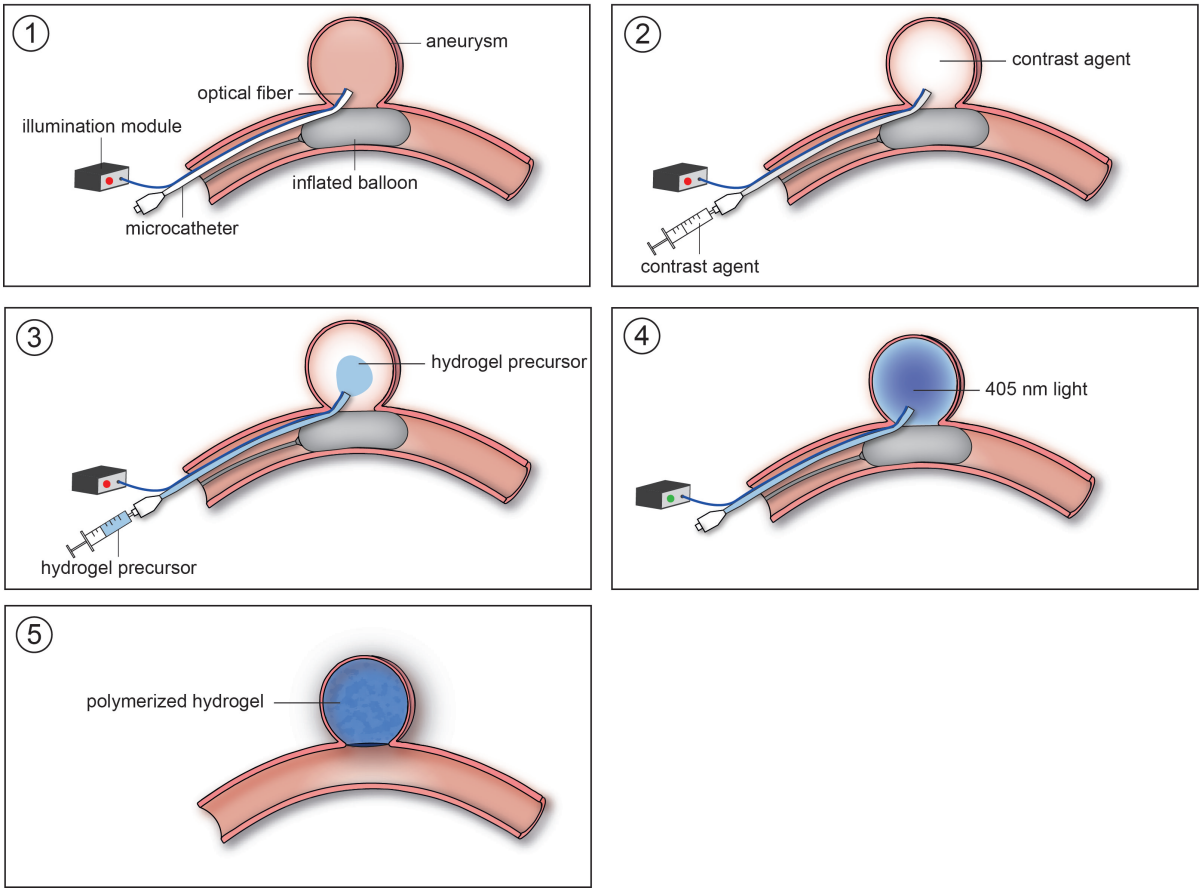

FIGURE 4.1: Schematic illustration of the different steps of the new treatment concept. (1) Positioning of the light-conducting microcatheter in the aneurysm and inflation of the balloon at the neck. (2) Rinsing of the aneurysm with contrast agent. (3) Injection of the hydrogel precursor. (4) 405 nm illumination and photopolymerization of the hydrogel. (5) Removal of the microcatheter and balloon.

4.3 Materials and Methods

4.3.1 Materials

All the chemicals were purchased from Sigma Aldrich (Merck, Switzerland). The reactions were performed under inert atmosphere of dry Argon using Schlenk techniques. Dry solvents were drawn from a commercial solvent drying system (Innovative Technology PURESOLV). The reaction flasks were dried in an oven overnight at 120°C before use. PEGDMA 6 kDa was prepared from poly(ethylene glycol) (PEG, M_n = 6000 g/mol) using a modified procedure from the previously reported one [175], as shown in Figure 4.2.A. The polymer (50 g) was loaded in a three necked 500 ml round bottomed flask equipped with an adapter for the Schlenk line and a Dean Stark condenser. The polymer was dissolved in 200 ml of toluene. The mixture was stirred at 600 rpm and warmed to 160°C. The mixture was refluxed for one hour and every

15 minutes an aliquot of 25 ml of solvent was removed using the Dean-Stark condenser. After 100 ml of solvent were removed, the mixture was cooled down to room temperature. Dry dichloromethane (100 ml) was added to the mixture followed by Et3N (distilled from CaCl2, stored in a Schlenk under Argon, 1.1 eq. for every OH) and methacrylic anhydride (distilled from CaCl2, stored in a Schlenk under Argon, 1.5 eq. for every OH). The mixture was protected from light and stirred at room temperature for 5 days. Subsequently, it was purified by filtration over a neutral alumina plug. The polymer was coagulated into diethyl ether and dried under high vacuum. The white powder was obtained in quantitative yield and characterized as the desired product via ^{1}H-NMR. The degree of functionalization was evaluated by integration of the ^{1}H-NMR resonances. The chemical structure of PEGDMA was confirmed using infrared spectroscopy (FT-IR, Bruker Tensor 27, Germany) in the infrared radiation range of 4000-400 cm^{-1} with a resolution of 4 cm^{-1} and 256 scans.
The iodine-based contrast medium Accupaque (350 mg/ml, GE Healthcare, Chicago, Illinois, US) was provided by the Bern University Hospital. Intralipid 20%, an intravenous fat emulsion, was purchased from Sigma Aldrich (Merck, Switzerland). The PEG-BAPO photoinitiator (PI) was synthetized by phospha-Michael addition of bis(mesitoyl)phosphane (BAP-H) to poly(ethylene glycol) methyl ether methacrylate (PEGMEM) followed by oxidation with aqueous H_2O_2, as previously reported [131]. The synthesis of PEG-BAPO is shown in Figure 4.2.B.

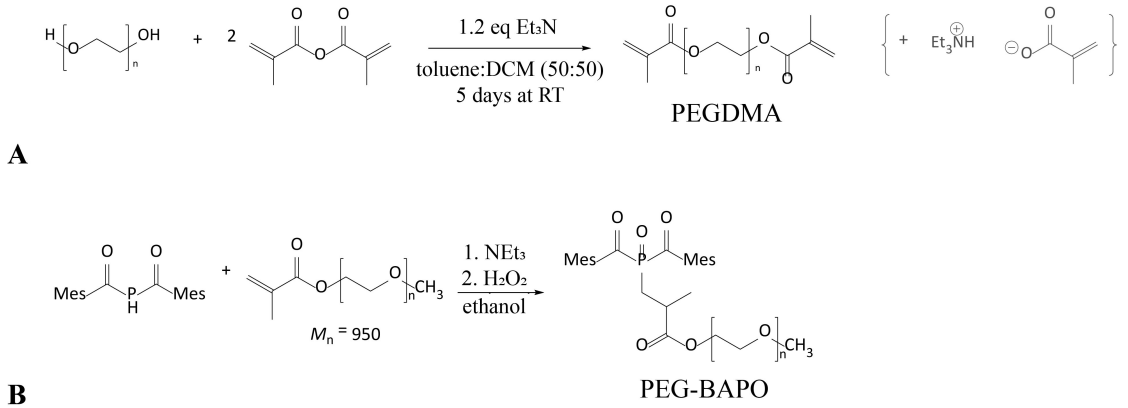

FIGURE 4.2: (A) Synthesis of PEGDMA polymer. (B) Synthesis of PEG-BAPO photoinitiator.

4.3.2 Hydrogel precursors preparation

The hydrogel precursor was prepared by dissolving PEGDMA (10 or 15 wt%) in equivalent weight concentrations of phosphate buffered saline (PBS) and Accupaque350. Since PEG-BAPO PI was shown to be more efficient (higher curing rate) than other commercially available water-soluble photoinitiators like Irgacure2959 [131], we decided to add this (0.1 wt%) to the formulation. These hydrogel precursor formulations were homogenized by Vortex for 5 min, degassed using a vacuum pump and then passed through a 0.22 μm syringe-filter (Rotilabo, Carl Roth, GmbH) for sterilization. Finally, intralipids (5 wt%) were added to the hydrogel precursor to enhance light-scattering and increase the polymerized volume during subsequent

illumination [231]. The precursors were named PEGDMA6k-10 and PEGDMA6k-15 for 10 and 15 wt% polymer concentration, respectively.

4.3.3 Injectability of the hydrogel precursors

The rheological properties of the hydrogel precursors were assessed with a modular compact rheometer 102 (Anton Paar, Peseux, Switzerland) by an oscillatory time sweep with a strain oscillation of 5% at a frequency of 1 Hz applied during 5 min. The dynamic viscosity was calculated as the average of the real part of the complex viscosity. The viscosity of the precursors was then compared with two reference samples, namely water and Accupaque350.
An injection test was also performed through a 430 μm inner diameter microcatheter (Echelon 10, Medtronic, Dublin, Ireland) using a 3 ml syringe connected to a syringe pump at a flow rate of 1 ml/min (Harvard Apparatus, Cambridge, MA, US).

4.3.4 Radiopacity of precursor and hydrogels

Using pulsed fluoroscopy (7.5-10 p/s) and serial angiography snapshots (70 kV, 23 mA) on a HDR flat detector monoplane system (154 μm pixel size, 16-bit digitization depth, Siemens Artis Zee, Erlangen, Germany), the radiopacity of 2 mm-thick samples of liquid precursor was assessed and compared to an equal volume of solid as-prepared hydrogel (immediately after polymerization) and swollen hydrogel (after incubation in PBS for 36 hours). The results were compared to pure Accupaque350 and to a single lumen occlusion balloon (Scopernic15, Balt, Montmorency, France) containing two radiopaque markers.

4.3.5 Photopolymerization

The kinetics of the hydrogels photopolymerization was evaluated by photorheology. The light from a 405 nm wavelength light laser diode was coupled to the modular compact rheometer 102 and a parallel 25 mm diameter disc configuration was used. 200 μl of the hydrogel precursor was tested directly after hydrogel preparation. A strain oscillation of 5% at a frequency of 10 Hz was applied and the temperature fixed at 37°C. Samples of 300 μm thickness were illuminated with a light intensity of 15 mW/cm^2 at 405 nm. The evolution of the storage modulus G' was recorded during 405 nm irradiation. The polymerization was considered complete when G' reached a plateau level. The time required to reach 95 % of the plateau level of G' was defined as polymerization time, noted t_{95}, as previously reported [187].
The volume of photopolymerized samples was also evaluated in function of the illumination time. A constant volume of the precursors was placed in an aneurysm mold of 8 mm in diameter and illuminated by a glass optical fiber connected to a laser diode controller (ThorLabs, Newton, NJ, US) at 405 nm and 15 mW/cm^2, as shown in Figure 4.9. The polymerized samples were then extracted from the aneurysm mold, immersed in PBS and dried to remove unreacted components and weighed.

4.3.6 *In vitro* aneurysm model

The feasibility of hydrogel injection, photopolymerization and implantation was evaluated in an *in vitro* aneurysm model shown in Figure 4.3. Since approximately 30% of IAs develop on the internal carotid artery, where flow rate and turbulence in the aneurysm are higher compared to more frequent aneurysm locations such as the anterior communicating or middle cerebral artery [232], we decided to model a paraophthalmic IA to simulate the worst hemodynamic conditions. The setup consisted of a wide necked, 5 x 6 mm left carotid ophthalmic aneurysm made of soft silicone (Elastrat, Geneva, Switzerland), connected to a peristaltic pump (Masterflex 7523-37, ColeParmer, Vernon Hills, IL, US) and head pump (Masterflex 7036-30, ColeParmer, Vernon Hills, IL, US) using 9.7 mm inner diameter silicone tubings (Masterflex 96410-36, ColeParmer, Vernon Hills, IL, US). The pump parameters were set to 1 Hz and 220 ml/min to mimic human internal carotid artery flow rate [233]. Additionally, a vertical 1.2 m liquid column inducing a constant pressure of 12 kPa (90 mmHg) to mimic intracranial arterial pressure conditions (91.2 ± 9.6 mmHg) [180] was implemented. The system was filled with a blood substitute composed of 36 vol% glycerol in water and PicroSirius Red dye (0.134 wt%) to match blood viscosity [234] and light absorbance, respectively. The dye concentration was determined using the Beer-Lambert law.

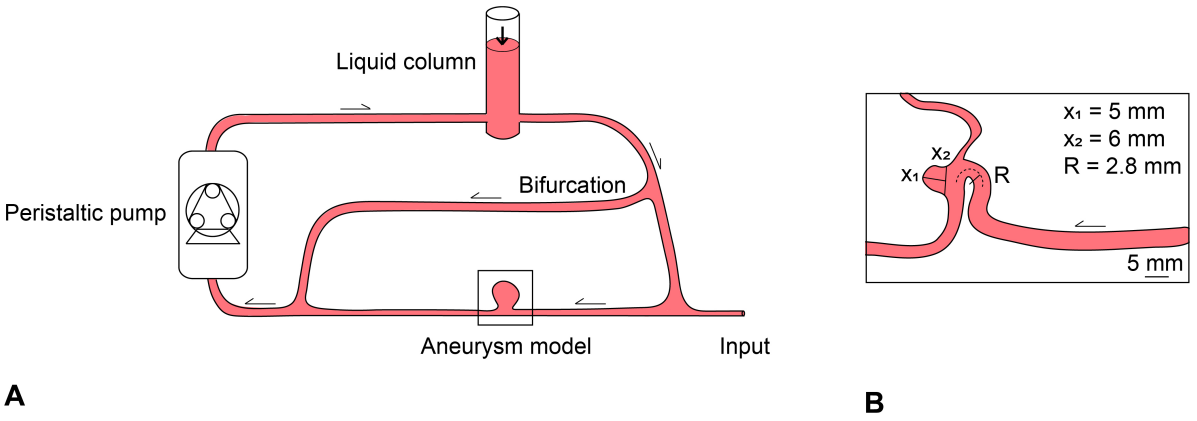

FIGURE 4.3: (A) Schematic illustration of the *in vitro* setup to evaluate the feasibility of the implantation. The peristaltic pump induced a pulsatile flow of 220 ml/min at 1 Hz. The height of the liquid column ensured a constant pressure of 12 kPa to the system. A parallel bifurcation channel, representing collateral shunting or outflow in the head and neck during balloon inflation at the aneurysm neck was added to dissipate over-pressurization and avoid bursting or displacing the balloon when inflated. The input represents access to the internal carotid artery through which a 9 French introducer sheath and an 8 French guiding catheter were placed, followed by navigation of the light-conducting microcatheter and balloon to the aneurysm site. (B) Schematic illustration of the *in vitro* aneurysm model, showing its dimensions and tortuous geometry.

4.3.7 *In vitro* proof-of-concept of the implementation

In order to bring light to the aneurysm to photopolymerize the hydrogel precursor *in situ*, two optical glass fibers (105 μm, 0.22 NA, 1.5 m, ThorLabs, Newton, NJ, US) were wrapped with

heat shrunk hydrophilic tube (Vesta, Lubrizol Company, Corona, CA, US) along the outer surface of a microcatheter typically used for IA coiling (Headway 17, MicroVention, Tustin, CA, US). The tip of the optical fibers was fixed to match the distal marker of the microcatheter and connected proximally to an illumination module composed of 405 nm, 200 mW light power laser diodes (Fibotec Fiberoptics GmbH, Meiningen, Germany), as shown in Figure 4.4. First, a 9F introducer sheath (Radifocus Introducer II, Terumo, Tokyo, Japan) and 8F guide catheter (Mach1, Boston Scientific, Marlborough, MA, US) were inserted in the input tubing. Under fluoroscopic guidance, the light-conducting microcatheter was placed in the aneurysm sac followed by the placement of an inflatable balloon (Scopernic15, Balt, Montmorency, France) at the neck of the aneurysm. The balloon was inflated, with a solution of Accupaque350 for radiopacity and black ink to prevent light from polymerizing leaked material in the parent artery. The blood substitute was flushed out from the aneurysm cavity with a contrast agent injected through the microcatheter under submaximal balloon inflation, in order to minimize light absorption caused by red dye and therefore maximize photopolymerization efficiency. The hydrogel precursor PEGDMA6k-10 was injected under blank roadmap fluoroscopy using a dedicated 3 ml syringe wrapped in aluminum foil (to avoid premature polymerization caused by ambient light) until the contents of the aneurysm were completely replaced and started to leak out downstream. After sealing the neck with maximal balloon inflation, the precursor was illuminated by the optical fibers for 8 min. Following photopolymerization, the microcatheter was removed under balloon inflation to avoid fragmentation followed by progressive balloon deflation and removal.

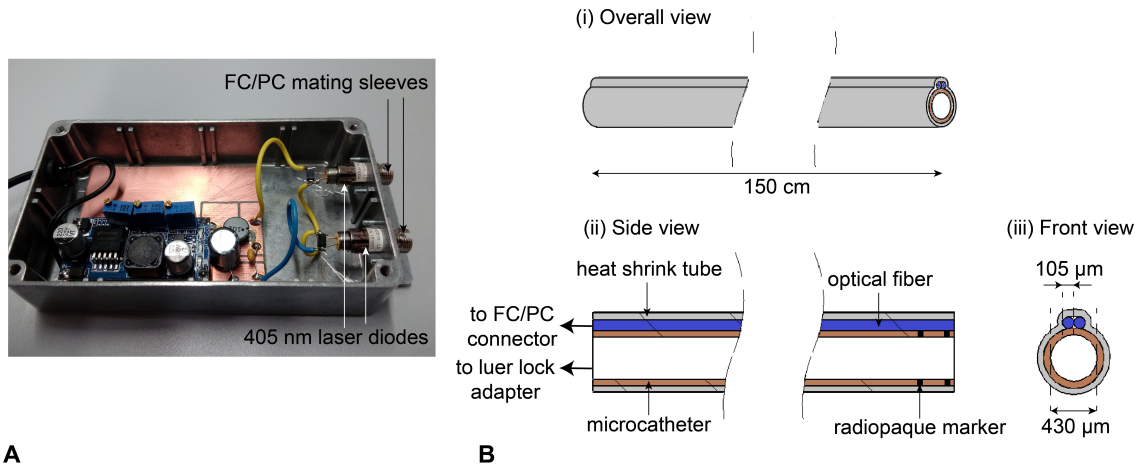

FIGURE 4.4: (A) Illumination module to which the optical fibers are connected. (B) Schematic of the light-conducting microcatheter from different views (i) overall, (ii) side and (iii) front view.

4.3.8 Statistical analysis

Each experiment was performed in triplicate or more and each statistical evaluation was done with MATLAB (Mathworks, Natick, MA, United States). All data are expressed as mean $\pm$ standard deviation. One-way analysis of variance (ANOVA) was used for comparison. $P < 0.05$

was considered as a significant result (denoted as *) and $p > 0.05$ non-significant (denoted ns). $p < 0.01$ was denoted as ** and $p < 0.001$ as ***.

4.4 Results

4.4.1 Characterization of PEGDMA polymer

The degree of functionalization of PEGDMA was found by ^{1}H-NMR integrals to be over 90%. The functionalisation of the PEG with methyl methacrylate ending units was confirmed by the FT-IR spectra, shown in Figure 4.5, recorded on the purified product. The signal arising from the C=O stretching methyl methacrylate substituent was visible at 1715.85 cm^{-1}. A peak at 841.20 cm^{-1} was also observed, corresponding to the C=C bending. Thus, the methacrylation functionalisation of the PEG polymer was confirmed by FT-IR.

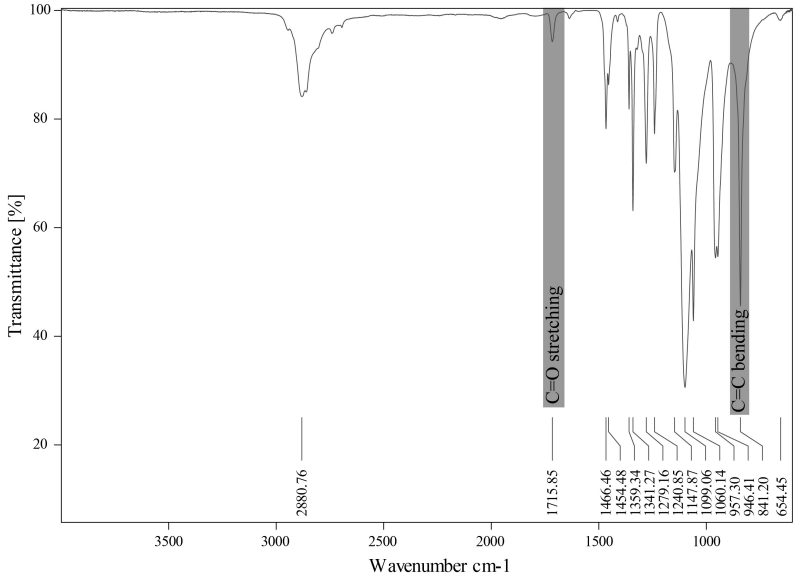

FIGURE 4.5: FT-IR spectra of PEGDMA polymer.

4.4.2 Injectability of hydrogels precursors

The dynamic viscosity at room temperature (23°C) of the precursors PEGDMA6k-10 and PEGDMA6k-15 and the contrast agent Accupaque350 were 6.53 $\pm$ 2.77, 16.83 $\pm$ 4.07 and 18.30 $\pm$ 4.85 mPa.s, respectively (Figure 4.6.A). Increasing the polymer concentration increases the dynamic viscosity of the precursor. The water viscosity of 1 mPa.s from literature was used as reference. Comparatively, PEGDMA6k-10 and PEGDMA6k-15 precursors viscosity was significantly higher than water (p=0.026 and 0.0025, respectively) but significantly lower than Accupaque350 value for PEGDMA6k-10 (p=0.022) and similar for PEGDMA6k-15 (p=0.71). In addition, viscosities of other liquid embolic agents, such as Onyx or PHIL, currently used in endovascular therapy, range from 16 to 72 mPa.s [235]. The injectability of the precursors

through a microcatheter of 430 μm inner diameter and 1.5 m length was confirmed by a syringe pump injection test, as shown in Figure 4.6.B.

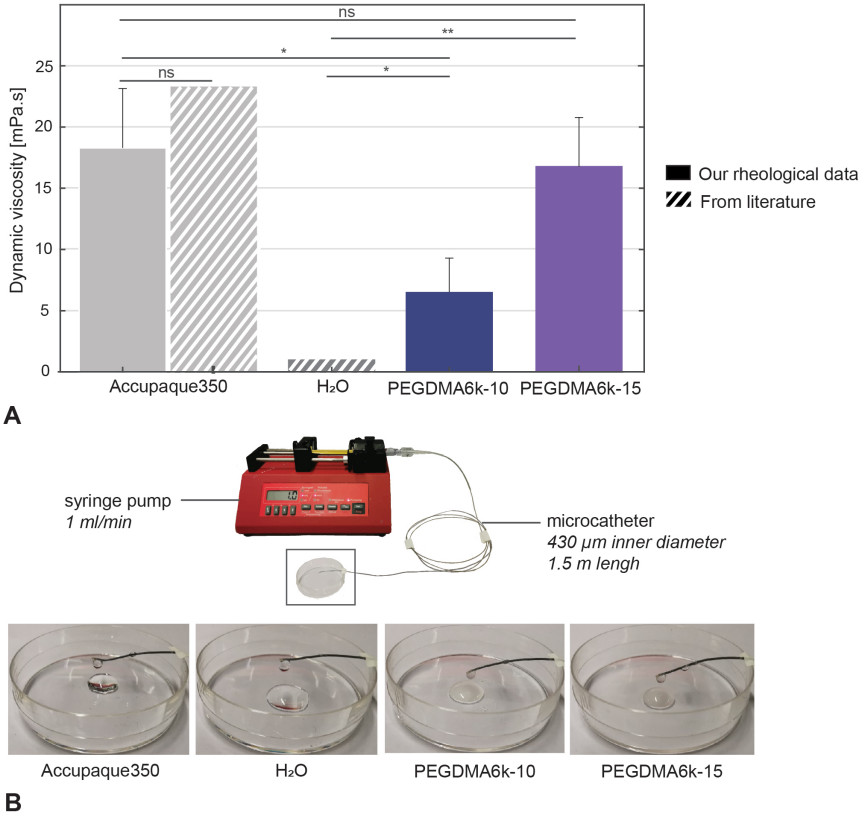

FIGURE 4.6: (A) Dynamic viscosities of Accupaque350, water and hydrogel precursors by rheology measurements (n=3). (B) Injectability of the Accupaque350, water and hydrogel precursors through a microcatheter of 430 μm inner diameter and 1.5 m length using a syringe pump.

4.4.3 Radiopacity of hydrogels precursors

The 2 mm-thick samples observed under fluoroscopy are shown in Figure 4.7. The radiopacity was compared with pure Accupaque350 and the two radiopaque markers of a single lumen occlusion balloon. The PEGDMA6k-10 precursor and as-prepared polymerized hydrogel were clearly visible under fluoroscopy, although less radiopaque than pure contrast agent, since the hydrogels are composed of 50% Accupaque and 50% PBS. As expected, the iodinated content of the hydrogel was no longer visible after 36 hours of incubation in PBS.

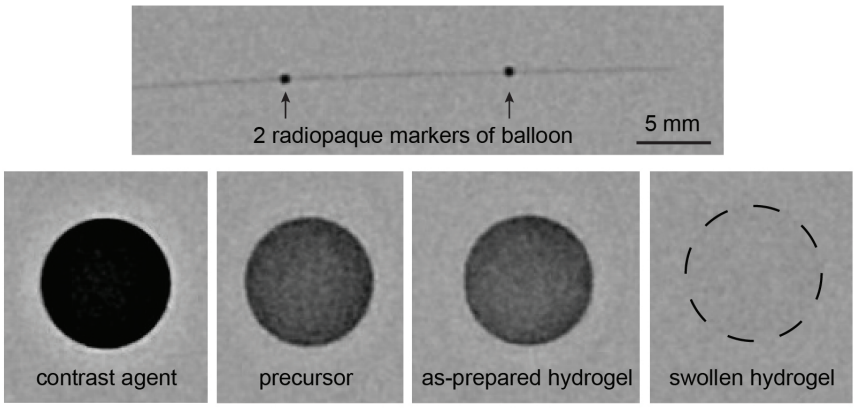

FIGURE 4.7: Radiography snapshot of a deflated balloon with its two proximal and distal radiopaque markers, pure contrast agent, hydrogel precursor, as-prepared hydrogel and swollen hydrogel.

4.4.4 Photopolymerization of hydrogels

As shown in Figure 4.8.A., the photopolymerization kinetics can be determined by photorheology with the evolution of the storage modulus G' over 405 nm illumination time. The cross-linking reaction and thus the propagation phase is identified by the rapid increase of G' while the termination phase is characterized by the G' plateau level. Photorheology measurements showed that the PEGDMA hydrogel precursors with 10 and 15% concentration completely polymerized after 8 min 15 s $\pm$ 1 min 36 s and 4 min 38 s $\pm$ 8 s, respectively, under a 405 nm illumination at 15 mW/cm^2, as shown in Figure 4.8.B. Therefore, increasing PEGDMA content significantly shortens the polymerization time. As comparison, PEGDMA6k-10 hydrogels with the commercially available LAP photoinitiator, polymerized in 10 min + 6 s $\pm$ 25 s, which is significantly longer than with PEG-BAPO photoinitiator (p=0.0321) and higher than the threshold of 10 min for intracranial aneurysms. Therefore, PEG-BAPO demonstrated a higher photo-reactivity than LAP.
When intralipids were added (5 wt%), the photopolymerization time t_{95} was non-significantly reduced to 7 min + 38 s $\pm$ 1 min 16 s and 4 min 23 s $\pm$ 45 s for PEGDMA6k-10 and PEGDMA6k-15 hydrogels (p=0.6318 and 0.6004, respectively). However, the addition of intralipids to the formulation has a significant impact on the polymerized volume of the hydrogels. As displayed in Figure 4.9, after the same 405 nm illumination time, the volume of the hydrogels samples was significantly higher with intralipids in the precursor formulation.

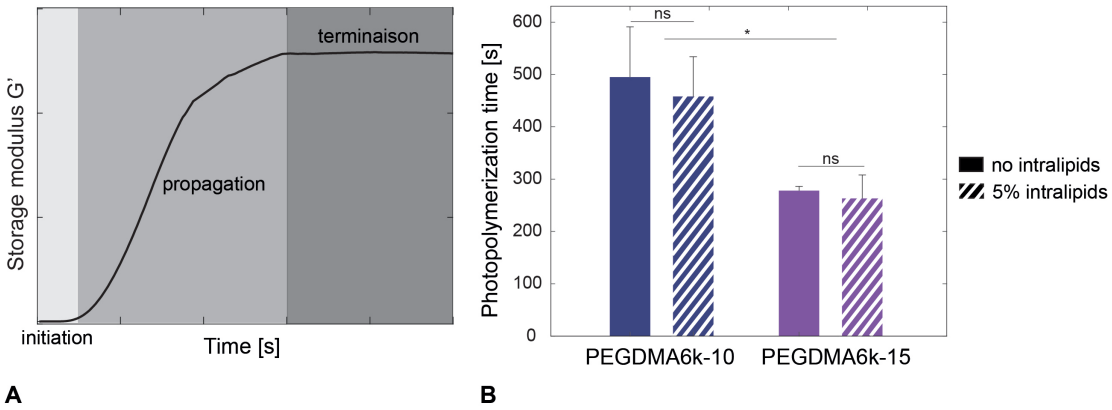

FIGURE 4.8: (A) Representative curve of the storage modulus G' evolution during the photopolymerization of PEGDMA hydrogels. (B) Photopolymerization time of PEGDMA hydrogels measured by photorheology (n=3), revealing a significant shortening of photopolymerization time when increasing the PEGDMA concentration and a non-significant decrease when adding intralipids.

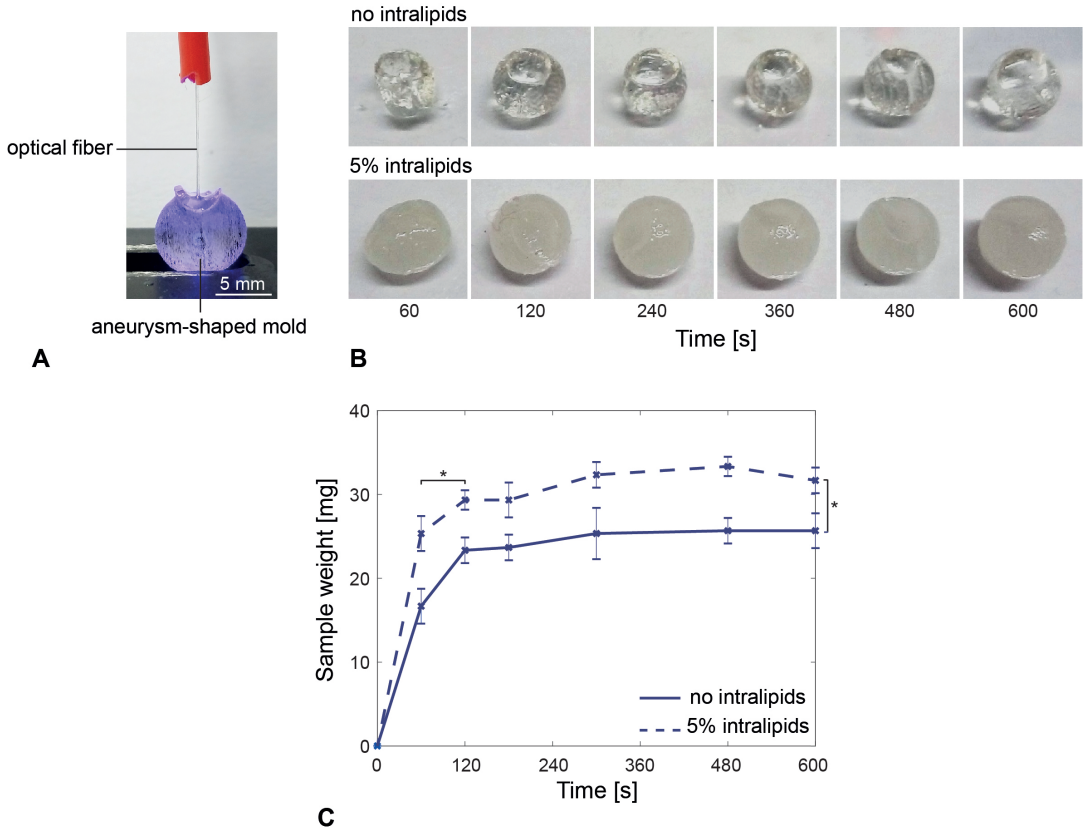

FIGURE 4.9: (A) 8 mm diameter aneurysm mold filled with hydrogel precursor and illuminated by a glass optical fiber. (B) PEGDMA6k-10 polymerized samples after different times of 405 nm illumination. (C) Weight of PEGDMA6k-10 polymerized samples in function of the 405 nm illumination time with and without intralipids (n=3), showing a significant increase of the sample weight when adding intralipids.

4.4.5 *In vitro* proof-of-concept of implementation

The light-conducting microcatheter (Figure 4.4.B.) was subjectively stiffer than the standard clinical microcatheter, due to the heat shrink tube wrapping around the glass optical fibers along the outer surface but this did not affect the navigation inside the silicone model and also ensured mechanical protection of the fibers. After positioning the balloon at the aneurysm neck in the parent vessel, the distal tip of the microcatheter (distal radiopaque marker) was placed inside the aneurysm within a few minutes, as shown in Figure 4.10.B. Figure 4.11 shows the optical fiber illumination *in situ*.
Fluoroscopically controlled balloon inflation was easily achieved (Figure 4.10.B.) followed by contrast agent injection to rinse the blood substitute volume out of the aneurysm cavity. Subsequently, the hydrogel precursor was injected through the microcatheter with a similar resistance to a regular contrast injection, according to the experienced neuro-interventionalist performing the injection (PJM) and depicted in Figure 4.10.C. The aneurysm was considered to be completely filled by the hydrogel precursor after all the contrast agent was replaced under blank map fluoroscopy (initially no contrast visible followed by negative contrast [white aspect] during contrast agent removal and finally positive contrast [black aspect] as the precursor filled the cavity). Direct visual inspection was used to confirm the complete filling of the aneurysm. A small residual inflow from the parent artery in the aneurysm was observed, despite maximal balloon inflation at the junction between the balloon and the microcatheter. This inflow was probably due to the rigidity and low compliance of the silicone model, a feature not generally observed in physiological conditions, unless the balloon leaks or is not sufficiently inflated. To match physiological conditions, the pump parameters were adapted until flow was almost stopped (25 ml/min) while the balloon was inflated. Despite this corrective measure, we observed some leakage of the precursor in the parent vessel and ophthalmic artery. The optical fibers connected to the illumination module were then used to illuminate the aneurysm with 25 mW/cm^2 of light at 405 nm. After 8 minutes of continuous *in situ* illumination of the hydrogel precursor (in a darkened room with no ambient light), the microcatheter was removed under fluoroscopy without fragmenting the hydrogel, suggesting minimal adhesion to the microcatheter.

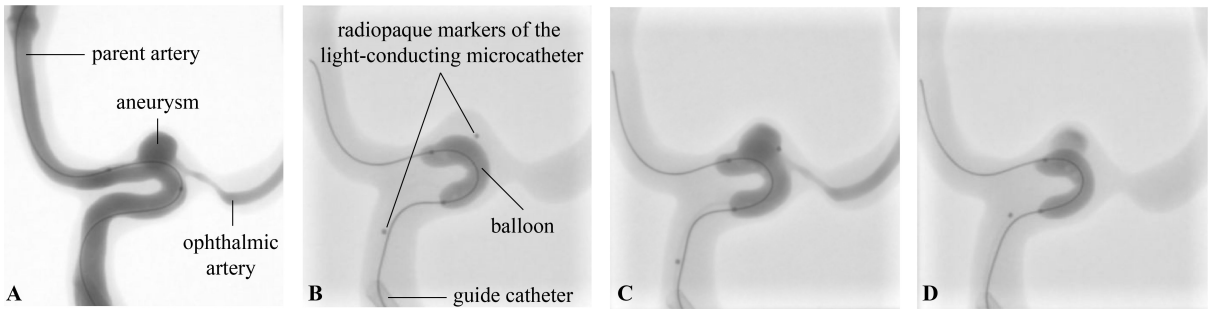

FIGURE 4.10: Subtracted (A) and (B-D) unsubtracted fluoroscopic images showing (A) contrast agent injection into the model to visualize the dimensions of the parent artery, aneurysm and ophthalmic artery; (B) guide catheter, inflated balloon (slightly prolapsing in the aneurysm) and light-conducting microcatheter in place; (C) injection of the hydrogel precursor through the microcatheter and (D) polymerized hydrogel after 8 minutes of 405 nm illumination and removal of the light-conducting microcatheter.

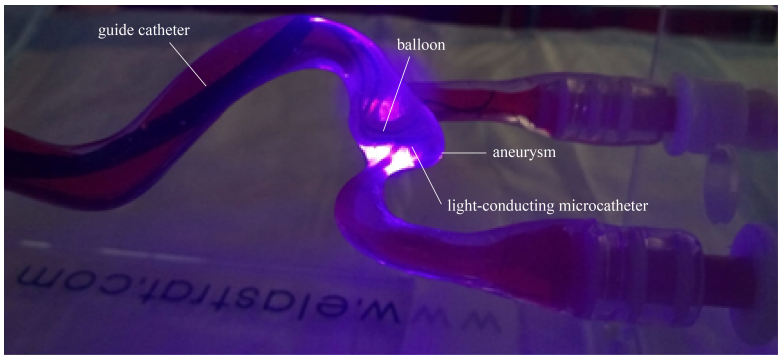

FIGURE 4.11: Optical fiber *in situ* illumination through the microcatheter in the aneurysm.

Figure 4.12 shows the progressive deflation and removal of the balloon and solidified photopolymerized hydrogel *in situ* in almost physiological hemodynamic conditions.

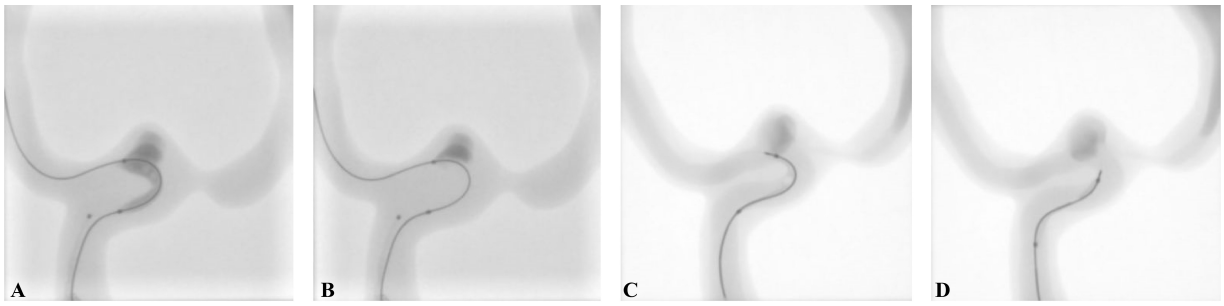

FIGURE 4.12: Unsubtracted fluoroscopic images of (A) deflation and (B-D) progressive removal of the balloon. Note that radiopacity is reduced compared to (A) due to slow residual inflow of blood substitute during polymerization. Recycled contrast agent after re-establishment of blood flow throughout the model is visible on (C) and (D).

4.5 Discussion

The present study is, to the best of our knowledge, the first to demonstrate the feasibility of *in situ* implementation using the same microcatheters as in clinical practice, as well as photoactivation and polymerization of hydrogels to treat intracranial aneurysms.

A major strength of our work is the development of low viscosity precursors injectable through the same microcatheters as those used for coiling i.e. with an inner diameter of 430 μm (1.7 French outer diameter). In comparison, the injectability of precursors until now was feasible through 4 to 6 French-catheters (1.33 to 2 mm outer diameter) [99], [107], [108], [224], [226], [236]. A pH-sensitive hydrogel was injected through a 2 French-catheter (490 μm inner diameter) [102], but so far we found no evidence of a similar or alternative hydrogel injectable through a 1.7 French-microcatheter or smaller. The viscosity of the precursors was affected by the PEGDMA concentration since higher concentration of polymer increases the precursor viscosity. The iodinated contrast agent also influenced the viscosity. By using other clinically

approved but less viscous contrast agents, it might be possible to further reduce resistance to injection in small microcatheters. Accupaque300 (GE Healthcare) or Visipaque270 (Nycomed), notably, have a viscosity at 20°C of 11.6 and 11.3 mPa.s, respectively, corresponding to a drop of almost 40%. Although both polymer concentration and iodinated contrast agent addition increase the viscosity of the precursors, it is worth mentioning that the precursors viscosity was still in the range of current injectable radiopaque agents viscosity and that their injectability through 430 μm microcatheters was validated.

Radiopacity of the hydrogel is indispensable for aneurysm embolization. In this study, the addition of 50 wt% iodinated contrast agent in the composition allowed both precursor and hydrogel to be radiopaque. It has been shown that hydrogel radiopacity remains acceptable under fluoroscopy with 20-25 wt% iodinated contrast medium [97], [99], [100], [102]. In other words, we could further decrease the radiopaque agent content in our formulation and hence viscosity, without significantly altering the fluoroscopic visibility of the liquid precursor. It is known that iodinated contrast agents are subject to leak to the surrounding environment [237], as it was demonstrated for our hydrogel over the following days due to the immersion process (Figure 4.7). In contrast to coiling or clipping [46] or use of EVOH agents [238] where artifacts are usually observed after treatment, the fast leakage of iodine has the potential to increase the quality of follow up imaging on Computed Tomography (CT) or Magnetic Resonance Imaging (MRI). The intra-aneurysmal content might become easier to evaluate in terms of recurrence without the need for follow up digital subtraction angiography (DSA), which requires arterial catheterization and still carries a small but relevant risk of iatrogenic ischemic stroke [239].

A further novelty of our approach is the use of a new type of water-soluble photoinitiator that is activated by visible light and allows the hydrogel to completely photopolymerize within 8 minutes for PEGDMA6k-10 and 5 min for PEGDMA6k-15. The presence of higher number of methacrylate groups in PEGDMA6k-15 hydrogels explained the shorter photopolymerization time. For biomedical applications, Irgacure2959 remains the most widely used water-soluble photoinitiator. Its major drawbacks are longer polymerization times, approximatively 25 minutes for 6kDa PEGDMA hydrogels [187], and the need for ultraviolet light, which may damage the DNA of the encapsulated cells or host tissues [229], [230]. Lithium phenyl2,4,6-trimethylbenzoylphosphinate (LAP) has recently appeared as a promising water-soluble photoinitiator sensitive to visible light for biomaterials. However, according to the photorheology results, LAP was found less photoreactive than PEG-BAPO. Other water-soluble visible photoinitiators, such as 2,2-azobis[2- methyl-n-(2-hydroxyethyl)propionamide] (VA-086) or eosin, used in tissue engineering [240] might also be of interest but were not assessed herein. Intralipids were added to the composition for their intrinsic scattering properties. These particles did not decrease the polymerization time but improved the volume of polymerized hydrogels. It should be noted that the photorheology bench test we performed was on thin samples (300 μm thickness) under homogeneous illumination using 405 nm light over the whole surface of the sample. The effect of light scattering particles becomes significant when the sample is polymerized in depth and when light is not homogeneously distributed [231]. This was confirmed by our test in the aneurysm mold, corresponding to polymerization in volumes similar to those

of intracranial aneurysms. Therefore, adding intralipids seems to enhance light distribution and photoactivation in complex environments such as a human brain aneurysm. In addition to the photopolymerization kinetics, it would also be relevant to determine the conversion rate by spectroscopy techniques, such as FT-IR and NMR.

A handful of studies have focused on the embolization of IAs using chemical and physical cross-linked hydrogels [99], [107], [226], usually limited by premature gelation or later dilution. Takao et al. [99] managed to embolize a wide-necked lateral wall aneurysm using a thermo-reversible hydrogel but with the drawback of solidifying into the microcatheter during delivery, rendering their applicability in humans unlikely. Consequently, a further benefit of the photopolymerizable hydrogel we have developed is the controllability of its solidification. Indeed, photoactivation can be triggered precisely by the operator by selectively switching the illumination module on. Moreover, it is theoretically possible to implement a feedback loop coupled to sound to monitor the solidification process by using light of a different wavelength through the same optical fiber [241].

The relevance of silicone aneurysms models for *in vitro* studies to test new devices, such as coils, stents or embolic agents was previously confirmed in multiple studies [242]. Similar *in vitro* pulsatile flow setups for aneurysm embolization (ranging from 100 to 300 ml/min) were developed in a few studies [107], [108]. A patient-specific carotid ophthalmic aneurysm silicone model enabled us to assess real-life navigation of the light-conducting microcatheter prototype, despite limitations such as the absence of endothelial lining or natural elastic and lubricity conditions. Nonetheless, microcatheterization of the aneurysm and visible light emission *in situ* was feasible in physiologically-approaching hemodynamic conditions. Although a similar optical system was developed by Barnett et al. [97] using a commercially available Excimer laser catheter sheath attached to a UV connection box for aortic and saccular aneurysm treatment, its minimal diameter of 0.9 mm limits its use for IAs, not to mention the danger of UV light previously discussed. Pushing an optical fiber through the inner lumen of a 430 μm microcatheter proved to be extremely time consuming in our experience and almost impossible in case of curvy or loopy anatomy. The risk of breaking the optic fiber was high, as well as the risk of vessel wall perforation related to the absence of radiopaque marker at the distal tip. The heat shrink tube ensured mechanical protection of the fibers but increased the bulkiness of the microcatheter. Braiding the optical fibers directly in the plastic wall of the microcatheter would be an elegant way to ensure mechanical protection without increasing the overall diameter.

A limitation of our implementation system is that it is difficult to rinse the blood out of the aneurysm entirely with the precursor and to keep the latter trapped inside to fill the whole volume before photoactivation. It is also challenging to avoid blood contamination from residual inflow during balloon inflation that could hinder the polymerization process. We tried to solve this issue by inflating the balloon in a submaximal fashion so that the precursor could be injected at a rate higher than the residual blood inflow until it leaked out into the parent artery, at which point the balloon was inflated to obtain complete sealing of the neck. It remains to be shown whether this technical feature is applicable in a real clinical situation.

4.6 Conclusion

Our study reveals the potential of photopolymerizable hydrogels for intracranial aneurysm treatment. The developed hydrogels were shown to have a low viscosity enabling injection through 430 μm microcatheters, to solidify within less than 8 minutes using visible light and to be radiopaque under fluoroscopy. The proof-of-concept of *in situ* implementation of the hydrogel was validated in a realistic flow model of a human brain aneurysm replica, using a customized light-conducting microcatheter. While this new type of liquid embolic agent has the potential to overcome the limitations of current endovascular implants, *in vivo* studies are needed to confirm these preliminary results and to evaluate other key features, such as clinical safety, thrombogenicity, tissue adherence, endothelialization and long-term durability.

Chapter 5

Toxicity evaluation of photopolymerizable poly(ethylene glycol) dimethacrylate-based precursors and hydrogels

5.1 Abstract

In the search for the ideal material for intracranial aneurysms embolization, *in situ* injectable photopolymerizable hydrogels are promising candidates. Hydrogels based on poly(ethylene glycol) dimethacrylate (PEGDMA) have been proposed due to their injectability, favorable mechanical properties and resistance to fatigue. However, their safety to be injected and photopolymerized *in situ* still needs to be demonstrated. This work thereby aims to evaluate the biocompatibility and thrombogenicity of the hydrogel precursor and assess the cytotoxicity of the polymerized hydrogels. To that end, *in vitro* cell viability and platelet aggregation assays were performed before moving to an *in vivo* systemic toxicity study in rats. The new visible photoinitiator PEG-BAPO was found biocompatible for concentrations below 0.1%. *In vitro* tests suggested that the precursors are biocompatible and do not induce platelet aggregation. The *in vivo* study in rats proved that PEGDMA hydrogel precursor up to 30 wt% concentration did not trigger any acute or delayed toxicity, thrombus formation or inflammation, even if 15 times the volume of the aneurysm was injected intravenously. Additionally, polymerized hydrogels did not affect the endothelial cells survival and did not support cell adhesion on their surfaces. Therefore, PEGDMA photopolymerizable hydrogels are expected to be biocompatible if injected for intracranial aneurysms treatment.

Keywords: biocompatibility, thrombogenicity, intracranial aneurysms (IAs), photopolymerizable hydrogels

5.2 Introduction

Endovascular therapy is nowadays the gold-standard in the treatment of intracranial aneurysms. Although solid coils remain the most common procedure, the use of adjunctive endovascular devices or liquid embolic agents are also emerging [45], [66]. On the one hand, adjunctive endovascular devices such as stents, flow diverters or disruptors have a lower recurrence rate than coils. Nevertheless, these devices require anti-platelet medication and are based on promoting fast intrasaccular aneurysm thrombosis, which may cause ischemic strokes due to the thrombus protrusion in the parent artery lumen or dislodgement of the intrasaccular thrombus [82]. On the other hand, liquid embolic agents can completely fill the aneurysm volume compared to the current coils, but also present significant limitations. First, off-target embolization due to spontaneous solidification in contact with blood is a serious complication since it may cause arterial occlusion and ischemic stroke. Second, the microcatheter can be entrapped within the solid embolic agent which makes difficult the retrieval of the microcatheter and even break the microcatheter tip [69]. Finally, precipitating agents contain dimethyl sulfoxide (DMSO) solvent which have shown to cause vasospasm and induce angionecrosis if injected too fast [70].

In order to address the shortcomings of the current treatments, novel types of liquid embolic agents are being developed [163]. Among them, *in situ* injectable hydrogels are of great interest. Their controllable solidification [171] could reduce the risk of off-target embolization. Moreover, their high water content and structural similarity to the extracellular matrix (ECM) of biological tissues [121] could lower their toxicity and thrombogenicity. Particularly, hydrogels based on poly(ethylene glycol) (PEG) are commonly used in tissue engineering applications [172] due to their hydrophilicity, non-toxicity, favorable mechanical properties and ease of chemical modification.

Herein, photopolymerizable hydrogels based on PEGDMA were developed with the aim of treating intracranial aneurysm. Previous works have demonstrated that the implementation and mechanical properties of PEGDMA hydrogels make them a promising candidate [169], [178]. Nonetheless, the safety of these biomaterials needs to be taken into consideration and be demonstrated in order to meet regulatory requirements. Indeed, the hydrogel precursor must be biocompatible and safe to be injected in its liquid state as a fraction of the precursor is bound to leak into the blood flow, even under balloon assistance. Moreover, the polymerized hydrogels must also be non-toxic, following ISO-10993 guidance (Figure 5.1).

This study is hence devoted to the evaluation of (1) the *in vitro* cell viability and platelet aggregation in contact with the PEG-BAPO photoinitiator and PEGDMA precursor, (2) the *in vivo* systemic toxicity of the precursors in rats to identify any acute or delayed toxicity, thrombus formation or inflammation and (3) the *in vitro* biocompatibility and cell adhesive properties of the polymerized hydrogels.

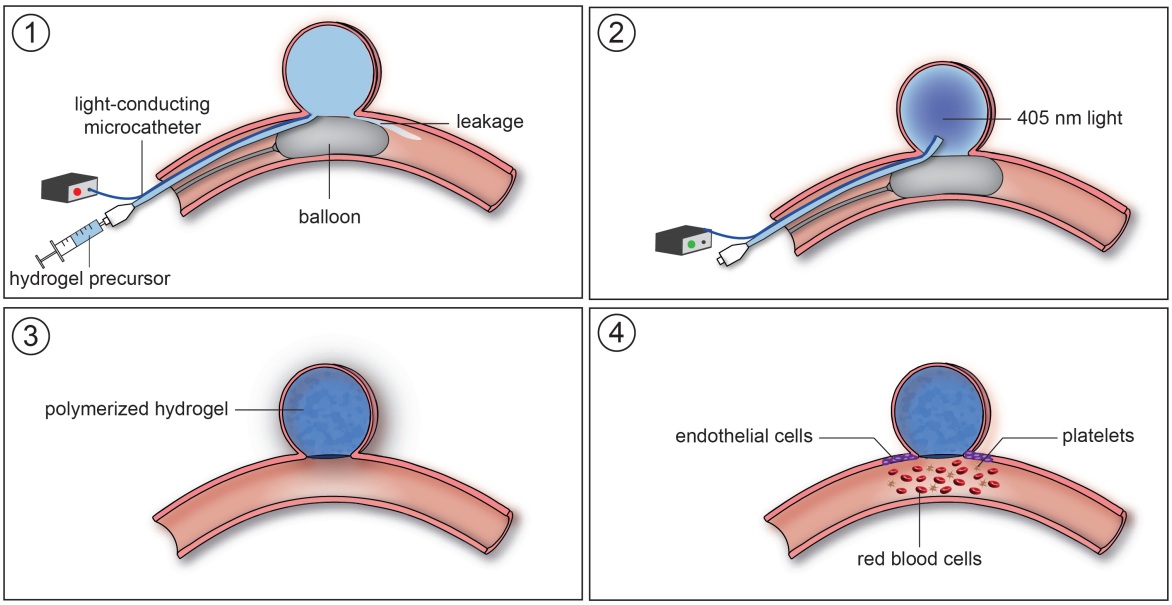

FIGURE 5.1: (1) Injection of the hydrogel precursor into the intracranial aneurysm, where leakage into the parent artery is bound to be expected even under balloon assistance. (2) 405 nm illumination to polymerize the hydrogel precursor. (3) Formation of the polymerized hydrogel and removal of the light-conducting microcatheter and balloon. (4) Biocompatibility of the precursor and hydrogel for the surrounding endothelial cells and absence of thrombus formation.

5.3 Materials and methods

5.3.1 Materials

PEGDMA was synthesized from poly(ethylene glycol) (PEG, M_n = 6000 g/mol) purchased from Sigma Aldrich (Merck, Switzerland) according to a modified procedure from Lin-Gibson, Bencherif, Cooper, *et al.* [175]. The iodine-based contrast medium Accupaque (350 mg/ml, GE Healthcare, Chicago, IL, United States) was provided by the Bern University Hospital and the intravenous fat emulsion Intralipid 20% was purchased from Sigma Aldrich (Merck, Switzerland). Poly(ethylene glycol) substituted bis(acyl)phosphane oxides (PEG-BAPO) photoinitiator was synthesized by phospha-Michael addition [131]. Human umbilical vein endothelial cells (HUVEC) were purchased from ATCC and EGM Endothelial Cell Growth Medium BulletKit (Lonza, Switzerland) was used for the cell culture and experiments.

5.3.2 Hydrogels preparation

The PEGDMA hydrogel precursor was composed of 10-30 wt% of PEGDMA with the molecular weight of 6 kDa and 0.1 wt% PEG-BAPO in equivalent weight concentrations of phosphate buffered saline (PBS) and Accupaque. The hydrogel precursors were homogenized by Vortex and degassed using a vacuum pump. Then, the precursors were sterilized through a 0.22 μm

syringe-filter (Rotilabo, Car Roth, GmbH). Finally, intralipids (5 wt%) were added to the precursors. The nomenclature used in the following was PEGDMA6k-a, where a represents the polymer concentration (10-30 wt%). All samples were illuminated for 10 min at a wavelength of 405 nm and an intensity of 15 mW/cm^2.

5.3.3 Evaluation of the biocompatibility and thrombogenicity of the hydrogels precursors

Cytotoxicity of PEG-BAPO photoinitiator

The cell proliferation in contact to PEG-BAPO photoinitiator at different concentrations (0.5, 0.1 and 0.05 w/v%) was determined using MTS assay (Cell Titer 96-Aqueous One Solution Cell Proliferation Assay, Promega). Bovine chondrocytes were cultured on a 96-well plate with 100 μl of culture medium in each well and incubated for 72h for cell attachment and confluence. The culture medium was aspirated and 100 μl photoinitiator solution was put in contact with cells during 1, 4 and 72 hours. 10 μl CellTiter was added and the plate was incubated for 90 minutes. The absorbance at 490 nm was then measured using a microplate reader (Wallac 1420 Victor2, PerkinElmer). Wells without PEG-BAPO solutions were considered as positive controls.

Cell viability assay

The cytotoxicity of the PEGDMA6k-10 precursor was investigated by cell viability assay. Human umbilical vein endothelial cells (HUVEC) were cultured on a 96-well plate with 10'000 cells/well and 100 μl of culture medium in each well. HUVEC were incubated for 48h and evaluated for cell attachment and confluence. The culture medium was aspirated and 100 μl of different conditions of precursor was put in contact with cells during one week. Constant concentrations of 0.1, 0.5, 1, 2.5, 5 and 10 vol% were tested. Three rounds of serial dilutions of the precursor were also performed. For each of the dilution rounds, pure precursor was placed in contact with HUVEC for 10 min, aiming to simulate the contact of HUVEC with the precursor during the injection and photopolymerization, 10 min being the maximum polymerization time required for aneurysm application. Then, the precursor was diluted at three different speeds, as shown in Figure 5.2, corresponding to the potential dilution of the precursor into the blood stream during leakage in the parent artery. To evaluate the cell viability after several time points (24h, 72h and 168h), the medium was aspirated and each well was filled with 100 μl of PBS with 10 vol% PrestoBlue assay (A13261, Life Technologies). The culture medium was replaced every 3 days. The fluorescence at 595 nm was measured by a microplate reader (Wallac 1420 Victor2, PerkinElmer) after 30 min of incubation. Wells without precursor were considered as positive controls.

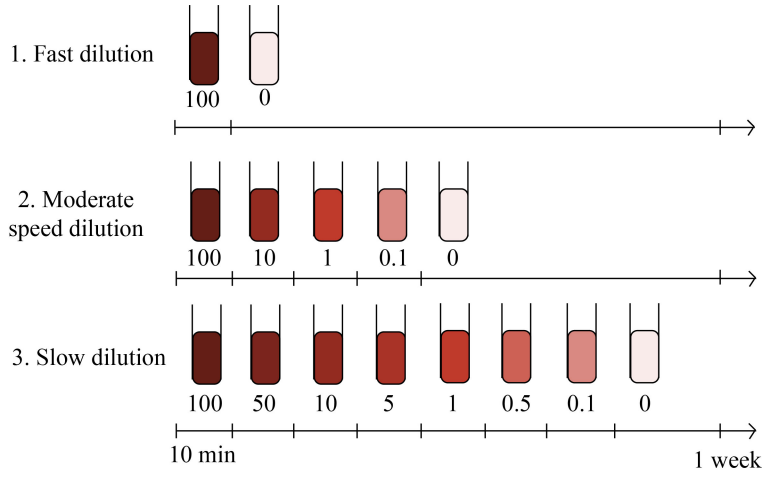

FIGURE 5.2: Progressive and instantaneous dilutions of the precursor to simulate the possible leakage of precursor into the blood flow.

Platelet aggregation assay

Platelet aggregation, for different concentrations of the PEGDMA6k-10 precursor ranging from 0.1 to 10 vol%, was determined as previously described [243]. Briefly, healthy human blood samples were centrifuged for 15 min, 200 g at room temperature (RT) and platelet-rich plasma (PRP) was collected. Blood samples were centrifuged again for 15 min, 500 g at RT and platelet poor plasma (PPP) was collected. 20 μl of different concentrations of precursor was put in a 384-well plate and 20 μl of PRP was added in each well. The plate was agitated for 15 min, 1200 RPM at RT. The absorbance at 595 nm was measured and platelet aggregation was determined by normalization with Tyrode buffer (0% aggregation) and PPP (100% aggregation). Collagen I (Mölab, ref 0203009) at 5 μg/ml was also used as positive control since collagen is a subendothelial thrombogenic protein responsible for platelet activation and aggregation.

In vivo evaluation of the hydrogel precursor toxicity

The *in vivo* study was approved by the Veterinary Office of the Canton of Zurich, Switzerland and followed the Swiss Animal Care Guidelines. The systemic toxicity of the hydrogel precursors was evaluated in healthy female Han Wistar rats for 21 days. Four animals per group (body weight BW 220-300 g) were included in the study and randomly assigned to the treatment groups. Two groups of hydrogel precursors were tested: PEGDMA with a molecular weight of 6 kDa at 10 and 30 wt% concentration (PEGDMA6k-10 and PEGDMA6k-30 groups). Administration of saline (0.9% NaCl) was used as control. After the acclimatization phase of 7 days at least, the hydrogel precursor was injected intravenously under anesthesia into the tail vein during 60 s at a dosage of 0.09 ml/100g BW. This dosage was fixed by assuming that 5 times the volume is required to properly fill the aneurysm and this volume was tripled to mimic an accidental overdose. Hence, the equivalent of 15 times the aneurysm volume was injected as safety factor.

Blood samples were taken directly before and after injection and at day 3, 7 and 21 after injection for hematology and biochemistry analysis in order to identify acute or delayed toxicity and thrombus formation. Hematology variables included hematocrit, hemoglobin, red blood cell count (RBC), mean corpuscular hemoglobin (MCH), mean corpuscular hemoglobin concentration (MCHC), mean corpuscular volume (MCV), leukocytes count, platelets count, mean platelet volume and plateletcrit. Biochemistry parameters included total bilirubin, urea, creatinine, albumin, alkaline phosphatase, aspartate aminotransferase (ASTA), alanine aminotransferase (ALTA) and gamma glutamyltransferase (GGT). After 3 weeks, the rats were sacrificed and subjected to gross necropsy. Heart, abdominal aorta, vena cava, liver, adrenals, kidneys, skin, spleen, muscle, brain, ovaries, lungs, bronchi and femur bone marrow were weighted and full organ histology was performed.

5.3.4 Evaluation of the biocompatiblity of the polymerized hydrogels

Cytotoxicity of polymerized hydrogels

To examine the possible toxicity of the solid, polymerized PEGDMA6k-10 hydrogels, HUVEC were cultured on a 48-well plate with 100 000 cells/well and 1 ml of culture medium in each well. The cells were incubated during 24 hours for cell attachment and confluence. Cell strainers (70 μm pluriStrainers, pluriSelect) were laid on the top of the wells and hydrogel samples were placed in the strainers. Since unreacted particles, mainly the radicals, can be released in the blood stream during hydrogel swelling process and have a negative impact on cell viability, we assessed their impact with a PrestoBlue assay immediately after polymerization (as-prepared hydrogels) and after 1 day of incubation in PBS (swollen hydrogels). The culture medium was replaced every 3 days.

Cell adhesion on hydrogel surfaces

The cell adhesive properties of the hydrogel surfaces were evaluated. PEGDMA6k-15 hydrogels were directly photopolymerized on a 96-well plate and incubated in PBS for 2h and then in culture medium for 12h to remove unreacted components prior to cell seeding. HUVEC were seeded on the surface of the hydrogels at a density of 20 000 cells/cm^2 and incubated prior to immunostaining assays. One day following the seeding, non-adherent cells were removed by washing several times with PBS and adherent cells were fixed using 4% paraformaldehyde solution for 10 min and permeabilized in 0.2% Triton X-100 for 10 min. The cytoskeleton of HUVEC was labeled with Alexa Fluor 488 phalloidin fluorescent dye (Life Technologies) and the nucleus with DAPI fluorescent dye. Fluorescent images were acquired using inverted fluorescence microscope (Nikon Eclipse Ts2R with 10x lens).

5.3.5 Statistical Analysis

Each experiment was performed in triplicate or more and the statistical data analysis was performed with MATLAB (Mathworks, Natick, MA, United States). All data are expressed as

mean ± standard deviation. One-way analysis of variance (ANOVA) was used for comparison. $p < 0.05$ was considered as a significant result (denoted as *) and $p > 0.05$ non-significant (denoted ns). $p < 0.01$ was denoted as **.

5.4 Results

5.4.1 Biocompatibility and thrombogenicity of the precursors

Cytotoxicity of PEG-BAPO photoinitiator

The cytotoxic effects of the PEG-BAPO photoinitiator solutions at different concentrations are shown in Figure 5.3. PEG-BAPO did not trigger a significant decrease of the cell viability for concentrations lower than 0.1% compared to the control without photoinitiator. However, when the cells were exposed to 0.5% PEG-BAPO, the cell survival significantly decreased to 11.59 $\pm$ 1.58 and 2.62 $\pm$ 1.35 after 1 and 72h of exposure, respectively. Low concentrations of PEG-BAPO ($\leq$ 0.1%) seem hence to be non-toxic for the cells. Accordingly, a concentration of 0.1% was used for all precursors and hydrogels in the following.

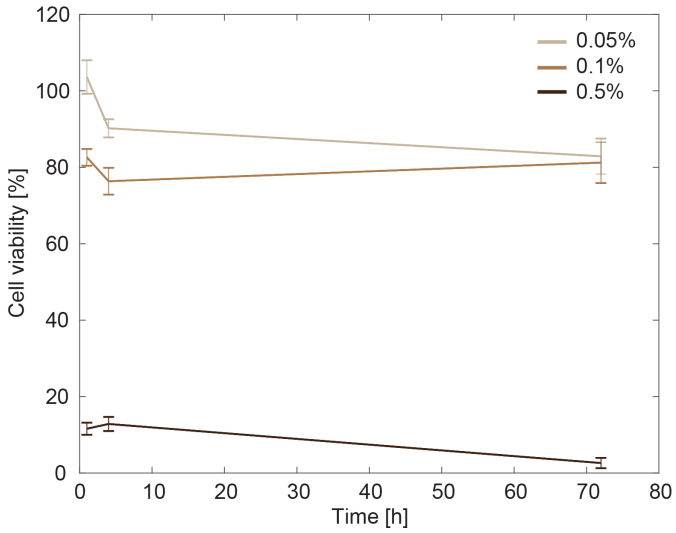

FIGURE 5.3: Cell viability after 1, 24 and 72h of contact with different concentrations of PEG-BAPO photoinitiator (n=3).

Cytotoxicity of the hydrogel precursor

As displayed in Figure 5.4, the PEGDMA6k-10 hydrogel precursor was diluted to different concentrations, ranging from 0.1 to 10%. The viability assay showed that a concentration of 10 vol% lead to 49.65 $\pm$ 3.77% cell death after 3 days of contact, which was non significantly different after 1 week of contact. For concentration lower than 5 vol%, the viability increased after 3 days and a decrease was noticed after 1 week. The cell viability was higher than 70% over one week in contact of precursors at concentrations lower than 5 vol%. Similarly, incubation of

HUVEC cells with pure PEGDMA6k-10 precursor during 10 min (representing the worst-case scenario with the most toxic concentration of leaked precursor in the parent artery during balloon inflation and *in situ* illumination) did not negatively impact viability, as shown for the serial dilutions at different speeds. This result suggests that longer contact time of low concentration precursor (<5 vol%) is highly unlikely to be toxic under realistic *in vivo* conditions.

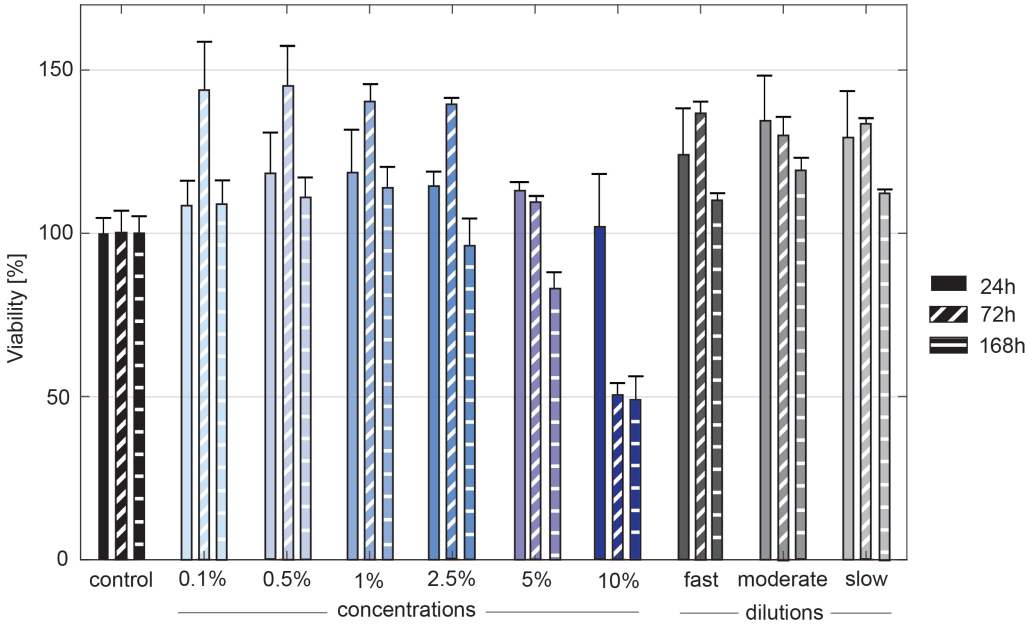

FIGURE 5.4: HUVEC viability after 1, 3 and 7 days of contact with different concentrations and dilutions of PEGDMA6k-10 hydrogel precursor (n=4).

Platelet aggregation of the hydrogel precursor

Platelet aggregation was measured for different concentrations of PEGDMA6k-10 precursor, ranging from 0.1 to 10 vol% and compared with Tyrode buffer as negative control and Collagen I and PPP, as positive controls, as shown in Figure 5.5. The assay indicated the aggregation of the precursor at different concentrations are not significantly different from the negative control, where the platelets did not aggregate. The negative values of aggregation might be explained by the sampling variations (n=3 donors, 3 samples/donor). Therefore, for concentration lower than 10 vol%, the PEGDMA6k-10 precursor seems not to induce any platelet aggregation.

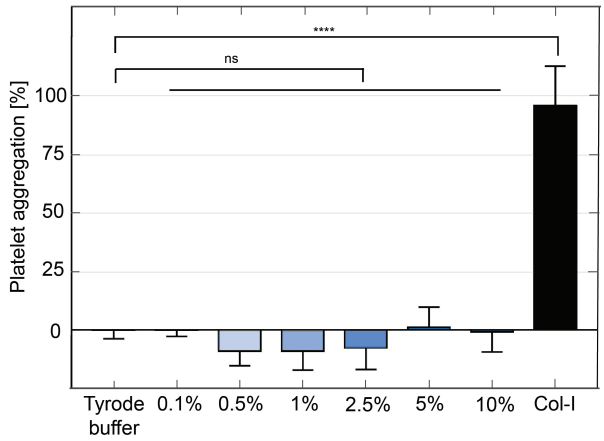

FIGURE 5.5: Platelet aggregation of different concentrations of PEGDMA6k-10 hydrogel precursor (n=3).

In vivo systemic toxicity of the precursors in rats

- General clinical examination and body weight

The systemic toxicity of the PEGDMA6k-10 and PEGDMA6k-30 precursors was evaluated in rats over a period of 21 days. No alterations in the animals well-being were noticed during the daily general clinical examination. Additionally, the body weight of the rats was monitored throughout the 21 days of the *in vivo* study. The gain in body weight of rats treated with PEGDMA6k-10 and PEGDMA6k-30 groups did not show significant difference compared with the control group, as shown in Figure 5.6.

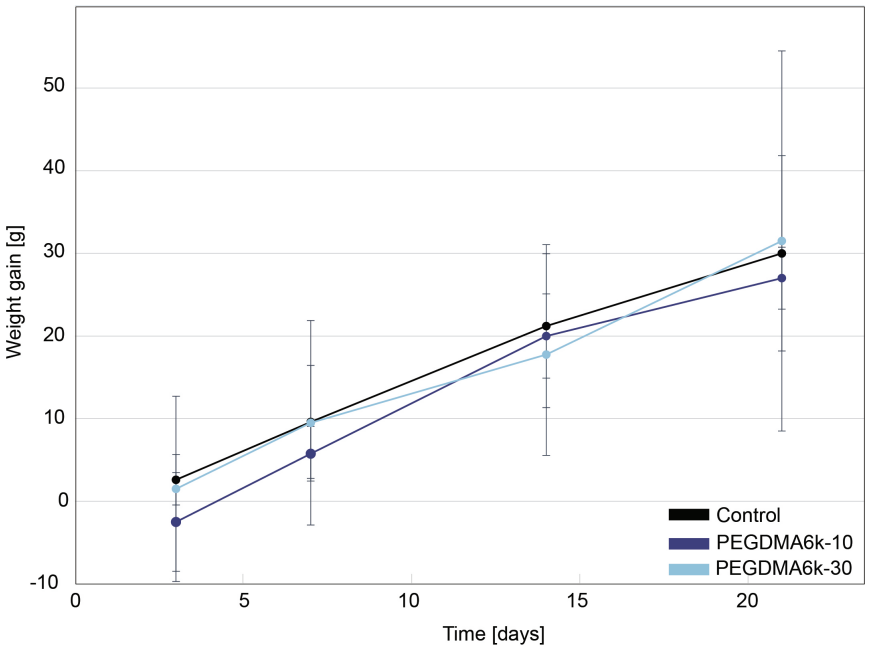

FIGURE 5.6: Gain in body weight of the rats during the experimental study, showing no variations between the treated and control groups (n=4).

The absolute values for all hematological and biochemical variables for control, PEGDMA6k-10 and PEGDMA6k-30 groups are summarized in Tables 5.1, 5.2 and 5.3 (Supplemental data), respectively.

- Hematological analysis

The results of the normalized hematological variables are presented in Figure 5.7. The results were normalized to the ones before injection (day 0 pre-injection). Hematological variables of treated groups were not significantly different than the control group, except isolated cases. For instance, a significant decrease in the platelets count and plateletcrit levels at day 3 was noticed for PEGDMA6k-30 group. Overall, no marked variations were noticed over the 21 days.

- Biochemical analysis

The results of the normalized biochemical blood variables are presented in Figure 5.8. Similar to hematological parameters, the biochemical blood analysis did not reveal any significant differences, except a decrease of urea at days 3 and 7 and a decrease of ALT at day 7 for PEGDMA6k-30 group. Directly after injection and after 21 days, all biochemical blood parameters of PEGDMA6k-10 and PEGDMA6k-30 precursor groups were not significantly different than the control group.

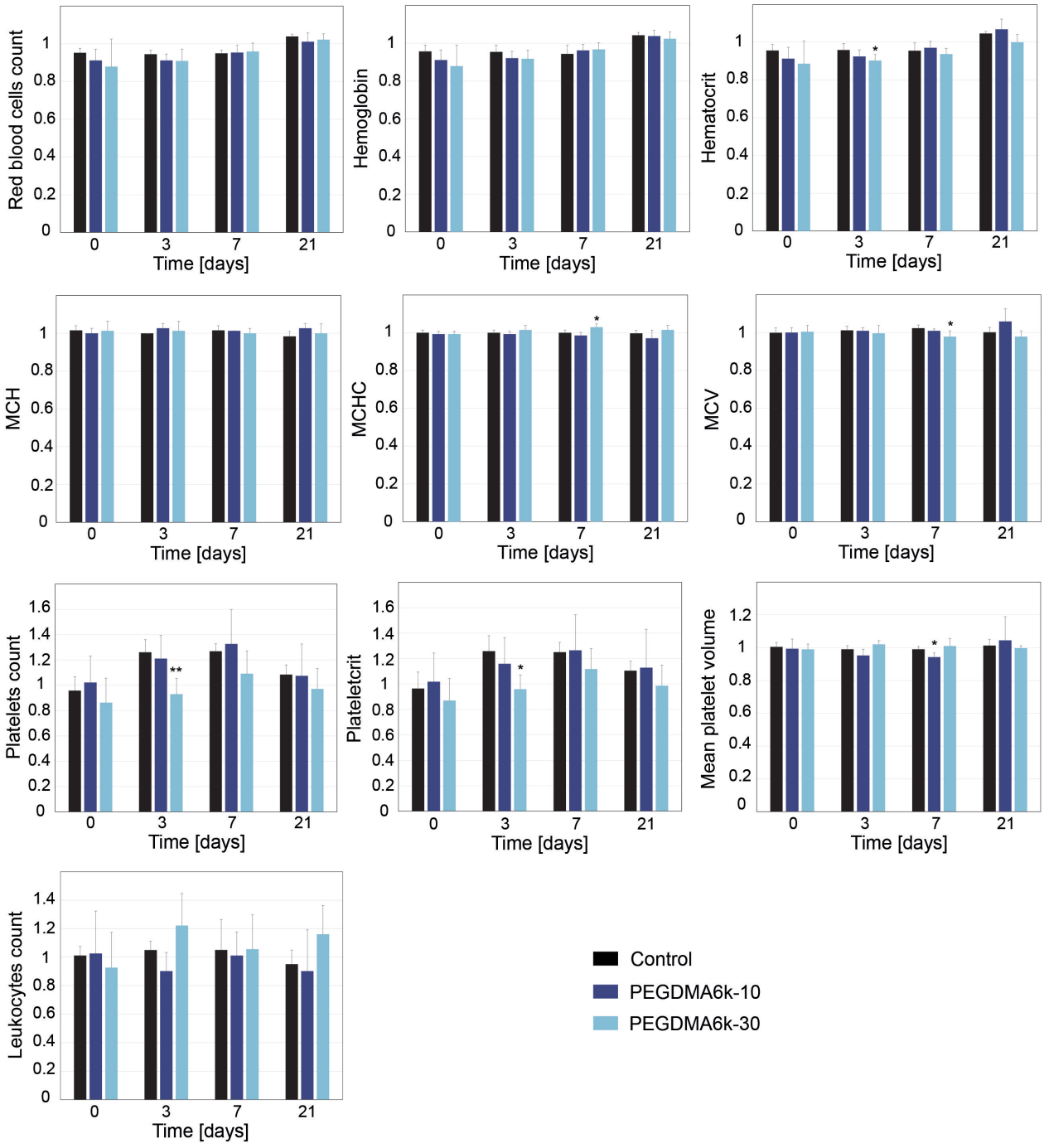

FIGURE 5.7: Normalized hematological variables to the ones before injection, showing no marked variations over the 21 days of the PEGDMA6k-10 and PEGDMA6k-30 groups compared to the control (* Statistically significant differences $p < 0.05$) (n=4).

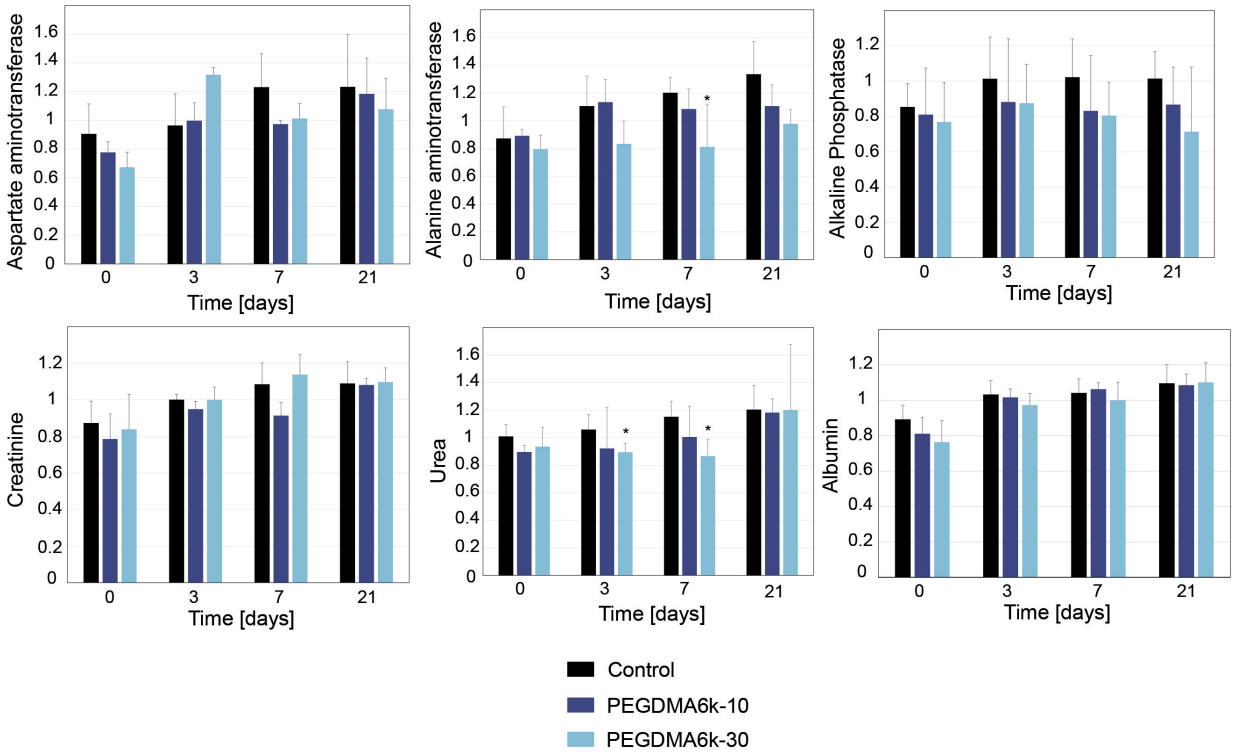

FIGURE 5.8: Normalized biochemical variables to the ones before injection, showing no significant variations over the 21 days of the PEGDMA6k-10 and PEGDMA6k-30 groups compared to the control (* Statistically significant differences $p < 0.05$) (n=4).

- Histopathological examination

After sacrifice, the animals organs presented normal morphology and no sign of necrosis. Furthermore, the organ weight to body weight ratio calculated after 21 days of injection was comparable between treated and untreated groups for heart, liver, spleen, brain, lungs, kidneys and adrenals (Figure 5.9). The histopathological examination was carried out for the major organs and revealed no changes in their cellular structure. No signs of thrombosis, inflammation reaction, tissue damage or necrosis was found for all organs of treated and control groups.

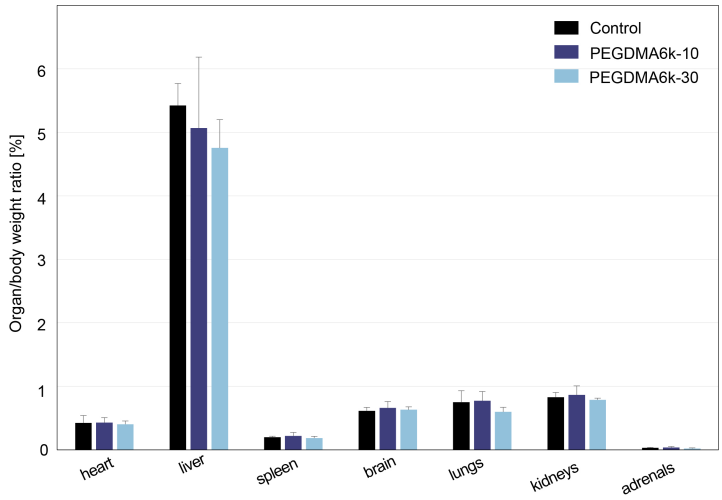

FIGURE 5.9: Organ weight to body weight ratio at 21 days after injection (n=4).

5.4.2 Biocompatibility of polymerized hydrogels

Beyond a week of contact with HUVEC, polymerized as-prepared and swollen PEGDMA6k-10 hydrogels exhibited a viability of 89.78 $\pm$ 14.65 and 97.65 $\pm$ 8.33%, respectively, as shown in Figure 5.10.A. The cytotoxicity of the as-prepared and swollen hydrogels was not significantly different. Potential unreacted particles into the polymerized hydrogels, such as radicals, did not show significant negative effects on the metabolic activity of the cells.
The cell adhesion on the polymerized hydrogel surface was also studied. The assay indicated that only a few cells were attached to the hydrogel surface after 1 day of incubation, as shown in Figure 5.10.B.

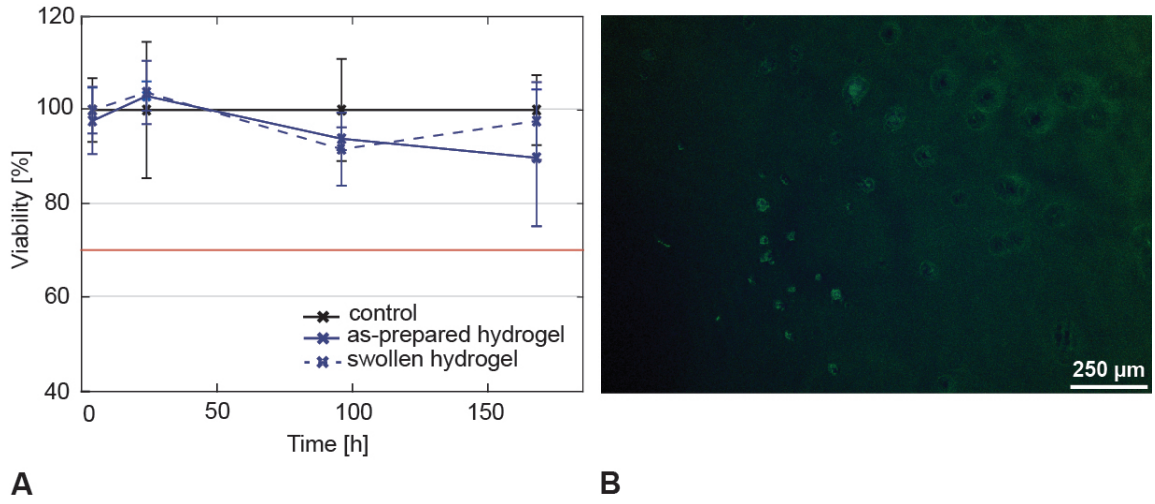

FIGURE 5.10: (A) HUVEC viability measured by PrestoBlue assay after 1 week of direct contact with as-prepared and swollen PEGDMA6k-10 hydrogels (n=3). (B) Microscopic image of immunostaining assay for PEGDMA6k-10 hydrogels after 1 day of HUVEC adhesion.

5.5 Discussion

The present study aimed to evaluate the toxicity of the precursors and hydrogels, mainly composed of PEGDMA polymer and a novel visible photoinitiator PEG-BAPO, designed for the treatment of intracranial aneurysms. Our work validates the safety of the injection in the neuro- and cardiovascular system of the PEGDMA precursor at a concentration up to 30% and suggested that PEGDMA hydrogel is biocompatible for the surrounding endothelial cells.

Since leakage of the hydrogel precursor into the parent artery is virtually inevitable and should be expected during the injection within the aneurysm, biocompatibility and non-thrombogenicity of the PEGDMA hydrogel precursor are essential. Compared to precipitating embolic agents containing potentially toxic DMSO [244], the photoactive PEGDMA hydrogel precursor we have developed consists of solvents already in clinical use, PBS and Accupaque. The biocompatibility of PEGDMA pre-polymer and PEG-BAPO photoinitiator components present in the formulation was, however, important to investigate. Our results showed that the cell survival was not negatively affected in contact to PEG-BAPO photoinitiator at a concentration below 0.1%. Specific tests were designed to simulate the dilution of the precursor into the blood stream. No toxicity for endothelial cells and no platelet aggregation were found. Additionally, contrary to chemical, temperature- or pH-sensitive hydrogel precursors that have a high risk of spontaneously polymerizing in the parent artery in case of leakage, our light-sensitive precursor is selectively polymerized on demand with visible light avoiding the risk of spontaneous polymerization. However, a limitation of our *in vitro* study is that the PEG-BAPO and precursor were not exposed to visible light illumination. Studies have demonstrated that the cell survival was not reduced after 10 min of 365 or 480 nm light exposure [245], [246]. Moreover, the use of 405 nm visible light was selected in this work to prevent the risks of phototoxicity induced by UV light [229], [230].

To supplement our *in vitro* results indicating that the precursor should be harmless if injected into the blood stream and determine potentially harmful effects, the systemic toxicity of the PEGDMA6k-10 and PEGDMA6k-30 precursors were further tested *in vivo* in rats by intravenous injection. The rodents were the preferred animal model for this study as it was recommended in ISO 10993-11. A safety factor was applied to the volume of injected precursor, corresponding to 15 times the aneurysm volume.
First, the evaluation of hematological variables enables the identification of adverse effects of foreign substances on the blood constituents, in particular red blood cells, platelets and leukocytes. Out of all the hematological variables assessed in this study, the PEGDMA6k-10 precursor did not show any significant variations throughout the 21 days after injection while only isolated changes were noticed for PEGDMA6k-30 precursor. The decrease of both platelet count and plateletcrit 3 days after the injection suggested that platelets have been excessively consumed [247]. After 7 days, the simultaneous augmentation of MCHC and reduction of MCV revealed contradictory effects. These variations were minor as MCHC and MCV showed normal values for the other time points. The hematological effects are hence unclear for PEGDMA6k-30 precursor, but seemed not substantially negative.

Second, the biochemical parameters are also useful to assess the liver functionality, since the liver plays a key role in the drug metabolism, involving the biotransformation and excretion of toxic exogenous substances. Alkaline phosphatase, GGT, ASTA and ALTA were used to test liver injury [248] and did not reveal any adverse alterations. No changes in the level of total bilirubin and albumin, two biomarkers of the liver function [248], also indicated that the liver is not affected by the precursors injection. Moreover, creatinine and urea, investigated in this study, are the standard biomarkers of kidney injury diagnosis [249]. The significant low level of urea for PEGDMA6k-30 group 3 and 7 days after injection might involve a higher kidney function. The functions of vital organs, such as the liver and the kidney, thereby seem not considerably affected by the overdose injections of PEGDMA6k at a concentration of 10 and 30%. Third, the organ weight to body weight ratio is also a proper indicator of the toxicity of a substance [250] and is mainly associated to atrophy or hypertrophy of an organ. Out of all the organs investigated in the study, the weight analysis did not show abnormalities, which corroborates with the preceding hematological and biochemical analysis. The histopathological analysis is consistent and supplements the toxicity study, revealing neither thrombosis nor inflammatory reactions.
Finally, the *in vivo* toxicity results imply that 6 kDa PEGDMA precursor up to 30% concentration do not trigger any acute or delayed toxic, thrombogenic and inflammatory effect and therefore is safe to be injected in the neuro- and cardiovascular systems.

With regard to the polymerized hydrogels, *in vitro* cell viability assay suggested that the hydrogels in the solid state are biocompatible as the hydrogels did not trigger any cytotoxicity for the endothelial cells, according to the ISO 10993-4 guidance. Moreover, the cell adhesion assay confirms that PEGDMA hydrogels are bioinert and do not induce any cell attachment [251]. This bioinert nature is due to the hydrophilicity of the PEGDMA polymer enabling protein adsorption repelling [252], [253]. On the one hand, this property could avoid platelet aggregation and thrombus formation at the hydrogel surface. On the other hand, the absence of cell adhesion could limit the endothelialization at the aneurysm neck. Finally, cytotoxicity and thrombogenicity of the hydrogels have to be further studied and confirmed *in vivo*, which we will test in an elastase aneurysm model in rabbits [254].

5.6 Conclusion

In the present study, the injection of PEGDMA photopolymerizable hydrogel precursors into the neuro- and cardiovascular systems, in overdose conditions, was demonstrated to be safe *in vivo*. PEGDMA precursors did not induce any acute or delayed toxicity, thrombus formation or inflammatory response. The polymerized PEGDMA hydrogels were also found to be biocompatible for endothelial cells and did not promote cell adhesion *in vitro*. Future work will involve an *in vivo* study in elastase-induced aneurysms in rabbits to evaluate the implantation, safety and long-term performance of the PEGDMA hydrogels.

5.7 Acknowledgements

We would like to thank Katja Nuss and the VetSuisse Faculty team for performing the *in vivo* study, Sandra Jaccoud for her assistance with cell experiments, Augusto Martins Lima and François Cuenot for performing the platelet aggregation assay.

5.8 Supplementary data

Control group	0 pre	0 post	3	7	21
Hematocrit [%]	42.65 ± 0.94	40.80 ± 1.33	40.90 ± 1.43	40.75 ± 1.71	44.65 ± 0.47
Hemoglobin [g/dl]	14.37 ± 0.49	13.75 ± 0.46	13.71 ± 0.5	13.56 ± 0.62	14.98 ± 0.22
RBC [x$10^6/\mu$l]	7.65 ± 0.15	7.28 ± 0.17	7.23 ± 0.15	7.27 ± 0.12	7.95 ± 0.09
MCH [pg]	19	19.3 ± 0.48	19	19.3 ± 0.48	18.7 ± 0.48
MCHC [g/dl]	33.65 ± 0.47	33.65 ± 0.47	33.65 ± 0.47	33.65 ± 0.47	33.55 ± 0.53
MCV [fl]	56 ± 1.41	55.95 ± 1.42	56.65 ± 1.25	57.3 ± 0.95	56.1 ± 1.43
Leukocytes count [x$10^3/\mu$l]	13.17 ± 0.82	13.32 ± 0.85	13.82 ± 0.86	13.84 ± 2.94	12.52 ± 1.24
Platelet count [x$10^3/\mu$l]	775.33 ± 95	742.65 ± 82	977.9 ± 97	983.95 ± 59	841.25 ± 64
Mean platelet volume [fl]	7.6 ± 0.16	7.64 ± 0.21	7.53 ± 0.17	7.53 ± 0.13	7.7 ± 0.29
Plateletcrit [%]	0.59 ± 0.08	0.57 ± 0.07	0.74 ± 0.09	0.74 ± 0.06	0.65 ± 0.05
Albumin [g/l]	47.00 ± 3.56	41.95 ± 3.35	48.55 ± 3.85	48.95 ± 3.93	51.55 ± 5.43
Alkaline Phosphate [U/l]	109.65 ± 12	93.6 ± 12	111.05 ± 26	112 ± 24	111.1 ± 17
Creatinine [μmol/l]	36.33 ± 3	31.7 ± 4	36.35 ± 1	39.4 ± 5	39.55 ± 5
Urea [mmol/l]	5.55 ± 0.25	5.6 ± 0.49	5.88 ± 0.65	6.39 ± 0.73	6.68 ± 1.18
ASTA [U/l]	80.33 ± 16	72.75 ± 15	77.4 ± 17	98.85 ± 23	99.05 ± 36
ALTA [U/l]	37.65 ± 7	32.85 ± 7	41.63 ± 9	45.25 ± 5	50.3 ± 12
GGT [U/l]	<3	<3	<3	<3	<3
Total bilurin [μmol/l]	<2.5	<2.5	<2.5	<2.5	<2.5
Body weight [g]	-	285.50 ± 24	286.75 ± 24	292.25 ± 24	312.50 ± 27

TABLE 5.1: Absolute values of the control group for all variables at day 0 pre and post-injection, 3, 7 and 21 after injection.

PEGDMA6k-10 group	0 pre	0 post	3	7	21
Hematocrit [%]	43.25 ± 0.96	39.5 ± 2.38	40 ± 1.41	42 ± 1.41	46.25 ± 2.5
Hemoglobin [g/dl]	14.55 ± 0.61	13.25 ± 0.7	13.4 ± 0.48	14 ± 0.45	15.1 ± 0.47
RBC [x$10^6/\mu$l]	7.74 ± 0.34	7.05 ± 0.43	7.05 ± 0.24	7.38 ± 0.28	7.82 ± 0.37
MCH [pg]	18.75 ± 0.5	18.75 ± 0.5	19.25 ± 0.5	19	19.25 ± 0.5
MCHC [g/dl]	34 ± 1.15	33.75 ± 0.5	33.75 ± 0.5	33.5 ± 0.58	33 ± 1.41
MCV [fl]	56 ± 1.41	56 ± 1.41	56.5 ± 1	56.5 ± 0.58	59.25 ± 4.03
Leukocytes count [x$10^3/\mu$l]	13.48 ± 2.66	13.83 ± 4.1	12.15 ± 1.59	13.63 ± 2.26	12.15 ± 3.53
Platelet count [x$10^3/\mu$l]	727 ± 149	743.25 ± 155	880.25 ± 161	964.5 ± 262	781 ± 197
Mean platelet volume [fl]	7.83 ± 0.51	7.78 ± 0.46	7.45 ± 0.29	7.38 ± 0.19	8.18 ± 1.18
Plateletcrit [%]	0.57 ± 0.1	0.58 ± 0.13	0.66 ± 0.13	0.72 ± 0.2	0.64 ± 0.19
Albumin [g/l]	43.75 ± 1.89	35.50 ± 3.32	44.50 ± 2.08	46.50 ± 1.73	47.50 ± 3
Alkaline Phosphate [U/l]	119.75 ± 36	97 ± 26	105.5 ± 38	99.5 ± 31	103.75 ± 22
Creatinine [μmol/l]	37.25 ± 5	29.25 ± 4	35.33 ± 2	34 ± 2	40.25 ± 2
Urea [mmol/l]	6.48 ± 0.53	5.8 ± 0.28	5.97 ± 1.77	6.50 ± 1.46	7.65 ± 0.77
ASTA [U/l]	76 ± 7	59 ± 4	75.75 ± 10	74 ± 2	90 ± 23
ALTA [U/l]	35.5 ± 11	31.67 ± 2	40.25 ± 7	38.5 ± 6	39.25 ± 6
GGT [U/l]	<3	<3	<3	<3	<3
Total bilurin [μmol/l]	<2.5	<2.5	<2.5	<2.5	<2.5
Body weight [g]	-	283.25 ± 18	280.75 ± 16	289 ± 15	310.25 ± 20

TABLE 5.2: Absolute values of the PEGDMA6k-10 group for all variables at day 0 pre and post-injection, 3, 7 and 21 after injection.

PEGDMA6k-30 group	0 pre	0 post	3	7	21
Hematocrit [%]	44 ± 2.16	39 ± 4.69	39.75 ± 1.26	41.25 ± 1.26	44 ± 1.83
Hemoglobin [g/dl]	14.63 ± 0.85	12.85 ± 1.44	13.43 ± 0.61	14.15 ± 0.5	14.98 ± 0.54
RBC [x$10^6/\mu$l]	7.6 ± 0.59	6.68 ± 0.98	6.9 ± 0.43	7.28 ± 0.33	7.76 ± 0.24
MCH [pg]	19.25 ± 1.26	19.5 ± 1	19.5 ± 1	19.25 ± 0.5	19.25 ± 0.96
MCHC [g/dl]	33.5 ± 0.58	33.25 ± 0.5	34 ± 0.82	34.5 ± 0.58	34 ± 0.82
MCV [fl]	58 ± 1.41	58.25 ± 1.89	57.75 ± 2.36	56.75 ± 1.71	56.75 ± 1.71
Leukocytes count [x$10^3/\mu$l]	8.1 ± 1.44	7.5 ± 1.87	9.9 ± 2.22	8.55 ± 2.06	9.4 ± 1.9
Platelet count [x$10^3/\mu$l]	993.5 ± 159	857.5 ± 166	923.5 ± 116	1084.75 ± 195	965.25 ± 155
Mean platelet volume [fl]	7.43 ± 0.15	7.35 ± 0.24	7.58 ± 0.17	7.5 ± 0.35	7.4 ± 0.12
Plateletcrit [%]	0.73 ± 0.11	0.63 ± 0.11	0.7 ± 0.08	0.81 ± 0.13	0.72 ± 0.12
Albumin [g/l]	46.50 ± 2.08	35.50 ± 4.36	45.25 ± 2.99	46.50 ± 4.80	51.25 ± 5.68
Alkaline Phosphate [U/l]	159.5 ± 39	122.5 ± 27	139.5 ± 31	128.25 ± 24	113.75 ± 42
Creatinine [μmol/l]	31 ± 1	26 ± 5	31 ± 2	35.25 ± 4	34 ± 3
Urea [mmol/l]	6.13 ± 0.64	5.73 ± 0.81	5.48 ± 0.34	5.3 ± 0.65	7.35 ± 3.49
ASTA [U/l]	90.25 ± 18	60.75 ± 6	80 ± 4	81 ± 9	87.25 ± 19
ALTA [U/l]	46.5 ± 3	37 ± 4	38.75 ± 6	37.75 ± 11	45.5 ± 5
GGT [U/l]	<3	<3	<3	<3	<3
Total bilurin [μmol/l]	<2.5	<2.5	<2.5	<2.5	<2.5
Body weight [g]	-	282.75 ± 20	284.25 ± 24	292.25 ± 21	314.25 ± 22

TABLE 5.3: Absolute values of the PEGDMA6k-30 group for all variables at day 0 pre and post-injection, 3, 7 and 21 after injection.

Chapter 6

Improving cell adhesive properties of photopolymerizable PEGDMA hydrogels by biofunctionalization with GelMA

6.1 Abstract

The regeneration of an endothelium layer at the aneurysm neck after implantation, called *in situ* endothelialization, seems to be essential for aneurysms healing. Endothelial cells migration, adhesion and proliferation as well as endothelial progenitor cells homing and differentiation are mechanisms promoting the endothelium growth. In this work, we propose the biofunctionalization of poly(ethylene glycol) dimethacrylate (PEGDMA) hydrogels by gelatin methacrylate (GelMA) as a strategy to enhance their bioactivity. The influence of GelMA concentration was evaluated in terms of cell adhesion and migration, compressive modulus, swelling characteristics, resistance to fatigue under pulsatile flow, viscosity and photopolymerization time. It was found that the endothelial cells migrated, adhered, spread and formed a cellular network after one week of culture on the hybrid hydrogels composed of 5% GelMA and 10% PEGDMA. In comparison, neat PEGDMA hydrogels did not promote any cell adhesion. The incorporation of GelMA into PEGDMA network significantly improved the cell adhesive properties of the hydrogels. The mechanical properties of the hybrid hydrogels were unchanged and matched the elastic modulus and compliance of aneurysmal tissue. In addition, the hydrogels withstood 5.5 million cycles without significant loss of weight or elastic modulus. The swelling characteristics were significantly reduced, reaching almost no swelling. Moreover, the hybrid hydrogel precursor demonstrated to be injectable through 430 μm microcatheters and polymerizable within 8 min of visible illumination. Further research is however necessary to confirm the *in situ* endothelialization potential of the PEGDMA-GelMA hydrogels.

Keywords: endothelialization, bioactivity, cell adhesion and migration, gelatin methacrylate, hybrid hydrogels, intracranial aneurysms

6.2 Introduction

The healing of intracranial aneurysms seems to be facilitated by the regeneration of a confluent, mature and healthy layer of endothelium in order to completely exclude the aneurysm from the parent artery [83], [255]. The endothelium plays a central role in maintaining hemostasis and regulating inflammation and thrombosis [256], [257]. The endothelialization serves as a physical barrier to prevent direct contact between the blood and the embolic agent, thereby prevent thrombosis and restore endothelium function. Endothelialization of the embolic agent can be achieved *in vitro* or *in situ*. *In vitro* endothelialization consists of endothelial cells (ECs) or endothelial progenitors cells (EPCs) seeding and surface modifications prior implantation. *In situ* endothelialization occurs by ECs migration, adhesion and proliferation and by circulating EPCs homing and differentiation into mature ECs after implantation *in vivo* [258]–[260], as displayed in Figure 6.1. *In situ* endothelialization is preferred over *in vitro* due to tedious and costly cell seeding, impracticality in case of emergency and high risks of contamination of the latter [83].

Several strategies have been developed on platinum coils to accelerate the *in situ* healing response of the aneurysm by coating bioabsorbable polyglycolic/polylactic acid (PGLA) copolymers or incorporating polyglycolic acid (PGA) polymer. These bioactive coils have demonstrated a fibrous tissue deposition at the aneurysm neck *in vivo* [62], [63], but the recurrence, recanalization and retreatment outcomes were not improved compared to platinum coils [64], [65]. Flow diverters also aim to induce endothelial cell growth along the device [216], however this technique is associated with long-term antiplatelet therapy.

Hydrogels have been tremendously used in the field of tissue engineering and regenerative medicine [261]. Notably, naturally-derived hydrogels possess inherent bioactive properties, promoting cell attachment and tissue regeneration [262]. In previous papers, we have proposed an *in situ* photopolymerizable hydrogel based on poly(ethylene glycol) dimethacrylate (PEGDMA) to treat intracranial aneurysms. Nonetheless, the synthetic origin of PEGDMA polymer imparts its bioinert nature and limits the cell attachment. As a result, various ECM-mimetic bioactive modifications, such as ECM-derived peptides and proteins, glycosaminoglycans (GAGs) and growth factors have arisen to overcome the lack of bioactivity of PEG [135]. Among the biofunctionalizations, gelatin is frequently used as ECM-derived protein as it is obtained by hydrolysis of collagen, the most abundant ECM protein. Gelatin as well as methacrylated gelatin (GelMA) contain numerous arginine-glycine-aspartic acid (RGD) adhesive peptide sequences and matrix metalloproteinase (MMP) sequences, favoring cell attachment and remodeling, respectively [263], [264]. The incorporation of GelMA into PEGDMA hydrogels has shown cell adhesive properties enhancement [142], [143].

Here, we explore the *in situ* endothelialization potential of PEGDMA hydrogels by incorporation of GelMA. The cell adhesive properties of the hydrid hydrogels in static and dynamic conditions were assessed according to GelMA concentration into the PEGDMA network, as well as the cell migration. In addition, the physical and mechanical properties of the hybrid hydrogels were evaluated by swelling, compression, fatigue testing while the injectability and

photopolymerization kinetics were determined by photorheology.

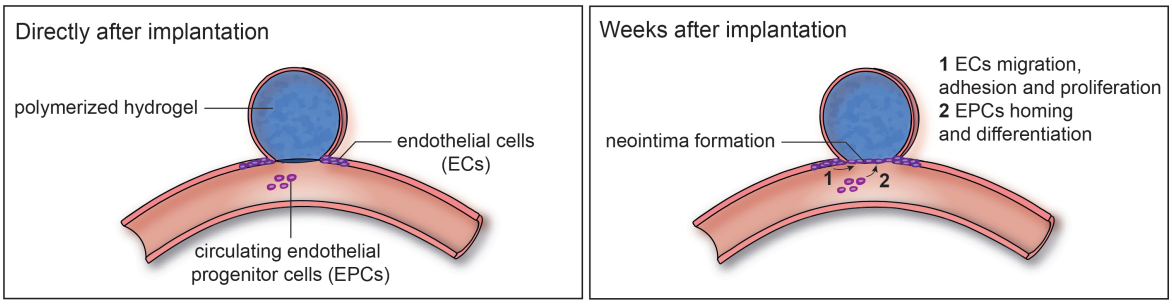

FIGURE 6.1: After several weeks of implantation, the polymerized hydrogels should promote neointima formation at the aneurysm neck to completely exclude the aneurysm from the parent artery. *In situ* endothelialization occurs by ECs migration, adhesion and proliferation and by circulating EPCs homing and differentiation into mature ECs.

6.3 Materials and Methods

6.3.1 Materials

Poly(ethylene glycol) (PEG, M_n = 6000 g/mol), gelatin from porcine skin (Type A, bloom 300) and methacrylic anhydride were purchased from Sigma Aldrich (Merck, Switzerland). The iodine-based contrast medium Accupaque (350 mg/ml, GE Healthcare, Chicago, IL, United States) was provided by the Bern University Hospital. Poly(ethylene glycol) substituted bis(acyl) phosphane oxides (PEG-BAPO) photoinitiator was synthesized by phospha-Michael addition [131]. Lithium phenyl(2,4,6-trimethylbenzoyl) phosphinate (LAP) photoinitiator was purchased from Sigma-Aldrich (Merck, Switzerland). Human umbilical vein endothelial cells (HUVEC) were purchased from ATCC and EGM Endothelial Cell Growth Medium BulletKit (Lonza, Switzerland) was used for the cell culture and experiments.

6.3.2 PEG and gelatin methacrylation

PEGDMA was synthesized from PEG according to a modified procedure [175].
The methacrylation of gelatin was performed according to an established protocol [265]. Briefly, gelatin was dissolved at 10 w/v% in PBS at 60°C. After complete dissolution, 4 g of methacrylic anhydride was added dropwise to the solution and stirred for 3h at 55°C. The solution was diluted several times with PBS to terminate the reaction. The solution was dialyzed in deionized water (diH_2O) for 24h to remove methacrylic acid byproducts and then lyophilized and stored at 4°C before use. The degree of functionalization of GelMA was found by ^{1}H-NMR integrals to be around 75%.

6.3.3 Hydrogels preparation

The precursors were prepared with a constant total polymer concentration of 15 wt%. PEGDMA and GelMA were mixed at 15:0, 14:1, 12.5:2.5, 10:5 and 0:15 ratios in equivalent weight concentrations of PBS and Accupaque at 37°C (to avoid spontaneous solidification of GelMA). 5 wt% Intralipids were added as well as 0.5 v/v% acetic acid to reduce the phase separation between PEGDMA and GelMa [142]. PEG-BAPO (0.1 wt%) or LAP (0.02 wt%) were used as photoinitiators. These weight concentrations are equivalent to 0.7 μmol/g for both photoinitiators. The nomenclature used for the hybrid hydrogels was: PEGDMAx-GelMAy where x is the PEGDMA concentration and y the GelMA concentration.

6.3.4 Cell adhesion on hydrogel surfaces

Hydrogels were directly photopolymerized on a 96-well plate and incubated in PBS for 2h and then in culture medium for 12h to remove unreacted components prior to cell seeding. HUVEC were seeded on the surface of the hydrogels at a density of 20'000 cells/cm^2 and incubated prior immunostaining assays. One and 7 days following the seeding, non-adherent cells were removed by washing several times with PBS and adherent cells were fixed using 4% paraformaldehyde solution for 10 min and permeabilized in 0.2% Triton X-100 for 10 min. The cytoskeleton of HUVEC was labeled with Alexa Fluor 488 phalloidin fluorescent dye (Life Technologies) and the nucleus with DAPI fluorescent dye. Fluorescent images were acquired using inverted fluorescence microscope (Nikon Eclipse Ts2R with 10x lens). Cells were counted at different positions of the surface and an interpolation was performed to calculate the number of cells per cm^2 of surface.

To assess the cell adhesion under flow, channel models were designed in SolidWorks (Dassault Systèmes, France) specifically to match the sticky-Slide I Luer and represented in Figure 6.2. Briefly, the models consisted of a channel of 5 mm wide to simulate a vessel and a cavity of 4 mm diameter to place the hydrogel. The channel models were fabricated in poly(methyl methacrylate) (PMMA) due to its biocompatibility, ease of sterilization and transparency. The channel model was stuck to the sticky-Slide I Luer (Ibidi) and connected to a peristaltic pump (Ismatec ISM597D, IDEX Corporation, Lake Forest, IL, United States) at a flow rate of 24 ml/min. The same immunostaining assay was repeated after passage of flow for 24h.

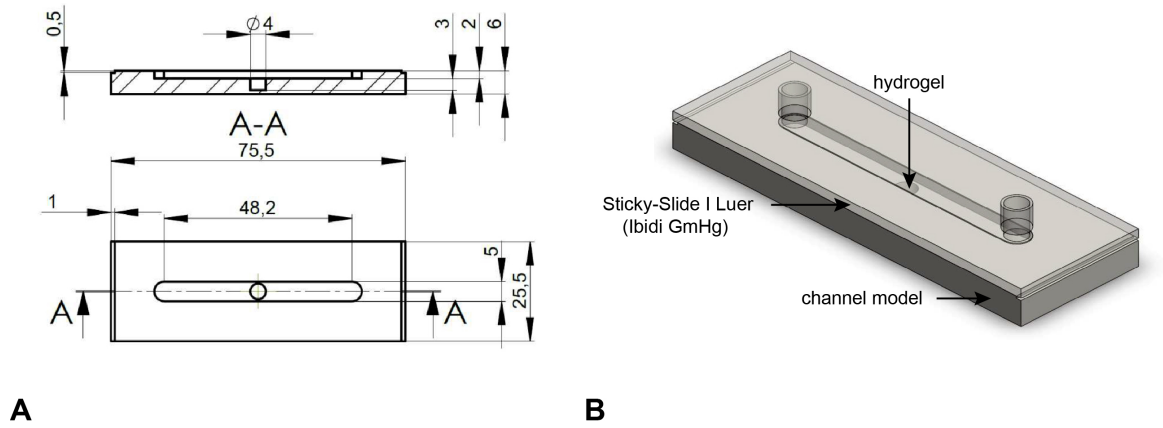

FIGURE 6.2: (A) Drawing of the channel models. (B) Illustration of the assembly of the designed channel model and the sticky-Slide I Luer (Ibidi GmHg).

6.3.5 Cell migration

Cell migration assay was performed on 6 cm petri dishes. A 5 mm diameter cylindrical hydrogel was placed at the center of the petri dish and fixed with a metallic clamp. 20 μl of HUVEC were placed at four points of the petri dish, approximately 1.5 cm away from the hydrogel, as shown in Figure 6.3. After 1h for the cells to attach, 5 ml of culture medium was added in the petri dish. HUVEC at the interface with PEGDMA10-GelMA5 hydrogels were observed after 1, 2, 5 and 8 days using inverted microscope (Nikon Eclipse Ts2R with 4x lens). Giemsa surface staining was performed after 8 days of culture to better observe the hydrogel interface.

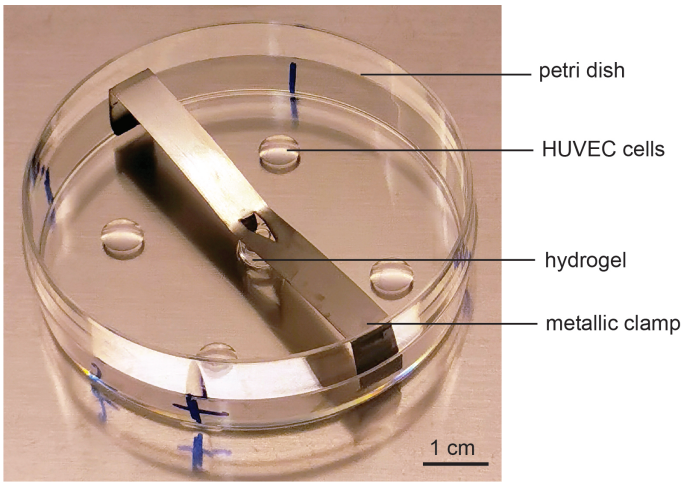

FIGURE 6.3: Cell migration setup.

6.3.6 Hydrogel physical and mechanical characterization

Swelling ratios

Hydrogel precursor samples were photopolymerized either in cylindrical molds before being extracted or within intracranial aneurysm models and kept inside them. The samples were immersed in PBS at 37°C and 5% CO_2, resulting in either a free swelling or constrained swelling with the exposure to the PBS solvent only at the aneurysm neck. The swelling study was performed during one month and the weight and volume swelling ratios, SR_w and SR_{vol}, at the time point t were determined using the following formulas:

$$SRw\ [\%] = 100(w_t\text{-}w_0)/w_0$$
$$SRvol\ [\%] = 100(V_t\text{-}V_0)/V_0$$

where w_0, V_0, w_t and V_t correspond to the weight and volume of the samples after synthesis and the weight and volume of the swollen samples after an immersion of a duration t, respectively. Volumes are calculated with Archimedes' principle by immersing the samples in extra pure hexane (99+%, Fisher Chemical) for free swelling and in pure ethanol for constrained swelling to avoid the PDMS swelling in hexane.

Swelling pressure

The pressure exerted by the swollen hydrogels was measured using a confined compression setup [176]. After synthesis, 0.1 N pre-load was applied on the sample to ensure proper confinement. The chamber was filled with PBS to enable the swelling of the samples and the load was monitored while keeping the displacement constant during 48h to reach the equilibrium swelling. The swelling pressure was defined as the maximum pressure reached during the test.

Mechanical testing

Mechanical properties of the hydrogels were evaluated using an Instron E3000 linear mechanical testing machine (Norwood, MA, USA) equipped with a 250 N load cell.
Hydrogel samples were compressed to 50% applied strain at a constant speed of 0.1 mm/s. Load and displacement were recorded and the elastic modulus E was calculated by linear regression of the true stress-strain curve between the strains of 10% to 20%. Samples were immersed in PBS and placed in the incubator at 37°C and 5% CO_2. After different immersion time points, the same compression test was repeated.
As-prepared hydrogels (after synthesis) were also compressed to 80% applied strain. Failure stress and strain were defined as the maximum stress and strain, respectively, before hydrogel breaking. The compliance of the hydrogels was determined and defined as the strains applied under pressures between 10.5 and 16 kPa, corresponding to the physiological systolic blood pressure (80-120 mmHg).

Fatigue test and characterization after long-term loading

The hydrogels were implanted into *in vitro* aneurysm models and dynamically loaded at 2.3 Hz by a pulsatile fluid flow system for one month, corresponding to 5.5 million cycles of circumferential stretch and shear stresses in total, as previously detailed [169]. After the cyclic loadings, the aneurysm model was dismantled to collect the hydrogel sample. To evaluate the performance of the hydrogel, the sample was weighed and cylindrical samples, obtained by a 5 mm diameter punch, were compressed using the mechanical test as described above. The results were compared to the hydrogel in the as-prepared state (after synthesis) and to the hydrogel in the swollen state (after one month of swelling).

6.3.7 Precursor characterization

Injectability of the hydrogel precursor

The rheological properties of the hydrogel precursor were assessed with a modular compact rheometer 102 (Anton Paar, Peseux, Switzerland) by an oscillatory time sweep with a strain oscillation of 5% at a frequency of 1 Hz applied during 5 min. The dynamic viscosity was calculated as the average of the real part of the complex viscosity.

Photopolymerization

For photorheology, the light from a 405 nm wavelength light laser diode was coupled to the modular compact rheometer 102 and a parallel 25 mm diameter disc configuration was used. 200 μl of the hydrogel precursor was tested directly after hydrogel preparation. A strain oscillation of 5% at a frequency of 10 Hz was applied and the temperature fixed at 37°C. Samples of 300 μm thickness were illuminated with a light intensity of 15 mW/cm^2 at 405 nm. The evolution of the storage modulus G' was recorded during the 405 nm irradiation. The polymerization was considered complete when G' reached a plateau level. The time required to reach 95 % of the plateau level of G' was defined as polymerization time, noted t_{95}, as previously reported [187].

6.3.8 Statistical analysis

Each experiment was performed in triplicate or more and the statistical data analysis was performed with MATLAB (Mathworks, Natick, MA, United States). All data are expressed as mean $\pm$ standard deviation. One-way analysis of variance (ANOVA) was used for comparison. $p < 0.05$ was considered as a significant result (denoted as *) and $p > 0.05$ non-significant (denoted ns). $p < 0.01$ was denoted as ** and $p < 0.001$ as ***.

6.4 Results

6.4.1 Cell adhesion on hydrogel surfaces

Influence of photoinitiator type

The influence of the photoinitiator type, PEG-BAPO and LAP, on the cell adhesion was studied, as shown for PEGDMA10-GelMA5 hydrogels in Figure 6.4. Endothelial cells on the LAP hydrogel surfaces had an elongated shaped-cytoskeleton whereas cells on the PEG-BAPO hydrogel surfaces had round shape. Both hydrogels presented cells on their surface, however only LAP hydrogels enabled the adhesion and spreading of cells. Thus, the photoinitiator type has an unexpected impact on the cell adhesive properties. Accordingly, LAP photoinitiator was used for all hydrogels in the following.

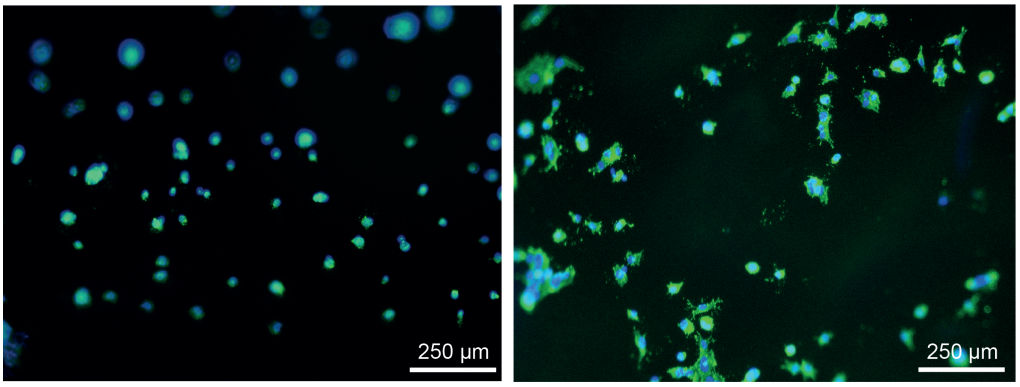

FIGURE 6.4: Microscopic images of immunostaining assay according to the photoinitiator type (PEG-BAPO or LAP) for PEGDMA10/GelMA5 hydrogels, after 1 day of HUVEC adhesion. The cytoskeleton of HUVEC is stained in green and nucleus in blue (n=3).

Influence of GelMA concentration into PEGDMA network

PEGDMA hydrogels were biofunctionalized with GelMA, at a concentration from 1 to 5%, for a total polymer concentration of 15%. The cell adhesion was investigated at 1 day and 1 week after cell seeding, as displayed in Figure 6.5. The incorporation of GelMA into PEGDMA network improved the cell adhesive properties of the hydrogels. HUVEC were observed at the surfaces of hydrogels comprising GelMA at a concentration below 2.5% after 24h. However, the cells had a round shape and hardly no cells were present after one week. For GelMA concentration of 5%, the hydrogels surfaces exhibited elongated cells after one day. The number of cells on the PEGDMA10-GelMA5 hydrogels surfaces were comparable to the surfaces of neat GelMA15 hydrogels. After one week of culture, HUVEC formed a cellular network on the hydrogels surfaces. However, this network was less dense for PEGDMA10-GelMA5 hybrid hydrogels than neat GelMA15 hydrogels.

Influence of fluid flow

The cell attachment of PEGDMA10-GelMA5 hydrogels was also evaluated after 24h of culture medium flow. Figure 6.6 shows adherent HUVEC at the interface channel/hydrogel and on the hydrogel surface. Due to the roughness of the channel surface, the cells did not attach to the channel, except at the boundaries. Cells were observed at the interface channel/hydrogel and on the hydrogel surface, before and after exposure to flow. Although slightly less cells were observed after 24h of flow than before the passage of flow, the cell adhesive properties of PEGDMA10-GelMA5 hydrogels seem to support the shear stresses induced by the fluid flow.

6.4.2 Cell migration

The migration of HUVEC towards the PEGDMA10-GelMA5 hydrogels was observed over 8 days of culture, as displayed in Figure 6.7.A. The cells significantly migrated towards the hydrogels, as an increase of the cells distribution around the hydrogels was observed. Figure 6.7.B. shows the cells distribution around the hydrogel after 8 days of culture. The morphology of the cells around the hydrogel were not altered compared to far from the hydrogel and cells were also observed under the hydrogel.

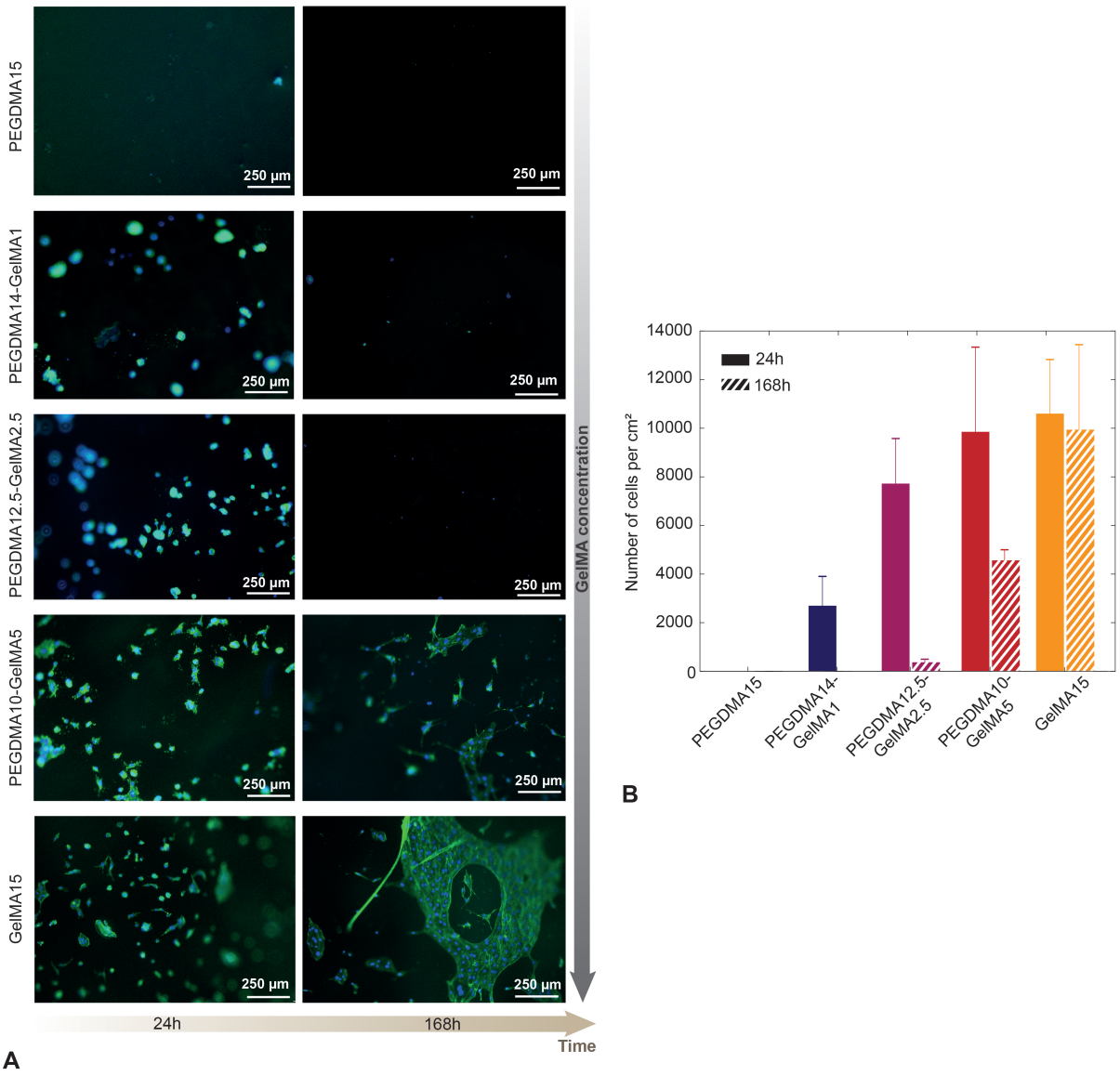

FIGURE 6.5: (A) Microscopic images of immunostaining assay according to the GelMA concentration into the hydrogels, after one day and one week of HUVEC adhesion. The cytoskeleton of HUVEC is stained in green and nucleus in blue. (B) Number of cells per cm^2 according to the GelMA concentration into the hydrogels, after one day and one week of HUVEC adhesion (n=3).

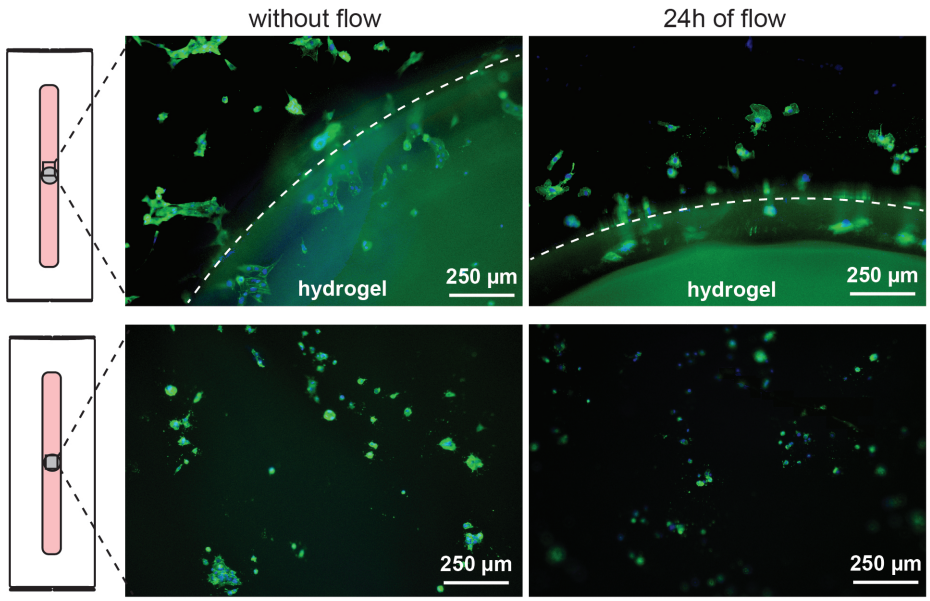

FIGURE 6.6: Microscopic images of immunostaining assay at the interface the channel/hydrogel and on the hydrogel surfaces, before and after 24h of fluid flow. The cytoskeleton of HUVEC is stained in green and nucleus in blue.

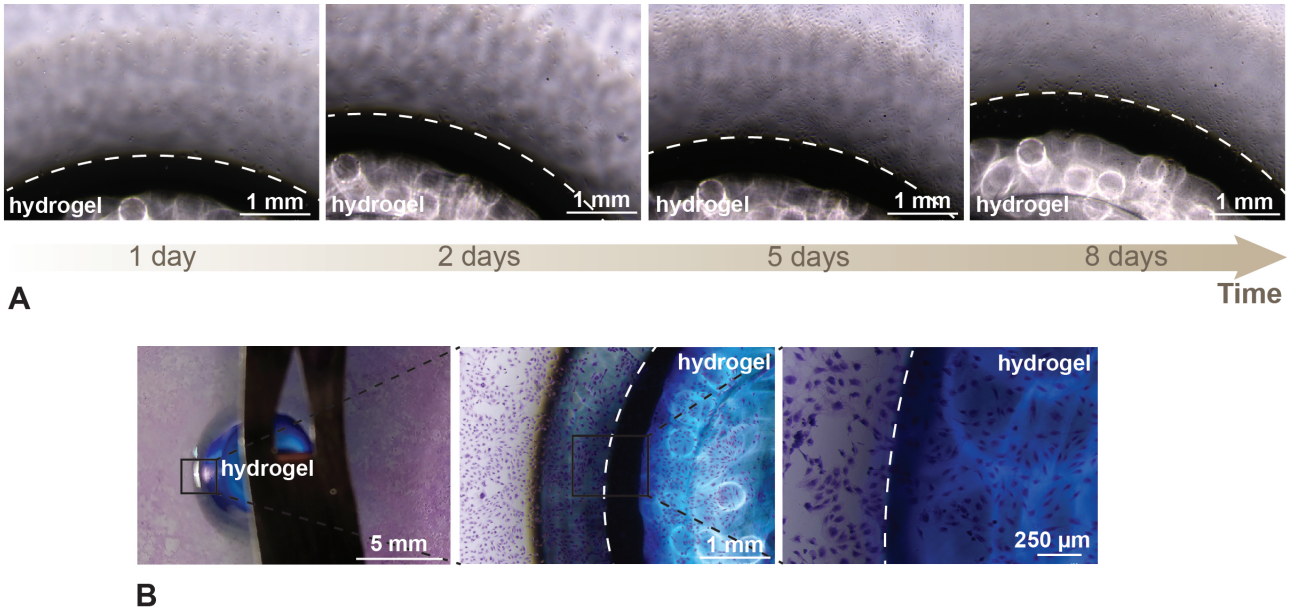

FIGURE 6.7: (A) Microscopic images of HUVEC around PEGDMA10-GelMA5 hydrogels, showing a migration of the cells, in function of the culture time. (B) Macroscopic (left) and microscopic (center and right) images around the PEGDMA10-GelMA5 hydrogel after 8 days of culture, showing that HUVEC migrated below the hydrogel.

6.4.3 Hydrogel physical and mechanical characterization

Note that, in this part, the results were compared with results of PEGDMA6k-15 hydrogels obtained in the Chapter 3.

The mechanical properties and swelling characteristics of the PEGDMA-GelMA hybrid hydrogels were evaluated to determine the influence of GelMA incorporation and compare with neat PEGDMA and GelMA hydrogels.
Figure 6.8.A revealed a significant reduction in volume swelling ratio when increasing GelMA concentration. In constrained swelling, PEGDMA15 samples exhibited a slightly increased volume (9 $\pm$ 7%), PEGDMA10-GelMA5 reached a volume swelling ratio of 1 $\pm$ 3%, while GelMA15 manifested a slightly decreased volume (-11 $\pm$ 6%). Accordingly, the swelling pressure also significantly diminished when increasing GelMA concentration (Figure 6.8.B).
The elastic modulus of PEGDMA15 and PEGDMA10-GelMA5 hydrogels were not significantly different, around 280 kPa, as shown in Figure 6.8.C. The elastic modulus of GelMA15 hydrogels was almost three times lower with 95 $\pm$ 11 kPa. In addition, the compliance was not significantly different for PEGDMA15 and PEGDMA10-GelMA5 samples (Figure 6.8.D). PEGDMA15, PEGDMA10-GelMA5 and GelMA15 samples failed under compression at a stress of 480 $\pm$ 127 kPa, 461 $\pm$ 145 kPa and 278 $\pm$ 89 kPa and an applied strain of 72 $\pm$ 7%, 60 $\pm$ 6% and 61 $\pm$ 4%, respectively.
The incorporation of a low concentration of GelMA (5%) into the PEGDMA network reduced the swelling behavior but did not affect the hydrogel mechanical properties.

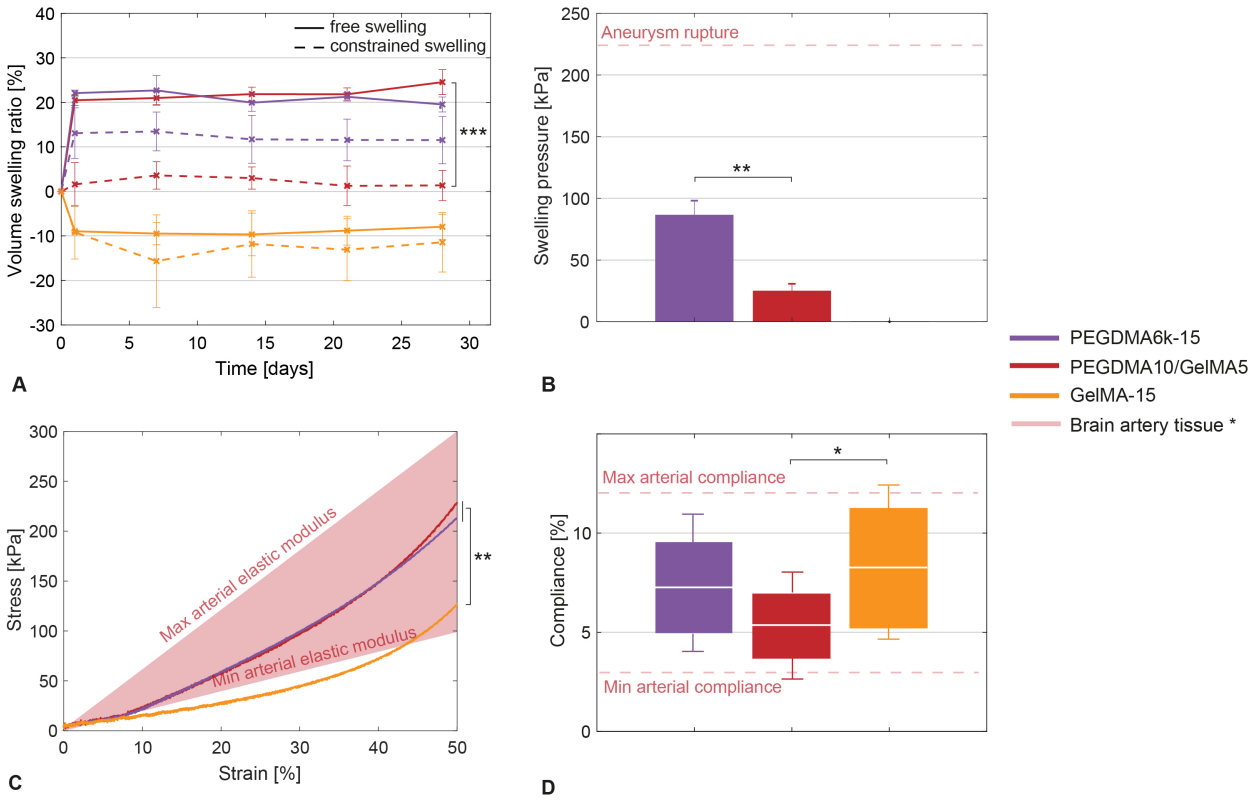

FIGURE 6.8: (A) Volume swelling ratio in free and constrained (within the aneurysm model) swelling conditions, revealing a significant decrease of the volume swelling ratio when incorporating GelMA into PEGDMA network. Statistically significant differences are only displayed between the free and constrained swelling conditions. (B) Maximal pressure induced by the swollen hydrogels, demonstrating a decrease of the swelling pressure when increasing GelMA concentration. (C) Strain-stress curve of the compression test, showing a significant lower elastic modulus of GelMA15 hydrogels. (D) Compliance of the hydrogels under physiological pressures (80-120 mmHg). Box plots depicted mean (white line) and values at 80 and 120 mmHg (bottom and top of the box).
* parent artery tissue data from literature [17], [158], [161]

The fatigue resistance of the PEGDMA10-GelMA5 hydrogels was subsequently assessed over one month of loading induced by pulsatile fluid flow. The hydrogels did not protrude or migrate into the parent artery and no signs of macroscopic damage was apparent (Figure 6.9.A). The weight and elastic modulus of PEGDMA10-GelMA5 hydrogels were similar after 5.5 million cycles compared to the as-prepared state (Figures 6.9.B and 6.9.C). However, a significant decrease of the weight was measured between as-prepared and swollen hydrogel.

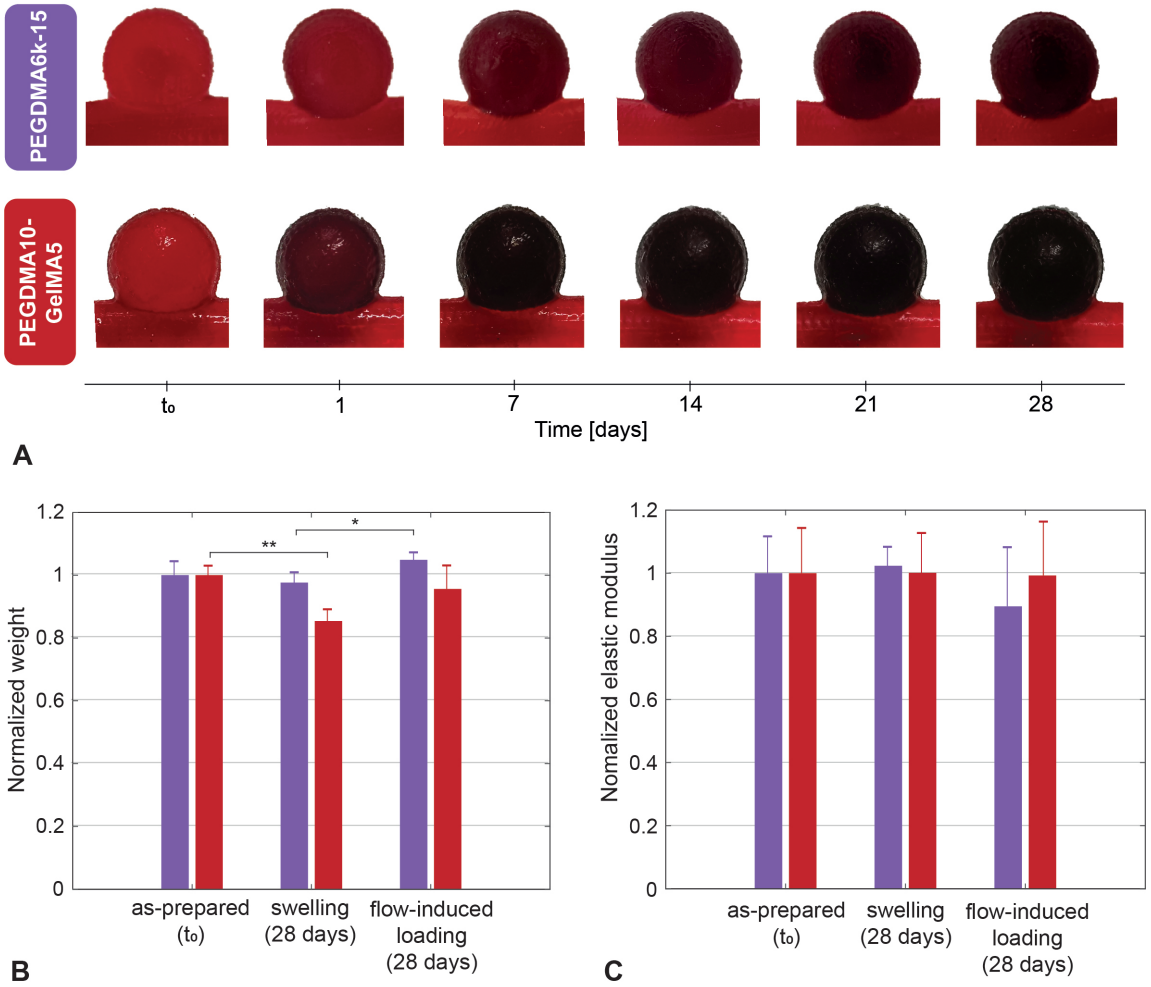

FIGURE 6.9: (A) Direct visualization of the hydrogels within the intracranial aneurysm model during one month of pulsatile fluid flow-induced loading showing complete occlusion without protrusion, migration, geometric distortion nor signs of macroscopic damage. (B) Weight and (C) Mechanical property variations, normalized to the as-prepared state of the hydrogel, after one month of swelling and one month of fluid flow-induced loading (n=3).

6.4.4 Precursor characterization

Note that, in this part, the results were compared with results of PEGDMA6k-15 hydrogels obtained in the Chapter 4.

The viscosity of the PEGDMA10-GelMA5 hydrogel precursor was evaluated by rheology. The dynamic viscosity of the precursor was measured to be 32 $\pm$ 6 mPa.s at 37°C and 233 $\pm$ 20

mPa.s at 22°C, as shown in Figure 6.10.A. The precursor was significantly affected by the temperature (p=8.10^{-5}), the precursor being more viscous when the temperature decreased. In comparison with PEGDMA15 precursor, the incorporation of 5% GelMA in 10% PEGDMA hydrogels significantly increased the viscosity of the precursor at 37°C (p=0.0396), but PEGDMA10-GelMA5 hydrogel was still injectable through 430 μm microcatheters.
The biofunctionalization of PEGDMA hydrogels with 5% GelMA significantly increased the time of photopolymerization from 4 min 23 s ± 45 s to 7 min 35 s ± 20 s, as shown in Figure 6.10.B.

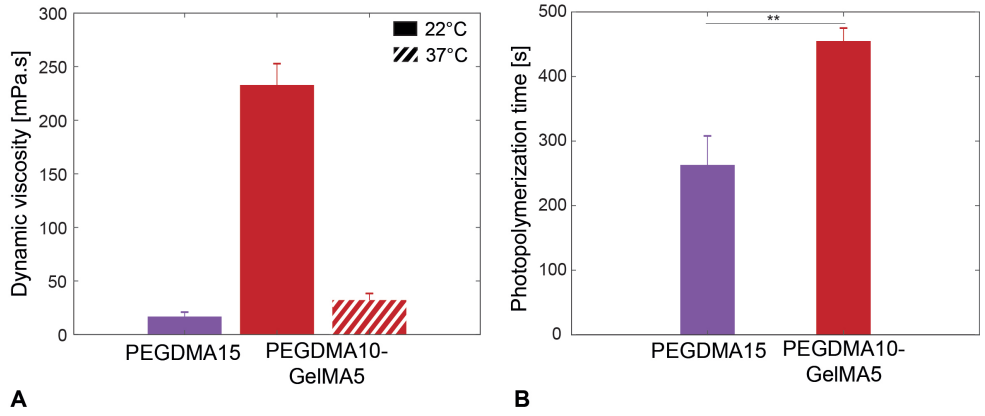

FIGURE 6.10: (A) Dynamic viscosity of PEGDMA15 and PEGDMA10-GelMA5 hydrogels at 22 and 37°C. (B) Time of photopolymerization of PEGDMA15 and PEGDMA10-GelMA5 hydrogels measured by photorheology.

6.5 Discussion

In the present study, a biofunctionalization of PEGDMA hydrogels with GelMA was proposed to promote the hydrogels bioactivity and, to a larger context, the *in situ* endothelialization. The main finding of our work is that the incorporation of a low concentration of GelMA (5%) into PEGDMA network improves the bioactivity of the hydrogels without significantly affecting the mechanical properties. GelMA modified the swelling and implantation properties, however the hybrid hydrogels meet the requirements for intracranial aneurysms embolic agents.

The endothelium layer growth at the hydrogel surfaces is a key aspect for the long-term success of the embolic agent implantation [258]. PEG hydrogels have been widely used in biomaterials. However, their lack of bioactivity and cell attachment sites [266], which was confirmed by our endothelial adhesion results, limits their use for tissue engineering and regenerative medicine. Many researches on PEG biofunctionalizations, such as collagen [140], [141], gelatin [142], [143], fibronectin [139], heparin [147] or vascular endothelial growth factor (VEGF) [152], have shown to foster cell attachment. Gelatin was chosen due to their biocompatiblity, ability to be modified with photocrosslinkable methacrylamide groups as well as better solubility and lower antigenicity compared to collagen [263], [267]. Our study on the cell adhesion by the incorporation of GelMA into PEGDMA hydrogels is consistent with recent studies [142],

[143], revealing a significant improvement of the cell adhesive properties. This enhancement is related to the presence in GelMA polymer of many RGD peptides sequences, identified as integrin-binding domains [268]. The cell adhesion assay in static conditions allowed us to identify the minimal GelMA concentration favoring cell adhesion. PEGDMA-GelMA hybrid hydrogels made of at least 5% GelMA showed cell attachment and spreading on their surfaces over one week of culture.

The hybrid hydrogels composed of 10% PEGDMA and 5% GelMA were then subjected to laminar shear stresses induced by fluid flow for one day, to assess if the cell adhesion will support the blood flow. It is important to highlight that the fluid shear stresses have differential effects on endothelial cell proliferation, survival, function and structure [269]. Indeed, the endothelial cells sense the hemodynamic forces and convert the mechanical stimuli into cellular signals [270]. This mechanotransduction mechanism allows maintaining the vascular homeostasis [271]. The preliminary results showed that the adherent cells withstood the flow. Nevertheless, it should be noted that the test was not performed under physiological conditions. A flow rate of 24 ml/min was set with the dynamic setup in order to avoid consequent volumes of culture medium. This flow rate was 10 times lower than the human intracranial arteries flow rate [233], inducing shear stresses of around 85 mPa, also significantly lower than the physiological shear stresses ranging from 1 to 5 Pa in intracranial arteries. Low shear stresses are associated to endothelial cell dysfunction and apoptosis [272]–[274] whereas higher shear stresses to the detachment of the endothelial cells [275]. Therefore, it would be of interest to study a range of shear stresses to determine if the endothelial cells also withstand higher shear stresses.

Although hybrid hydrogels composed of PEGDMA and GelMA polymers demonstrated proper adhesive properties and suitable support for the endothelial cells to migrate, the present study cannot determine whether these hydrogels would promote the endothelialization at the aneurysm neck. Indeed, the cell adhesion and migration were studied only for one week. An extensive evaluation should be performed to determine the proliferation of cells under flow conditions for longer culture times. Moreover, a limitation of our work is that the hydrogels surfaces were seeded with endothelial cells, which will not be the case in a real clinical situation. A pulsatile flow bioreactor system could be developed by coating the microchannel developed in this work for cells to attach and form an endothelial layer. A peristaltic pump enabling an average flow rate and shear stresses could be connected to the system to simulate closer physiological conditions.

It is worth mentioning that the effects of the photoinitiator type on cell attachment were unexpected. Numerous published data reported the influence of the photoinitiator on polymerization kinetics, mechanical properties or biocompatibility properties [128], [130], but to our knowledge, none have studied the impact on cell adhesion. Since the polymerized hydrogels were washed in PBS and culture medium prior cell seeding, potentially toxic unreacted products, in particular radicals, should have been removed. The molar concentration for both PEG-BAPO and LAP was similar, hence the number of produced radicals were equivalent and thus cannot explain the differences in cell adhesion.

A question associated with the incorporation of GelMA into the PEGDMA hydrogel network is its impact on others properties such as the mechanical, physical and implantation properties. Since all the hydrogel properties are interrelated, the minimal GelMA concentration promoting cell adhesion (5%) was chosen to limit changes in others properties. The present study is consistent with and supplements the PEGDMA-GelMA hybrid hydrogels characterization reported in literature [142], [143], [276]. When incorporating GelMA into PEGDMA network, the volume swelling ratio and swelling pressure were lower than neat PEGDMA15 and higher than GelMA15. This can be explained by the biodegradability of GelMA polymer [267] due to the presence of MMP-sensitive degradation sites. The GelMA biofunctionalization was found to not influence the mechanical properties of the hydrogels. A recent study demonstrated that the tensile properties of hybrid hydrogels were enhanced compared to neat PEGDMA hydrogels [142]. In this work, we have focused on the characterization of compressive properties. The hybrid hydrogels exhibited an elastic modulus and compliance, covering those of the native aneurysm tissue and far withstood physiological blood pressures and circumferential stresses.
Subsequently, the fatigue resistance of the hybrid hydrogels was also evaluated under pulsatile flow-induced loadings for one month. The results between neat PEGDMA and hybrid hydrogels were similar. PEGDMA10-GelMA5 hydrogels preserved their shape, weight and elastic modulus after 5.5 million of cycles.
It was indispensable to also assess the injectability and photopolymerization time to ensure the minimal invasiveness and fast solidification of the technique. GelMA is known to be a thermosensitive polymer, with an upper critical solution temperature (UCST) of 25–35°C [277]. This explains the significant increase of the dynamic viscosity at room temperature compared to 37°C. Although the incorporation of GelMA into PEGDMA network makes the PEGDMA10-GelMA5 precursor more viscous, their viscosity at 37°C is in the range of current liquid embolic agents [235]. Therefore, the precursor should be stored at 37°C before being injected into aneurysms through 430 μm microcatheters. Due to the effect of the photoinitiator type on cell adhesion, LAP was used as photoinitator for hybrid and GelMA hydrogels. LAP is less photoreactive than PEG-BAPO, which explains the longer time of photopolymerization of PEGDMA10-GelMA5 hydrogels. The hybrid hydrogels still satisfy the threshold of 10 minutes of solidification required for intracranial aneurysm treatment.

6.6 Conclusion

The present study demonstrated that the biofunctionalization of PEGDMA hydrogels with GelMA significantly enhanced the bioactivity of the hydrogels. The endothelial cells adhered and spread to the hybrid surfaces forming a cellular network after one week of culture, whereas neat PEGDMA hydrogels did not promote any cell adhesion. The cells also migrated towards the hydrogels surfaces. Moreover, the mechanical properties were not influenced by GelMA incorporation and the hydrogels were resistant to 5.5 million cycles of loading induced by pulsatile flow. Others properties such as swelling, viscosity and photopolymerization time, were

significantly changed but without negative impacts on the success of the implantation into intracranial aneurysms. Nonetheless, the *in situ* endothelialization potential of the PEGDMA-GelMA hybrid hydrogels must be thoroughly investigated in closer physiological conditions and for longer period of times.

6.7 Acknowledgements

We would like to thank Peyman Karami who synthesized the GelMA polymer.

Chapter 7

Conclusion and Perspectives

7.1 Summary of findings

The overall objective of this work was to develop an *in situ* photopolymerizable hydrogel for the minimally-invasive treatment of intracranial aneurysms (IAs). *In situ* forming hydrogels have been investigated as IAs embolic materials during the last two decades, but no standard definition of the ideal IA embolic material has clearly been approved yet. The first step of this work was thereby to identify and establish clear specifications to develop an ideal embolic material, in accordance with the literature and surgeons guidelines. The present thesis focused accordingly on four major axes: (1) the development and characterization of fatigue-resistant hydrogels, (2) the implantation of the hydrogels into aneurysm models, (3) the evaluation of the safety of the precursor and hydrogel and (4) the enhancement of the cell adhesive properties of the hydrogels.

The first part of this thesis (Chapter 3) aimed at optimizing the swelling behavior and mechanical properties of the hydrogels and assessing their fatigue-resistance. Poly(ethylene glycol) dimethacrylate (PEGDMA) hydrogels were characterized according to their molecular weights (2 to 20 kDa) and concentrations (10 to 20 wt%). Denser covalently cross-linked hydrogel networks were obtained by decreasing the molecular weight and increasing the polymer concentration, which was consistent with published data. PEGDMA hydrogels of 6 kDa molecular weight at a concentration of 10 to 15 wt% presented the optimal properties to serve as an aneurysm embolic agent. Their elastic modulus and compliance covered the range of native aneurysm tissue of 200 to 600 kPa. Moreover, the hydrogels withstood the physiological blood pressures of approximately 15 kPa as well as the circumferential stresses of 100-150 kPa. The hydrogels also presented a minimal swelling volume ratio avoiding protrusion in the parent artery and a low swelling pressure preventing excessive aneurysm wall stresses. These characteristics make the optimized hydrogels promising candidates for IA embolization and therefore were further examined in dynamic conditions. To that end, *in vitro* aneurysms models, mimicking the dimensions and mechanical properties of human aneurysms, were fabricated by casting PDMS around 3D printed water-soluble sacrificial PVA molds. Subsequently, the hydrogels were photopolymerized in the aneurysm model and dynamically loaded by a pulsatile flow inducing circumferential and shear stresses. The strains applied on the aneurysm wall, measured by digital image correlation, were significantly reduced compared to untreated aneurysm model. The hydrogels were then exposed to a realistic fatigue test of 5.5 million cycles of circumferential and shear stresses, corresponding to an implantation of two months *in vivo*. The shape, weight

and mechanical properties of the selected hydrogels were preserved over the cyclic loading. Slight erosion defects were observed at the surface in contact with the blood substitute fluid. The fatigue resistance of the optimized hydrogels confirms their promising long-term integrity and stability into intracranial aneurysms.

The second part (Chapter 4) was devoted to validate the proof-of-concept of the photopolymerizable hydrogel implementation into an aneurysm model from a clinical standpoint. The rheology results demonstrated that the low viscosity of the precursors, composed of PEGDMA 6 kDa at 10 to 15%, enabled their injectabilitiy through 430 μm microcatheters. The new visible photoinitiator PEG-BAPO allowed to reach a complete polymerization in less than 8 minutes of visible light illumination. Higher concentration of PEGDMA polymer increased the precursor viscosity but shortened the polymerization time. The addition of iodinated contrast agent in the precursor solution was associated with its visibility under fluoroscopy during delivery and after polymerization. A specifically customized light-conducting microcatheter was fabricated by fixing optical fibers along the outer surface of a microcatheter and was connected to an illumination module. The light-conducting microcatheter enables the solidification to be temporally and spatially controlled, in contrast to conventional liquid embolic agents. The implementation of the hydrogel into an *in vitro* aneurysm model with tortuous anatomy in flow conditions was successfully achieved. The appropriate implantation properties of the developed hydrogel precursors combined with the use of the light-conducting microcatheter ensures the minimal invasiveness of the IA embolization with photopolymerizable hydrogels.

The third part (Chapter 5) focused on the evaluation of the toxicity of the PEGDMA-based precursors and hydrogels. The biocompatibility of the hydrogel precursor was investigated by specific *in vitro* endothelial cell viability and platelet aggregation assays to simulate the precursor dilution into the blood flow. It was found that the precursor was not toxic and did not induce thrombus formation. The *in vivo* study in rats corroborated these results. An intravenous injection in overdose conditions (15 times the aneurysm volume) of precursor PEGDMA 6 kDa at a concentration up to 30% did not cause any acute or delayed toxicity, thrombogenicity or inflammation after 3 weeks. Subsequently, *in vitro* cytotoxicity assays suggested that the polymerized hydrogels did not affect the endothelial cells survival after one week of contact. It was also confirmed that PEGDMA hydrogels did not promote any cell adhesion. According to these results, PEGDMA photopolymerizable hydrogels seem to be biocompatible if injected for intracranial aneurysm treatment.

Finally, the fourth part of this thesis (Chapter 6) investigated the *in situ* endothelialization potential of the PEGDMA photopolymerizable hydrogels by incorporation of gelatin methacrylate (GelMA). The *in vitro* assays revealed that the endothelial cells migrated, adhered, spread and formed a cellular network after one week of culture on the hybrid hydrogels composed of 10% PEGDMA and 5% GelMA, whereas neat PEGDMA hydrogels did not promote any cell adhesion. The hybrid hydrogels were then exposed to shear stresses induced by laminar flow for one day. The adherent endothelial cells withstood the flow. The biofunctionalization of PEGDMA with GelMA significantly improved the cell adhesive properties of the hydrogels. The GelMA

incorporation did not affect the mechanical properties and fatigue-resistance of the hydrogels. The swelling characteristics were significantly reduced, reaching almost no swelling. Moreover, the hybrid hydrogel precursor demonstrated to be injectable through 430 μm microcatheters and photopolymerizable within 8 min of visible illumination. The enhancement of the bioactivity of the PEGDMA-GelMA hydrogels could promote the endothelialization at the aneurysm neck.

7.2 Perspectives and future work

7.2.1 Towards further characterization of hydrogels

The mechanical properties of the hydrogels is of great importance to withstand the continuous interaction with the blood. Although these properties were optimized to match those of native aneurysm tissue, a more detailed investigation on several aspects is required. The fatigue-resistance is, among others, a key property of the hydrogel since the embolic agent is subjected to many years of cyclic loading. Although the hydrogel possess a great integrity and stability over 5.5 million cycles, the fatigue-resistance evaluation needs to be extended to a longer loading time. It is worthwhile to thoroughly examine the erosion phenomena observed in our study. This entails to expose the hydrogels to fluid flow for different time points and to determine the number of cycles initiating the erosion. Furthermore, our hypotheses on the erosion consequences, namely the stroke risk due to possible hydrogel fragments moving downstream or the promotion of cell adhesion and endothelialization, need to be verified. Finally, the erosion observation in this research work paves the way towards erosion study for others applications such as the synovial fluid flow in cartilage [278].

The hydrogel adhesion to the endothelial tissue also needs to be further investigated to avoid hydrogel migration into the parent artery, particularly for wide-necked aneurysms, and enhance the hydrogel integration with the surrounding tissue. This involves bovine or porcine arteries tissue samples preparation and adhesion and tear strength tests. It would also be of interest to study the degradation and porosity of the hydrogels, which could foster the endothelium regeneration.

7.2.2 Towards pulsatile flow bioreactor system

Further research could also be proposed on the development of a pulsatile flow bioreactor. Casting PDMS around PVA sacrificial molds provides an efficient technique to fabricate *in vitro* aneurysm models and could be adapted to replicate more tortuous geometries of aneurysms and even patient-specific geometries. These *in vitro* models have a great potential to be customized to a pulsatile flow bioreactor system. Endothelial cells could be seeded on the vessel surfaces thanks to the biocompatibility and sterilization of both materials used in the fabrication process. The system driven by a peristaltic pump enables to simulate realistic hemodynamic conditions, combining circumferential and shear stresses. The bioreactor could hence be used to assess the endothelialization of the hydrogel surfaces for longer period of times and closer physiological conditions.

7.2.3 Towards *in vivo* embolization and clinical implantation

The implementation of photopolymerizable hydrogels was successfully achieved in *in vitro* aneurysms models and an *in vivo* pilot study in elastase-induced aneurysms in rabbits is currently on-going. Some improvements and challenges need to be explored, mainly in the design of the light-conducting microcatheter and in the photopolymerization process.

The light-conducting microcatheter prototype we have developed enables *in vitro* implementation, but its simple design could be improved. First, it is known that glass material surfaces initiate blood coagulation [279]. Although protected by the heat shrink tube, the glass-made optical fiber fixed to the microcatheter might cause blood coagulation at its tip, which can prevent the light diffusion. Consequently, coatings to prevent blood clotting could be used such as liquid perfluorocarbons coatings [280]. Second, in the developed implantation approach, the aneurysm embolization is estimated in function of the radiopacity of the hydrogel precursor. It is of interest to integrate a pressure sensor at the microcatheter tip to assess the pressure applied on aneurysm wall during the precursor delivery and thereby avoid excessive pressure which could cause aneurysm rupture. Finally, an optimal solution is to directly braid the optical fiber in the plastic wall of the microcatheter.

The photopolymerization of our precursor was achieved within 8 minutes, which was lower than the threshold of 10 minutes established from the clinical point of view. However, it is preferred to decrease this polymerization time to several seconds or less than a minute, to reduce the risks of ischemic stroke and vessel injury. Consequently, further research should be performed to reduce this time, by modification of the PEG-BAPO photoinitiator, using others photoinitiators or employing a light-diffusing optical fiber tip [281] to homogeneously distribute the light in the aneurysm volume. Besides, it is of interest to monitor the polymerization process by employing a feedback loop using light of a different wavelength through the same optical fiber [241], to ensure a complete curing of the hydrogel. Moreover, it was found difficult to rinse blood out of the aneurysm, which would challenge the photopolymerization due to the visible light absorption of blood [282]. Although our implementation was performed using blood substitute fluid with light absorption similar to the one of blood, the implantation needs to be confirmed in real clinical situation.

Finally, the proposed photopolymerizable hydrogels also hold great potential for other transarterial embolization therapies, such as arteriovenous malformations and vascular tumors.

Bibliography

[1] M. H. M. Vlak, A. Algra, R. Brandenburg, and G. J. E. Rinkel, "Prevalence of unruptured intracranial aneurysms, with emphasis on sex, age, comorbidity, country, and time period: A systematic review and meta-analysis," *The Lancet Neurology*, vol. 10, no. 7, pp. 626–636, 2011, ISSN: 14744422.

[2] Z. Vrselja, H. Brkic, S. Mrdenovic, R. Radic, and G. Curic, "Function of circle of Willis," *Journal of Cerebral Blood Flow and Metabolism*, vol. 34, no. 4, pp. 578–584, 2014, ISSN: 0271-678X.

[3] A. Keedy, "An overview of intracranial aneurysms," *McGill Journal of Medicine*, vol. 9, no. 2, pp. 141–146, 2006, ISSN: 1201026X.

[4] V. L. Feigin, G. J. E. Rinkel, C. M. M. Lawes, A. Algra, D. A. Bennett, J. Van Gijn, and C. S. Anderson, "Risk factors for subarachnoid hemorrhage: An updated systematic review of epidemiological studies," *Stroke*, vol. 36, no. 12, pp. 2773–2780, 2005, ISSN: 00392499.

[5] Medical Advisory Secretariat, "Coil embolization for intracranial aneurysms: an evidence-based analysis.," *Ontario health technology assessment series*, vol. 6, no. 1, pp. 1–114, 2006, ISSN: 1915-7398.

[6] J. van Gijn, R. S. Kerr, and G. J. E. Rinkel, "Subarachnoid haemorrhage," *Lancet*, vol. 369, no. 9558, pp. 306–318, 2007, ISSN: 1474-547X.

[7] K.-H. Jung, "New Pathophysiological Considerations on Cerebral Aneurysms," *Neurointervention*, vol. 13, no. 2, pp. 73–83, 2018, ISSN: 2093-9043.

[8] N. Etminan, B. A. Buchholz, R. Dreier, P. Bruckner, J. C. Torner, H.-J. Steiger, D. Hänggi, and R. L. Macdonald, "Cerebral Aneurysms: Formation, Progression, and Developmental Chronology," *Translational Stroke Research*, vol. 5, no. 2, pp. 167–173, 2014, ISSN: 1868-4483.

[9] P. Texakalidis, A. Sweid, N. Mouchtouris, E. C. Peterson, C. Sioka, L. Rangel-Castilla, J. Reavey-Cantwell, and P. Jabbour, "Aneurysm Formation, Growth, and Rupture: The Biology and Physics of Cerebral Aneurysms," *World Neurosurgery*, vol. 130, pp. 277–284, 2019, ISSN: 18788750.

[10] F. Signorelli, S. Sela, L. Gesualdo, S. Chevrel, F. Tollet, C. Pailler-Mattei, L. Tacconi, F. Turjman, A. Vacca, and D. B. Schul, "Hemodynamic Stress, Inflammation, and Intracranial Aneurysm Development and Rupture: A Systematic Review," *World Neurosurgery*, vol. 115, pp. 234–244, 2018, ISSN: 18788750.

[11] J. D. Humphrey, "Coupling haemodynamics with vascular wall mechanics and mechanobiology to understand intracranial aneurysms," *International Journal of Computational Fluid Dynamics*, vol. 23, no. 8, pp. 569–581, 2009, ISSN: 1061-8562.

[12] N. Chalouhi, B. L. Hoh, and D. Hasan, "Review of Cerebral Aneurysm Formation, Growth, and Rupture," *Stroke*, vol. 44, no. 12, pp. 3613–3622, 2013, ISSN: 0039-2499.

[13] V. S. Fennell, M. Y. S. Kalani, G. Atwal, N. L. Martirosyan, and R. F. Spetzler, "Biology of Saccular Cerebral Aneurysms: A Review of Current Understanding and Future Directions," *Frontiers in Surgery*, vol. 3, 2016, ISSN: 2296-875X.

[14] MedlinePlus, *Circle of Willis*.

[15] A. Raabe, D. Bervini, and J. Goldberg, *Unruptured cerebral aneurysms*.

[16] J. C. Lasheras, "The Biomechanics of Arterial Aneurysms," *Annual Review of Fluid Mechanics*, vol. 39, pp. 293–319, 2007.

[17] A. P. Ebrahimi, "Mechanical properties of normal and diseased cerebrovascular system.," *Journal of vascular and interventional neurology*, vol. 2, no. 2, pp. 155–62, 2009, ISSN: 1941-5893.

[18] N. Wang, Zhijie and Golob, Mark J. and Chesler, "Viscoelastic Properties of Cardiovascular Tissues," in *Viscoelastic and Viscoplastic Materials*, 2016, ch. 7.

[19] J. M. Rhodes and M. Simons, "The extracellular matrix and blood vessel formation : not just a scaffold," *Journal of Cellular and Molecular Medicine*, vol. 11, no. 2, pp. 176–205, 2007.

[20] A. M. Robertson and P. N. Watton, "Mechanobiology of the Arterial Wall," *Transport in Biological Media*, pp. 275–347, 2013.

[21] R. M. K. W. Lee, "Morphology of cerebral arteries," *Pharmacology Therapeutics*, vol. 66, no. 94, pp. 149–173, 1995.

[22] J. D. Humphrey, "Vascular Adaptation and Mechanical Homeostasis at Tissue , Cellular, and Sub-cellular Levels," *Cell Biochemistry and Biophysics*, vol. 50, pp. 53–78, 2008.

[23] A. Can and R. Du, "Association of Hemodynamic Factors With Intracranial Aneurysm Formation and Rupture," *Neurosurgery*, vol. 78, no. 4, pp. 510–520, 2016, ISSN: 0148-396X.

[24] H. Meng, Z. Wang, Y. Hoi, L. Gao, E. Metaxa, D. D. Swartz, and J. Kolega, "Complex Hemodynamics at the Apex of an Arterial Bifurcation Induces Vascular Remodeling Resembling Cerebral Aneurysm Initiation," *Stroke*, vol. 38, no. 6, pp. 1924–1931, 2007, ISSN: 0039-2499.

[25] S. Zhou, P. A. Dion, and G. A. Rouleau, "Genetics of Intracranial Aneurysms," *Stroke*, vol. 49, no. 3, pp. 780–787, 2018, ISSN: 0039-2499.

[26] B. Krischek and M. Tatagiba, "The influence of genetics on intracranial aneurysm formation and rupture: current knowledge and its possible impact on future treatment," in *Advances and Technical Standards in Neurosurgery*, 2008, pp. 131–147.

[27] G. Ailawadi, C. W. Moehle, H. Pei, S. P. Walton, Z. Yang, I. L. Kron, C. L. Lau, and G. K. Owens, "Smooth muscle phenotypic modulation is an early event in aortic aneurysms," *The Journal of Thoracic and Cardiovascular Surgery*, vol. 138, no. 6, pp. 1392–1399, 2009, ISSN: 00225223.

[28] R. M. Starke, N. Chalouhi, D. Ding, D. M. S. Raper, M. S. Mckisic, G. K. Owens, D. M. Hasan, R. Medel, and A. S. Dumont, "Vascular Smooth Muscle Cells in Cerebral Aneurysm Pathogenesis," *Translational Stroke Research*, vol. 5, no. 3, pp. 338–346, 2014, ISSN: 1868-4483.

[29] N. Chalouhi, M. S. Ali, P. M. Jabbour, S. I. Tjoumakaris, L. F. Gonzalez, R. H. Rosenwasser, W. J. Koch, and A. S. Dumont, "Biology of Intracranial Aneurysms: Role of Inflammation," *Journal of Cerebral Blood Flow Metabolism*, vol. 32, no. 9, pp. 1659–1676, 2012, ISSN: 0271-678X.

[30] Y. Kanematsu, M. Kanematsu, C. Kurihara, Y. Tada, T.-L. Tsou, N. van Rooijen, M. T. Lawton, W. L. Young, E. I. Liang, Y. Nuki, and T. Hashimoto, "Critical Roles of Macrophages in the Formation of Intracranial Aneurysm," *Stroke*, vol. 42, no. 1, pp. 173–178, 2011, ISSN: 0039-2499.

[31] R. Ishibashi, T. Aoki, M. Nishimura, N. Hashimoto, and S. Miyamoto, "Contribution of Mast Cells to Cerebral Aneurysm Formation," *Current Neurovascular Research*, vol. 7, no. 2, pp. 113–124, 2010, ISSN: 15672026.

[32] T. Aoki, H. Kataoka, M. Morimoto, K. Nozaki, and N. Hashimoto, "Macrophage-Derived Matrix Metalloproteinase-2 and -9 Promote the Progression of Cerebral Aneurysms in Rats," *Stroke*, vol. 38, no. 1, pp. 162–169, 2007, ISSN: 0039-2499.

[33] J. Frosen, A. Piippo, A. Paetau, M. Kangasniemi, M. Niemela, J. Hernesniemi, and J. Jaaskelainen, "Remodeling of saccular cerebral artery aneurysm wall is associated with rupture," *Stroke*, vol. 35, no. 10, pp. 2287–2293, 2004, ISSN: 0039-2499.

[34] T. Aoki, H. Kataoka, R. Ishibashi, K. Nozaki, R. Morishita, and N. Hashimoto, "Reduced Collagen Biosynthesis Is the Hallmark of Cerebral Aneurysm," *Arteriosclerosis, Thrombosis, and Vascular Biology*, vol. 29, no. 7, pp. 1080–1086, 2009, ISSN: 1079-5642.

[35] A. J. Molyneux, "International Subarachnoid-Aneurysm Trial (ISAT) of neurosurgical clipping versus endovascular coiling in 2143 patients with ruptured intracranial aneurysms: a randomised trial," *The Lancet*, vol. 360, pp. 1267–1274, 2002.

[36] A. J. Molyneux, J. Birks, A. Clarke, M. Sneade, and R. S. C. Kerr, "The durability of endovascular coiling versus neurosurgical clipping of ruptured cerebral aneurysms: 18 year follow-up of the UK cohort of the International Subarachnoid Aneurysm Trial (ISAT)," *The Lancet*, vol. 385, no. 9969, pp. 691–697, 2015, ISSN: 1474547X.

[37] C. G. McDougall, R. F. Spetzler, J. M. Zabramski, S. Partovi, N. K. Hills, P. Nakaji, and F. C. Albuquerque, "The barrow ruptured aneurysm trial: Clinical article," *Journal of Neurosurgery*, vol. 116, no. 1, pp. 135–144, 2012, ISSN: 00223085.

[38] R. F. Spetzler, C. G. Mcdougall, J. M. Zabramski, F. C. Albuquerque, N. K. Hills, J. J. Russin, S. Partovi, P. Nakaji, and R. C. Wallace, "The Barrow Ruptured Aneurysm Trial: 6-year results," *Journal of Neurosurgery*, vol. 123, no. September, pp. 609–617, 2015.

[39] R. F. Spetzler, C. G. McDougall, J. M. Zabramski, F. C. Albuquerque, N. K. Hills, P. Nakaji, J. P. Karis, and R. C. Wallace, "Analysis of saccular aneurysms in the Barrow Ruptured Aneurysm Trial," *Journal of Neurosurgery*, vol. 128, no. 3, pp. 120–125, 2018, ISSN: 19330693.

[40] R. F. Spetzler, C. G. McDougall, J. M. Zabramski, F. C. Albuquerque, N. K. Hills, P. Nakaji, J. P. Karis, and R. C. Wallace, "Ten-year analysis of saccular aneurysms in the Barrow Ruptured Aneurysm Trial," *Journal of Neurosurgery*, vol. 132, no. 3, pp. 771–776, 2020, ISSN: 19330693.

[41] S. Tamatani, Y. Ito, H. Abe, T. Koike, S. Takeuchi, and R. Tanaka, "Evaluation of the stability of aneurysms after embolization using detachable coils: Correlation between stability of aneurysms and embolized volume of aneurysms," *American Journal of Neuroradiology*, vol. 23, no. 5, pp. 762–767, 2002, ISSN: 01956108.

[42] K. Yagi, K. Satoh, J. Satomi, S. Matsubara, and S. Nagahiro, "Evaluation of Aneurysm Stability After Endovascular Embolization With Guglielmi Detachable Coils: Correlation Between Long-Term Stability and Volume Embolization Ratio," *Neurologia medico-chirurgica*, vol. 45, no. 11, pp. 561–566, 2005, ISSN: 0470-8105.

[43] M. Piotin, S. Mandai, K. J. Murphy, K. Sugiu, P. Gailloud, J. B. Martin, and D. A. Rüfenacht, "Dense packing of cerebral aneurysms: An in vitro study with detachable platinum coils," *American Journal of Neuroradiology*, vol. 21, no. 4, pp. 757–760, 2000, ISSN: 01956108.

[44] M. Piotin and R. Blanc, "Balloons and stents in the endovascular treatment of cerebral aneurysms: Vascular anatomy remodeled," *Frontiers in Neurology*, vol. 5 APR, no. April, pp. 1–9, 2014, ISSN: 16642295.

[45] J. K. Campos, B. V. Lien, A. S. Wang, and L. M. Lin, "Advances in endovascular aneurysm management: Coiling and adjunctive devices," *Stroke and Vascular Neurology*, vol. 5, no. 1, pp. 14–21, 2020, ISSN: 20598696.

[46] L. Pierot, L. Spelle, X. Leclerc, C. Cognard, A. Bonafé, and J. Moret, "Endovascular treatment of unruptured intracranial aneurysms: Comparison of safety of remodeling technique and standard treatment with coils," *Radiology*, vol. 251, no. 3, pp. 846–855, 2009, ISSN: 00338419.

[47] L. Fan, X. Tan, Y. Xiong, K. Zheng, Z. Li, D. Liu, M. Zhong, and B. Zhao, "Stent-assisted coiling versus coiling alone of ruptured anterior communicating artery aneurysms: A single-center experience," *Clinical Neurology and Neurosurgery*, vol. 144, pp. 96–100, 2016, ISSN: 18726968.

[48] Y. Hong, Y. J. Wang, Z. Deng, Q. Wu, and J. M. Zhang, "Stent-assisted coiling versus coiling in treatment of intracranial aneurysm: A systematic review and meta-analysis," *PLoS ONE*, vol. 9, no. 1, pp. 1–8, 2014, ISSN: 19326203.

[49] X. Zhang, Q. Zuo, H. Tang, G. Xue, P. Yang, R. Zhao, Q. Li, Y. Fang, Y. Xu, B. Hong, Q. Huang, and J. Liu, "Stent assisted coiling versus non-stent assisted coiling for the management of ruptured intracranial aneurysms: a meta-analysis and systematic review," *Journal of NeuroInterventional Surgery*, vol. 11, no. 5, pp. 489–496, 2019, ISSN: 1759-8478.

[50] S. Fischer, Z. Vajda, M. A. Perez, E. Schmid, N. Hopf, H. Bäzner, and H. Henkes, "Pipeline embolization device (PED) for neurovascular reconstruction: Initial experience in the treatment of 101 intracranial aneurysms and dissections," *Neuroradiology*, vol. 54, no. 4, pp. 369–382, 2012, ISSN: 00283940.

[51] L. Giacomini, R. L. Piske, C. E. Baccin, M. Barroso, A. F. Joaquim, and H. Tedeschi, "Neurovascular reconstruction with flow diverter stents for the treatment of 87 intracranial aneurysms: Clinical results," *Interventional Neuroradiology*, vol. 21, no. 3, pp. 292–299, 2015, ISSN: 1591-0199.

[52] Y. Zhang, Y. Zhou, P. Yang, J. Liu, Y. Xu, B. Hong, W. Zhao, Q. Chen, and Q. H. Huang, "Comparison of the flow diverter and stent-assisted coiling in large and giant aneurysms: safety and efficacy based on a propensity score-matched analysis," *European Radiology*, vol. 26, no. 7, pp. 2369–2377, 2016, ISSN: 14321084.

[53] A. A. Dmytriw, M. M. Salem, V. X. Yang, T. Krings, V. M. Pereira, J. M. Moore, and A. J. Thomas, "Endosaccular Flow Disruption: A New Frontier in Endovascular Aneurysm Management," *Clinical Neurosurgery*, vol. 86, no. 2, pp. 170–181, 2020, ISSN: 15244040.

[54] V. Da Ros, A. Bozzi, C. Comelli, V. Semeraro, S. Comelli, N. Lucarelli, N. Burdi, and R. Gandini, "Ruptured Intracranial Aneurysms Treated with Woven Endobridge Intrasaccular Flow Disruptor: A Multicenter Experience," *World Neurosurgery*, vol. 122, e498–e505, 2019, ISSN: 18788769.

[55] C. Papagiannaki, L. Spelle, A. C. Januel, A. Benaissa, J. Y. Gauvrit, V. Costalat, H. Desal, F. Turjman, S. Velasco, X. Barreau, P. Courtheoux, C. Cognard, D. Herbreteau, J. Moret, and L. Pierot, "WEB intrasaccular flow disruptor-Prospective, multicenter experience in 83 patients with 85 aneurysms," *American Journal of Neuroradiology*, vol. 35, no. 11, pp. 2106–2111, 2014, ISSN: 1936959X.

[56] A. S. Arthur, A. Molyneux, A. L. Coon, I. Saatci, I. Szikora, F. Baltacioglu, A. Sultan, D. Hoit, J. E. Delgado Almandoz, L. Elijovich, S. Cekirge, J. V. Byrne, and D. Fiorella, "The safety and effectiveness of the woven endobridge (web) system for the treatment of wide-necked bifurcation aneurysms: Final 12-month results of the pivotal web intrasaccular therapy (web-it) study," *Journal of NeuroInterventional Surgery*, vol. 11, no. 9, pp. 924–930, 2019, ISSN: 17598486.

[57] H. Ferral, "Hydrogel-Coated Coils: Product Description and Clinical Applications," *Seminars in Interventional Radiology*, vol. 32, no. 04, pp. 343–348, 2015, ISSN: 0739-9529.

[58] C. A. Taschner, R. Chapot, V. Costalat, P. Machi, P. Courthéoux, X. Barreau, J. Berge, L. Pierot, K. Kadziolka, B. Jean, R. Blanc, A. Biondi, H. Brunel, S. Gallas, A. Berlis, D. Herbreteau, J. Berkefeld, H. Urbach, S. Elsheikh, J. Fiehler, H. Desal, E. Graf, and A. Bonafé, "Second-generation hydrogel coils for the endovascular treatment of intracranial aneurysms a randomized controlled trial," *Stroke*, vol. 49, no. 3, pp. 667–674, 2018, ISSN: 15244628.

[59] P. M. White, S. C. Lewis, A. Gholkar, R. J. Sellar, H. Nahser, C. Cognard, L. Forrester, and J. M. Wardlaw, "Hydrogel-coated coils versus bare platinum coils for the endovascular treatment of intracranial aneurysms (HELPS): A randomised controlled trial," *The Lancet*, vol. 377, no. 9778, pp. 1655–1662, 2011, ISSN: 01406736.

[60] J. Raymond, R. Klink, M. Chagnon, S. L. Barnwell, A. J. Evans, J. Mocco, B. H. Hoh, A. S. Turk, R. D. Turner, H. Desal, D. Fiorella, S. Bracard, A. Weill, F. Guilbert, S. Lanthier, A. J. Fox, T. E. Darsaut, P. M. White, and D. Roy, "Hydrogel versus bare platinum coils in patients with large or recurrent aneurysms prone to recurrence after endovascular treatment: A randomized controlled trial," *American Journal of Neuroradiology*, vol. 38, no. 3, pp. 432–441, 2017, ISSN: 1936959X.

[61] T. Gunnarsson, F. C. Tong, P. Klurfan, C. M. Cawley, and J. E. Dion, "Angiographic and clinical outcomes in 200 consecutive patients with cerebral aneurysm treated with hydrogel-coated coils," *American Journal of Neuroradiology*, vol. 30, no. 9, pp. 1657–1664, 2009, ISSN: 01956108.

[62] S. Geyik, O. Ertugrul, K. Yavuz, P. Geyik, I. Saatci, and H. S. Cekirge, "Comparison of bioactive coils and bare platinum coils for treatment of intracranial aneurysms: a matched-pair analysis," *Journal of Neurosurgery*, vol. 112, no. 4, pp. 709–713, 2010, ISSN: 0022-3085.

[63] Y. Murayama, S. Tateshima, N. R. Gonzalez, and F. Vinuela, "Matrix and bioabsorbable polymeric coils accelerate healing of intracranial aneurysms: Long-term experimental study," *Stroke*, vol. 34, no. 8, pp. 2031–2037, 2003, ISSN: 00392499.

[64] S. W. Youn, S. H. Cha, H. S. Kang, Y. D. Cho, and M. H. Han, "Matrix 2 coils in embolization of intracranial aneurysms: 1-Year outcome and comparison with bare platinum coil group in a single institution," *American Journal of Neuroradiology*, vol. 32, no. 9, pp. 1745–1750, 2011, ISSN: 01956108.

[65] S. A. Ansari, E. J. Dueweke, Y. Kanaan, N. Chaudhary, D. Gandhi, B. G. Thompson, and J. J. Gemmete, "Embolization of intracranial aneurysms with second-generation Matrix-2 detachable coils: mid-term and long-term results," *Journal of NeuroInterventional Surgery*, vol. 3, no. 4, pp. 324–330, 2011, ISSN: 1759-8478.

[66] F. Brassel and D. Meila, "Evolution of Embolic Agents in Interventional Neuroradiology," *Clinical Neuroradiology*, vol. 25, no. S2, pp. 333–339, 2015, ISSN: 1869-1439.

[67] S. Vaidya, K. R. Tozer, and J. Chen, "An overview of embolic agents," *Seminars in Interventional Radiology*, vol. 25, no. 3, pp. 204–215, 2008, ISSN: 07399529.

[68] M. S. Kilani, J Izaaryene, F Cohen, A Varoquaux, J. Y. Gaubert, G Louis, A Jacquier, J. M. Bartoli, G Moulin, and V Vidal, "Ethylene vinyl alcohol copolymer (Onyx ®) in peripheral interventional radiology : Indications , advantages and limitations," *Diagnostic and Interventional Imaging*, vol. 96, no. 4, pp. 319–326, 2015, ISSN: 2211-5684.

[69] B. P. Walcott, J. L. Gerrard, R. G. Nogueira, B. V. Nahed, A. R. Terry, and C. S. Ogilvy, "Microsurgical retrieval of an endovascular microcatheter trapped during Onyx embolization of a cerebral arteriovenous malformation," *Journal of NeuroInterventional Surgery*, vol. 3, no. 1, pp. 77–79, 2011, ISSN: 1759-8478.

[70] K. Takeda, M. Pokorski, Y. Sato, Y. Oyamada, and Y. Okada, "Respiratory Toxicity of Dimethyl Sulfoxide," in, 2015, pp. 89–96.

[71] J. N. Rodriguez, W. Hwang, J. Horn, T. L. Landsman, A. Boyle, M. A. Wierzbicki, S. M. Hasan, D. Follmer, J. Bryant, W. Small, and D. J. Maitland, "Design and biocompatibility of endovascular aneurysm filling devices," *Journal of Biomedical Materials Research - Part A*, vol. 103, no. 4, pp. 1577–1594, 2015, ISSN: 15524965.

[72] J. Wu, C. Hu, Z. Tang, Q. Yu, X. Liu, and H. Chen, "Tissue-engineered Vascular Grafts: Balance of the Four Major Requirements," *Colloids and Interface Science Communications*, vol. 23, no. February, pp. 34–44, 2018, ISSN: 22150382.

[73] S. Pashneh-Tala, S. MacNeil, and F. Claeyssens, "The tissue-engineered vascular graft - Past, present, and future," *Tissue Engineering - Part B: Reviews*, vol. 22, no. 1, pp. 68–100, 2016, ISSN: 19373376.

[74] M. J. McClure, P. S. Wolfe, I. A. Rodriguez, and G. L. Bowlin, "Bioengineered vascular grafts: Improving vascular tissue engineering through scaffold design," *Journal of Drug Delivery Science and Technology*, vol. 21, no. 3, pp. 211–227, 2011, ISSN: 17732247.

[75] A. Tortoriello and G. Pedrizzetti, "Flow-tissue interaction with compliance mismatch in a model stented artery," *Journal of Biomechanics*, vol. 37, no. 1, pp. 1–11, 2004, ISSN: 00219290.

[76] L. Morris, F. Stefanov, and T. McGloughlin, "Stent graft performance in the treatment of abdominal aortic aneurysms: The influence of compliance and geometry," *Journal of Biomechanics*, vol. 46, no. 2, pp. 383–395, 2013, ISSN: 00219290.

[77] M. R. Diagbouga, S. Morel, P. Bijlenga, and B. R. Kwak, "Role of hemodynamics in initiation/growth of intracranial aneurysms," *European Journal of Clinical Investigation*, vol. 48, no. 9, e12992, 2018, ISSN: 00142972.

[78] Y. H. Ding, D. Dai, D. A. Lewis, H. J. Cloft, and D. F. Kallmes, "Angiographic and histologic analysis of experimental aneurysms embolized with platinum coils, Matrix, and HydroCoil," *American Journal of Neuroradiology*, vol. 26, no. 7, pp. 1757–1763, 2005, ISSN: 01956108.

[79] R. T. Higashida, B. J. Lahue, M. T. Torbey, L. N. Hopkins, E Leip, and D. F. Hanley, "Treatment of Unruptured Intracranial Aneurysms: A Nationwide Assessment of Effectiveness," *American Journal of Neuroradiology*, vol. 28, pp. 146–151, 2007.

[80] A. M. Spiotta, T. Bhalla, M. S. Hussain, T. Sivapatham, A. Batra, F. Hui, P. A. Rasmussen, and S. I. Moskowitz, "An Analysis of Inflation Times During Balloon-Assisted Aneurysm Coil Embolization and Ischemic Complications," *Stroke*, vol. 42, no. 4, pp. 1051–1055, 2011, ISSN: 0039-2499.

[81] S. Rudin, D. R. Bednarek, and K. R. Hoffmann, "Endovascular image-guided interventions (EIGIs)," *Medical Physics*, vol. 35, no. 1, pp. 301–309, 2008, ISSN: 00942405.

[82] J. E. Cohen, E. Yitshayek, J. Moshe, S. Grigoriadis, G. Raphaeli, S. Spektor, and G. Rajz, "Spontaneous thrombosis of cerebral aneurysms presenting with ischemic stroke," *Journal of Neuroscience*, vol. 254, pp. 95–98, 2007.

[83] J. H. Pang, Y. Farhatnia, F. Godarzi, A. Tan, J. Rajadas, B. G. Cousins, and A. M. Seifalian, "In situ Endothelialization : Bioengineering Considerations to Translation," *Small*, vol. 11, no. 47, pp. 6248–6264, 2015.

[84] J. Hu, H. Albadawi, B. W. Chong, A. R. Deipolyi, R. A. Sheth, A. Khademhosseini, and R. Oklu, "Advances in Biomaterials and Technologies for Vascular Embolization," *Advanced Materials*, vol. 31, no. 33, pp. 1–52, 2019, ISSN: 15214095.

[85] C. Y. Wang, J. Hu, R. A. Sheth, and R. Oklu, "Emerging embolic agents in endovascular embolization: an overview," *Progress in Biomedical Engineering*, vol. 2, no. 1, p. 012 003, 2020.

[86] A. Metcalfe, A. C. Desfaits, I. Salazkin, L. Yahia, W. M. Sokolowski, and J. Raymond, "Cold hibernated elastic memory foams for endovascular interventions," *Biomaterials*, vol. 24, no. 3, pp. 491–497, 2003, ISSN: 01429612.

[87] J. Ortega, D. Maitland, T. Wilson, W. Tsai, Ö. Savaş, and D. Saloner, "Vascular dynamics of a shape memory polymer foam aneurysm treatment technique," *Annals of Biomedical Engineering*, vol. 35, no. 11, pp. 1870–1884, 2007, ISSN: 00906964.

[88] M. Cabanlit, D. Maitland, T. Wilson, S. Simon, T. Wun, M. E. Gershwin, and J. Van De Water, "Polyurethane shape-memory polymers demonstrate functional biocompatibility in vitro," *Macromolecular Bioscience*, vol. 7, no. 1, pp. 48–55, 2007, ISSN: 16165187.

[89] W. Hwang, B. L. Volk, F. Akberali, P. Singhal, J. C. Criscione, and D. J. Maitland, "Estimation of aneurysm wall stresses created by treatment with a shape memory polymer foam device," *Biomechanics and Modeling in Mechanobiology*, vol. 11, no. 5, pp. 715–729, 2012, ISSN: 16177959.

[90] T. L. Landsman, R. L. Bush, A. Glowczwski, J. Horn, S. L. Jessen, E. Ungchusri, K. Diguette, H. R. Smith, S. M. Hasan, D. Nash, F. J. Clubb, and D. J. Maitland, "Design and verification of a shape memory polymer peripheral occlusion device," *Journal of the Mechanical Behavior of Biomedical Materials*, vol. 63, pp. 195–206, 2016, ISSN: 18780180.

[91] A. J. Boyle, M. A. Wierzbicki, S. Herting, A. C. Weems, A. Nathan, W. Hwang, and D. J. Maitland, "In vitro performance of a shape memory polymer foam-coated coil embolization device," *Medical Engineering Physics*, vol. 49, pp. 56–62, 2017, ISSN: 13504533.

[92] J. N. Rodriguez, Y. J. Yu, M. W. Miller, T. S. Wilson, J. Hartman, F. J. Clubb, B. Gentry, and D. J. Maitland, "Opacification of shape memory polymer foam designed for treatment of intracranial aneurysms," *Annals of Biomedical Engineering*, vol. 40, no. 4, pp. 883–897, 2012, ISSN: 00906964.

[93] J. N. Rodriquez, F. J. Clubb, T. S. Wilson, M. W. Miller, T. W. Fossum, J. Hartman, E. Tuun, P. Singhal, and D. J. Maitland, "In vivo tissue responses following implantation of shape memory polyurethane foam in a porcine aneurysm model," *Journal of Biomedical Materials Research Part A*, vol. 102, no. 5, pp. 1231–1242, 2014.

[94] J. Horn, W. Hwang, S. L. Jessen, B. K. Keller, M. W. Miller, E. Tuzun, J. Hartman, F. J. Clubb, and D. J. Maitland, "Comparison of shape memory polymer foam versus bare metal coil treatments in an in vivo porcine sidewall aneurysm model," *Journal of Biomedical Materials Research - Part B Applied Biomaterials*, vol. 105, no. 7, pp. 1892–1905, 2017, ISSN: 15524981.

[95] T. A. Becker, D. R. Kipke, and T. Brandon, "Calcium alginate gel: A biocompatible and mechanically stable polymer for endovascular embolization," *Journal of Biomedical Materials Research*, vol. 54, no. 1, pp. 76–86, 2001, ISSN: 00219304.

[96] T. A. Becker, M. C. Preul, W. D. Bichard, D. R. Kipke, and C. G. McDougall, "Preliminary investigation of calcium alginate gel as a biocompatible material for endovascular aneurysm embolization in vivo," *Neurosurgery*, vol. 60, no. 6, pp. 1119–1127, 2007, ISSN: 0148396X.

[97] B. P. Barnett, A. H. Hughes, S. Lin, A. Arepally, and P. H. Gailloud, "In Vitro Assessment of EmboGel and UltraGel Radiopaque Hydrogels for the Endovascular Treatment of Aneurysms," *Journal of Vascular and Interventional Radiology*, vol. 20, no. 4, pp. 507–512, 2009, ISSN: 10510443.

[98] S. A. Brady, E. K. Fox, C. Lally, and O. M. Clarkin, "Optimisation of a novel glass-alginate hydrogel for the treatment of intracranial aneurysms," *Carbohydrate Polymers*, vol. 176, pp. 227–235, 2017, ISSN: 01448617.

[99] H Takao, Y Murayama, T Saguchi, T Ishibashi, M Ebara, K Irie, H Yoshioka, Y Mori, S Ohtsubo, F Viñuela, and T Abe, "Endovascular treatment of experimental cerebral aneurysms using thermoreversible liquid embolic agents.," *Interventional neuroradiology : journal of peritherapeutic neuroradiology, surgical procedures and related neurosciences*, vol. 12, no. Suppl 1, pp. 154–157, 2006, ISSN: 1591-0199.

[100] A. Fatimi, J. M. Coutu, G. Cloutier, and S. Lerouge, "Rheological Studies of an Injectable Radiopaque Hydrogel for Embolization of Abdominal Aortic Aneurysms," *Advanced Materials Research*, vol. 409, pp. 129–135, 2011, ISSN: 1662-8985.

[101] A. Fatimi, P. Chabrot, S. Berrahmoune, J. M. Coutu, G. Soulez, and S. Lerouge, "A new injectable radiopaque chitosan-based sclerosing embolizing hydrogel for endovascular therapies," *Acta Biomaterialia*, vol. 8, no. 7, pp. 2712–2721, 2012, ISSN: 17427061.

[102] Q. V. Nguyen, M. S. Lee, J. S. Lym, Y. I. Kim, H. J. Jae, and D. S. Lee, "pH-Sensitive sulfamethazine-based hydrogels as potential embolic agents for transcatheter vascular embolization," *Journal of Materials Chemistry B*, vol. 4, no. 40, pp. 6524–6533, 2016, ISSN: 2050-750X.

[103] C. M. Riley, R. McLemore, M. C. Preul, and B. L. Vernon, "Gelling process differences in reverse emulsion, in situ gelling polymeric materials for intracranial aneurysm embolization, formulated with injectable contrast agents," *Journal of Biomedical Materials Research - Part B Applied Biomaterials*, vol. 96 B, no. 1, pp. 47–56, 2011, ISSN: 15524973.

[104] C. R. Brennecka, M. C. Preul, and B. L. Vernon, "In vitro delivery, cytotoxicity, swelling, and degradation behavior of a liquid-to-solid gelling polymer system for cerebral aneurysm embolization," *Journal of Biomedical Materials Research - Part B Applied Biomaterials*, vol. 100 B, no. 5, pp. 1298–1309, 2012, ISSN: 15524973.

[105] C. R. Brennecka, M. C. Preul, T. A. Becker, and B. L. Vernon, "In vivo embolization of lateral wall aneurysms in canines using the liquid-to-solid gelling PPODA-QT polymer system: 6-month pilot study: Laboratory investigation," *Journal of Neurosurgery*, vol. 119, no. 1, pp. 228–238, 2013, ISSN: 00223085.

[106] C. R. Brennecka, M. C. Preul, W. D. Bichard, and B. L. Vernon, "In vivo experimental aneurysm embolization in a swine model with a liquid-to-solid gelling polymer system: Initial biocompatibility and delivery strategy analysis," *World Neurosurgery*, vol. 78, no. 5, pp. 469–480, 2012, ISSN: 18788769.

[107] H. H. Bearat, M. C. Preul, and B. L. Vernon, "Cytotoxicity, in vitro models and preliminary in vivo study of dual physical and chemical gels for endovascular embolization of cerebral aneurysms," *Journal of Biomedical Materials Research Part A*, vol. 101A, no. 9, pp. 2515–2525, 2013, ISSN: 15493296.

[108] A. Ishikawa and A. Nakayama, "In Vitro Study of Photocurable Embolization Agent for Cerebral Aneurysms," *Journal of Biotechnology Biomaterials*, vol. 02, no. 02, 2012, ISSN: 2155952X.

[109] N. A. Peppas, P Bures, W Leobandung, and H Ichikawa, "Hydrogels in pharmaceutical formulations Hydrogels in pharmaceutical formulations," *European Journal of Pharmaceutics and Biopharmaceutics*, vol. 50, no. August, pp. 27–46, 2000.

[110] R. Dimatteo, N. J. Darling, and T. Segura, "In situ forming injectable hydrogels for drug delivery and wound repair," *Advanced Drug Delivery Reviews*, vol. 127, pp. 167–184, 2018, ISSN: 18728294.

[111] N. Oliva, J. Conde, K. Wang, and N. Artzi, "Designing Hydrogels for On-Demand Therapy," *Accounts of Chemical Research*, vol. 50, no. 4, pp. 669–679, 2017, ISSN: 15204898.

[112] J. Schmidt, J. Rowley, and H. Kong, "Hydrogels used for cell-based drug delivery," *Journal of Biomedical Materials Research - Part A*, vol. 87, no. 4, pp. 1113–1122, 2008, ISSN: 1549-3296.

[113] G. D. Nicodemus and S. J. Bryant, "Cell encapsulation in biodegradable hydrogels for tissue engineering applications," *Tissue Engineering - Part B: Reviews*, vol. 14, no. 2, pp. 149–165, 2008, ISSN: 19373368.

[114] G. Choe, J. Park, H. Park, and J. Y. Lee, "Hydrogel biomaterials for stem cell microencapsulation," *Polymers*, vol. 10, no. 9, pp. 1–17, 2018, ISSN: 20734360.

[115] A. Sivashanmugam, R. Arun Kumar, M. Vishnu Priya, S. V. Nair, and R. Jayakumar, "An overview of injectable polymeric hydrogels for tissue engineering," *European Polymer Journal*, vol. 72, pp. 543–565, 2015, ISSN: 00143057.

[116] Sebastián L. Vega, Mi Y. Kwon1 and J. A. Burdick1, "Recent Advances In Hydrogels For Cartilage Tissue," *Eur Cell Mate*, pp. 59–75, 2018.

[117] B. Peña, M. Laughter, S. Jett, T. J. Rowland, M. R. Taylor, L. Mestroni, and D. Park, "Injectable Hydrogels for Cardiac Tissue Engineering," *Macromolecular Bioscience*, vol. 18, no. 6, pp. 1–22, 2018, ISSN: 16165195.

[118] M. C. Catoira, L. Fusaro, D. Di Francesco, M. Ramella, and F. Boccafoschi, "Overview of natural hydrogels for regenerative medicine applications," *Journal of Materials Science: Materials in Medicine*, vol. 30, no. 10, 2019, ISSN: 15734838.

[119] D. A. Gyles, L. D. Castro, J. O. C. Silva, and R. M. Ribeiro-Costa, "A review of the designs and prominent biomedical advances of natural and synthetic hydrogel formulations," *European Polymer Journal*, vol. 88, no. 01, pp. 373–392, 2017, ISSN: 00143057.

[120] E. M. Ahmed, "Hydrogel: Preparation, characterization, and applications: A review," *Journal of Advanced Research*, vol. 6, no. 2, pp. 105–121, 2015, ISSN: 20901232.

[121] K. T. Nguyen and J. L. West, "Photopolymerizable hydrogels for tissue engineering applications," *Biomaterials*, vol. 23, no. 22, pp. 4307–4314, 2002, ISSN: 01429612. arXiv: arXiv:1011.1669v3.

[122] K. S. Anseth and J. a. Burdick, "New directions in photopolymerizable biomaterials," *MRS Bulletin*, vol. 27, no. 2, pp. 130–136, 2002, ISSN: 0883-7694.

[123] J. R. Choi, K. W. Yong, J. Y. Choi, and A. C. Cowie, "Recent advances in photo-crosslinkable hydrogels for biomedical applications," *BioTechniques*, vol. 66, no. 1, pp. 40–53, 2019, ISSN: 0736-6205.

[124] B. Amsden, "Photo-Crosslinking Methods to Design Hydrogels," *World Scientific*, pp. 201–218, 2016.

[125] S. Naficy, H. R. Brown, J. M. Razal, G. M. Spinks, and P. G. Whitten, "Progress toward robust polymer hydrogels," *Australian Journal of Chemistry*, vol. 64, no. 8, pp. 1007–1025, 2011, ISSN: 00049425.

[126] J. Elisseeff, K. Anseth, D. Sims, W. Mcintosh, M. Randolph, and R. Langer, "Transdermal photopolymerization for minimally invasive implantation," *Proceedings of the National Academy of Sciences of the United States of America*, vol. 96, no. 6, pp. 3104–3107, 1999, ISSN: 00278424.

[127] W. Tomal and J. Ortyl, "Water-soluble photoinitiators in biomedical applications," *Polymers*, vol. 12, no. 5, pp. 1–30, 2020, ISSN: 20734360.

[128] B. Fairbanks, M. Schwartz, C. Bowman, and K. Anseth, "Photoinitiated polymerisation of PEG-diacrylate with lithium phenyl-2,4,6-trimethylbenzoylphosphinate: polymerisation rate ans cytocompatibility.," *Biomaterials*, vol. 30, no. 35, pp. 6702–6707, 2009.

[129] P. Occhetta, R. Visone, L. Russo, L. Cipolla, M. Moretti, and M. Rasponi, *VA-086 methacrylate gelatine photopolymerizable hydrogels: A parametric study for highly biocompatible 3D cell embedding*, 2015.

[130] C. T. Meereis, F. B. Leal, G. S. Lima, R. V. De Carvalho, E. Piva, and F. A. Ogliari, "BAPO as an alternative photoinitiator for the radical polymerization of dental resins," *Dental Materials*, vol. 30, no. 9, pp. 945–953, 2014, ISSN: 01095641.

[131] J. Wang, S. Stanic, A. A. Altun, M. Schwentenwein, K. Dietliker, L. Jin, J. Stampfl, S. Baudis, R. Liska, and H. Grützmacher, "A highly efficient waterborne photoinitiator for visible-light-induced three-dimensional printing of hydrogels," *Chemical Communications*, 2018, ISSN: 1359-7345.

[132] W. M. Palin, M. A. Hadis, J. G. Leprince, G. Leloup, L. Boland, G. J. Fleming, G. Krastl, and D. C. Watts, "Reduced polymerization stress of MAPO-containing resin composites with increased curing speed, degree of conversion and mechanical properties," *Dental Materials*, vol. 30, no. 5, pp. 507–516, 2014, ISSN: 01095641.

[133] H. Shih and C. C. Lin, "Visible-light-mediated thiol-ene hydrogelation using eosin-Y as the only photoinitiator," *Macromolecular Rapid Communications*, vol. 34, no. 3, pp. 269–273, 2013, ISSN: 10221336.

[134] J. A. Killion, L. M. Geever, D. M. Devine, J. E. Kennedy, and C. L. Higginbotham, "Mechanical properties and thermal behaviour of PEGDMA hydrogels for potential bone regeneration application," *Journal of the Mechanical Behavior of Biomedical Materials*, vol. 4, no. 7, pp. 1219–1227, 2011, ISSN: 17516161.

[135] J. Zhu, "Bioactive modification of poly(ethylene glycol) hydrogels for tissue engineering," *Biomaterials*, vol. 31, no. 17, pp. 4639–4656, 2010, ISSN: 01429612.

[136] T. Liu, S. Liu, K. Zhang, J. Chen, and N. Huang, "Review Article Endothelialization of implanted cardiovascular biomaterial surfaces : The development from in vitro to in vivo," *Journal of Biomedical Materials Research - Part A*, vol. 102A, pp. 3754–3772, 2014.

[137] M. Avci-Adali, G. Ziemer, and H. P. Wendel, "Induction of EPC homing on biofunctionalized vascular grafts for rapid in vivo self-endothelialization - A review of current strategies," *Biotechnology Advances*, vol. 28, no. 1, pp. 119–129, 2010, ISSN: 07349750.

[138] A. de Mel, G. Jell, M. M. Stevens, and A. M. Seifalian, "Biofunctionalization of biomaterials for accelerated in situ endothelialization: A review," *Biomacromolecules*, vol. 9, no. 11, pp. 2969–2979, 2008, ISSN: 15257797.

[139] D. Missirlis and J. P. Spatz, "Combined effects of PEG hydrogel elasticity and cell-adhesive coating on fibroblast adhesion and persistent migration," *Biomacromolecules*, vol. 15, no. 1, pp. 195–205, 2014, ISSN: 15257797.

[140] T. D. Sargeant, A. P. Desai, S. Banerjee, A. Agawu, and J. B. Stopek, "An in situ forming collagen-PEG hydrogel for tissue regeneration," *Acta Biomaterialia*, vol. 8, no. 1, pp. 124–132, 2012, ISSN: 17427061.

[141] J. X. Chen, J. Yuan, Y. L. Wu, P. Wang, P. Zhao, G. Z. Lv, and J. H. Chen, "Fabrication of tough poly(ethylene glycol)/collagen double network hydrogels for tissue engineering," *Journal of Biomedical Materials Research - Part A*, vol. 106, no. 1, pp. 192–200, 2018, ISSN: 15524965.

[142] J. Liang, Z. Guo, A. Timmerman, D. Grijpma, and A. Poot, "Enhanced mechanical and cell adhesive properties of photo-crosslinked PEG hydrogels by incorporation of gelatin in the networks," *Biomedical Materials*, vol. 14, no. 2, 2019, ISSN: 1748605X.

[143] C. B. Hutson, J. W. Nichol, H. Aubin, H. Bae, S. Yamanlar, S. Al-Haque, S. T. Koshy, and A. Khademhosseini, "Synthesis and characterization of tunable poly(ethylene glycol): gelatin methacrylate composite hydrogels.," *Tissue engineering. Part A*, vol. 17, no. 13-14, pp. 1713–23, 2011, ISSN: 1937-335X.

[144] D. L. Hern and J. A. Hubbell, "Incorporation of adhesion peptides into nonadhesive hydrogels useful for tissue resurfacing," *Journal of Biomedical Materials Research*, vol. 39, no. 2, pp. 266–276, 1998, ISSN: 00219304.

[145] R. R. Asawa, J. C. Belkowski, D. A. Schmitt, E. M. Hernandez, A. E. Babcock, C. K. Lochner, H. N. Baca, C. M. Rylatt, I. S. Steffes, J. J. VanSteenburg, K. E. Diaz, and D. M. Doroski, "Transient cellular adhesion on poly(ethyleneglycol)-dimethacrylate hydrogels facilitates a novel stem cell bandage approach," *PLoS ONE*, vol. 13, no. 8, pp. 1–20, 2018, ISSN: 19326203.

[146] W. J. Seeto, Y. Tian, and E. A. Lipke, "Peptide-grafted poly(ethylene glycol) hydrogels support dynamic adhesion of endothelial progenitor cells," *Acta Biomaterialia*, vol. 9, no. 9, pp. 8279–8289, 2013, ISSN: 17427061.

[147] A. Janse van Rensburg, N. H. Davies, A. Oosthuysen, C. Chokoza, P. Zilla, and D. Bezuidenhout, "Improved vascularization of porous scaffolds through growth factor delivery from heparinized polyethylene glycol hydrogels," *Acta Biomaterialia*, vol. 49, pp. 89–100, 2017, ISSN: 18787568.

[148] D. S. Benoit and K. S. Anseth, "Heparin functionalized PEG gels that modulate protein adsorption for hMSC adhesion and differentiation," *Acta Biomaterialia*, vol. 1, no. 4, pp. 461–470, 2005, ISSN: 17427061.

[149] T. Nie, R. E. Akins, and K. L. Kiick, "Production of heparin-containing hydrogels for modulating cell responses," *Acta Biomaterialia*, vol. 5, no. 3, pp. 865–875, 2009, ISSN: 17427061.

[150] S. Ouasti, R. Donno, F. Cellesi, M. J. Sherratt, G. Terenghi, and N. Tirelli, "Network connectivity, mechanical properties and cell adhesion for hyaluronic acid/PEG hydrogels," *Biomaterials*, vol. 32, no. 27, pp. 6456–6470, 2011, ISSN: 01429612.

[151] J. Christoffersson, C. Aronsson, M. Jury, R. Selegård, D. Aili, and C. F. Mandenius, "Fabrication of modular hyaluronan-PEG hydrogels to support 3D cultures of hepatocytes in a perfused liver-on-a-chip device," *Biofabrication*, vol. 11, no. 1, 2019, ISSN: 17585090.

[152] J. E. Leslie-Barbick, J. J. Moon, and J. L. West, "Covalently-immobilized vascular endothelial growth factor promotes endothelial cell tubulogenesis in poly(ethylene glycol) diacrylate hydrogels," *Journal of Biomaterials Science, Polymer Edition*, vol. 20, no. 12, pp. 1763–1779, 2009, ISSN: 15685624.

[153] S. A. DeLong, J. J. Moon, and J. L. West, "Covalently immobilized gradients of bFGF on hydrogel scaffolds for directed cell migration," *Biomaterials*, vol. 26, no. 16, pp. 3227–3234, 2005, ISSN: 01429612.

[154] N. Chen, Z. Zhang, B. Soontornworajit, J. Zhou, and Y. Wang, "Cell adhesion on an artificial extracellular matrix using aptamer-functionalized PEG hydrogels," *Biomaterials*, vol. 33, no. 5, pp. 1353–1362, 2012, ISSN: 01429612.

[155] M. Filippi, B. Dasen, J. Guerrero, F. Garello, G. Isu, G. Born, M. Ehrbar, I. Martin, and A. Scherberich, "Magnetic nanocomposite hydrogels and static magnetic field stimulate the osteoblastic and vasculogenic profile of adipose-derived cells," *Biomaterials*, vol. 223, no. April, p. 119 468, 2019, ISSN: 18785905.

[156] K. Ono, M. Ishihara, Y. Ozeki, H. Deguchi, M. Sato, Y. Saito, H. Yura, M. Sato, M. Kikuchi, A. Kurita, and T. Maehara, "Experimental evaluation of photocrosslinkable chitosan as a biologic adhesive with surgical applications," *Surgery*, vol. 130, no. 5, pp. 844–850, 2001, ISSN: 00396060.

[157] Y. Hong, F. Zhou, Y. Hua, X. Zhang, C. Ni, D. Pan, Y. Zhang, D. Jiang, L. Yang, Q. Lin, Y. Zou, D. Yu, D. E. Arnot, X. Zou, L. Zhu, S. Zhang, and H. Ouyang, "A strongly adhesive hemostatic hydrogel for the repair of arterial and heart bleeds," *Nature Communications*, vol. 10, no. 1, pp. 1–11, 2019, ISSN: 20411723.

[158] E. van Haaften, C. Bouten, and N. Kurniawan, "Vascular Mechanobiology: Towards Control of In Situ Regeneration," *Cells*, vol. 6, no. 3, p. 19, 2017, ISSN: 2073-4409.

[159] E. Lehmann, K. Hopkins, and R. Gosling, "Aortic compliance measurements using doppler ultrasound: In vivo biochemical correlates," *Ultrasound in Medicine Biology*, vol. 19, no. 9, pp. 683–710, 1993, ISSN: 03015629.

[160] X. Ma, Z. He, L. Li, G. Liu, Q. Li, D. Yang, Y. Zhang, and N. Li, "Development and in vivo validation of tissue-engineered, small-diameter vascular grafts from decellularized aortae of fetal pigs and canine vascular endothelial cells," *Journal of Cardiothoracic Surgery*, vol. 12, no. 1, pp. 1–11, 2017, ISSN: 17498090.

[161] B. Ciszek, K. Cieslicki, P. Krajewski, and S. K. Piechnik, "Critical pressure for arterial wall rupture in major human cerebral arteries," *Stroke*, vol. 44, no. 11, pp. 3226–3228, 2013, ISSN: 00392499.

[162] L. A. Eadie, G. Soulez, M. W. King, and L. W. Tse, "Graft durability and fatigue after in situ fenestration of endovascular stent grafts using radiofrequency puncture and balloon dilatation," *European Journal of Vascular and Endovascular Surgery*, vol. 47, no. 5, pp. 501–508, 2014, ISSN: 15322165.

[163] J. Lord, H. Britton, S. G. Spain, and A. L. Lewis, "Advancements in the development on new liquid embolic agents for use in therapeutic embolisation," *Journal of Materials Chemistry B*, pp. 8207–8218, 2020, ISSN: 2050-750X.

[164] "Biological evaluation of medical devices - ISO 10993-4."

[165] R. Galante, T. J. Pinto, R. Colaço, and A. P. Serro, "Sterilization of hydrogels for biomedical applications: A review," *Journal of Biomedical Materials Research - Part B Applied Biomaterials*, vol. 106, no. 6, pp. 2472–2492, 2018, ISSN: 15524981.

[166] G. Lippi, D. Adcock, A. M. Simundic, A. Tripodi, and E. J. Favaloro, "Critical laboratory values in hemostasis: toward consensus," *Annals of Medicine*, vol. 49, no. 6, pp. 455–461, 2017, ISSN: 13652060.

[167] M. Pai, K. A. Moffat, E. Plumhoff, and C. P. Hayward, "Critical values in the coagulation laboratory," *American Journal of Clinical Pathology*, vol. 136, no. 6, pp. 836–841, 2011, ISSN: 00029173.

[168] M. Weber, H. Steinle, S. Golombek, L. Hann, C. Schlensak, H. P. Wendel, and M. Avci-Adali, "Blood-Contacting Biomaterials: In Vitro Evaluation of the Hemocompatibility," *Frontiers in Bioengineering and Biotechnology*, vol. 6, no. July, 2018, ISSN: 2296-4185.

[169] O. Poupart, R. Conti, A. Schmocker, L. Pancaldi, C. Moser, K. M. Nuss, M. S. Sakar, T. Dobrocky, H. Grützmacher, P. J. Mosimann, and D. P. Pioletti, "Pulsatile Flow-Induced Fatigue-Resistant Photopolymerizable Hydrogels for the Treatment of Intracranial Aneurysms," *Frontiers in Bioengineering and Biotechnology*, vol. 8, no. January, pp. 1–12, 2021.

[170] N. Uchiyama, S. Kida, M. Nomura, M. Hasegawa, T. Yamashima, J. Yamashita, and O. Matsui, "Significance of Volume Embolization Ratio as a Predictor of Recanalization on Endovascular Treatment of Cerebral Aneurysms with Guglielmi Detachable Coils," *Interventional Neuroradiology*, vol. 6, no. Suppl 1, pp. 59–63, 2000, ISSN: 1591-0199.

[171] N. Corrigan, J. Yeow, P. Judzewitsch, J. Xu, and C. Boyer, "Seeing the Light: Advancing Materials Chemistry through Photopolymerization," *Angewandte Chemie International Edition*, vol. 58, no. 16, pp. 5170–5189, 2019, ISSN: 14337851.

[172] G. Burke, V. Barron, T. Geever, L. Geever, D. M. Devine, and C. L. Higginbotham, "Evaluation of the materials properties, stability and cell response of a range of PEGDMA hydrogels for tissue engineering applications," *Journal of the Mechanical Behavior of Biomedical Materials*, vol. 99, pp. 1–10, 2019, ISSN: 17516161.

[173] L. Wang, S. Wu, G. Cao, Y. Fan, N. Dunne, and X. Li, "Biomechanical studies on biomaterial degradation and co-cultured cells: mechanisms, potential applications, challenges and prospects," *Journal of Materials Chemistry B*, vol. 7, no. 47, pp. 7439–7459, 2019, ISSN: 20507518.

[174] H. Kamata, X. Li, U. I. Chung, and T. Sakai, "Design of Hydrogels for Biomedical Applications," *Advanced Healthcare Materials*, vol. 4, no. 16, pp. 2360–2374, 2015, ISSN: 21922659.

[175] S. Lin-Gibson, S. Bencherif, J. A. Cooper, S. J. Wetzel, J. M. Antonucci, B. M. Vogel, F. Horkay, and N. R. Washburn, "Synthesis and Characterization of PEG Dimethacrylates and Their Hydrogels," *Biomacromolecules*, vol. 5, no. 4, pp. 1280–1287, 2004, ISSN: 1525-7797.

[176] P.-E. Schmocker, Andreas and Khoushabi, Azadeh and Frauchiger, Daniela A. and Gantenbein, Benjamin and Schizas, Constantin and Moser, Christophe and Bourban and P. D. P., "A photopolymerized composite hydrogel and surgical implanting tool for a nucleus pulposus replacement," *Biomaterials*, vol. 88, pp. 110–119, 2016.

[177] ASTM, "Standard Test Method for Strength Properties of Tissue Adhesives in Tension," *Annual Book of ASTM Standards*, vol. 05, no. Reapproved 2010, pp. 3–7, 2011.

[178] O. Poupart, A. Schmocker, R. Conti, C. Moser, K. M. Nuss, H. Grützmacher, P. J. Mosimann, and D. P. Pioletti, "In vitro Implementation of Photopolymerizable Hydrogels as a Potential Treatment of Intracranial Aneurysms," *Frontiers in Bioengineering and Biotechnology*, vol. 8, no. April, pp. 1–13, 2020.

[179] L. Zarrinkoob, K. Ambarki, A. Wåhlin, R. Birgander, A. Eklund, and J. Malm, "Blood flow distribution in cerebral arteries," *Journal of Cerebral Blood Flow and Metabolism*, vol. 35, no. January, pp. 648–654, 2015, ISSN: 15597016.

[180] A. M. Netlyukh, V. M. Shevaga, L. M. Yakovenko, A. V. Payenok, V. M. Salo, and O. J. Kobyletskiy, "Invasive Intracranial Arterial Pressure Monitoring During Endovascular Cerebral Aneurysms Embolization for Cerebral Perfusion Evaluation," in *Neurovascular Events After Subarachnoid Hemorrhage*, Cham: Springer International Publishing, 2015, pp. 177–181.

[181] C. Sherif, G. Kleinpeter, G. Mach, M. Loyoddin, T. Haider, R. Plasenzotti, H. Bergmeister, A. Di Ieva, D. Gibson, and M. Krssak, "Evaluation of cerebral aneurysm wall thickness in experimental aneurysms: Comparison of 3T-MR imaging with direct microscopic measurements," *Acta Neurochirurgica*, vol. 156, no. 1, pp. 27–34, 2014, ISSN: 00016268.

[182] J. Krejza, M. Arkuszewski, S. E. Kasner, J. Weigele, A. Ustymowicz, R. W. Hurst, B. L. Cucchiara, and S. R. Messe, "Carotid artery diameter in men and women and the relation to body and neck size," *Stroke*, vol. 37, no. 4, pp. 1103–1105, 2006, ISSN: 00392499.

[183] R. Blankena, R. Kleinloog, B. H. Verweij, P. Van Ooij, B. Ten Haken, P. R. Luijten, G. J. E. Rinkel, and J. J. M. Zwanenburg, "Thinner regions of intracranial aneurysm wall correlate with regions of higher wall shear stress: A 7T MRI study," *American Journal of Neuroradiology*, vol. 37, no. 7, pp. 1310–1317, 2016, ISSN: 1936959X.

[184] C. Grochowski, J. Litak, B. Kulesza, P. Szmygin, D. Ziemianek, P. Kamieniak, D. Szczepanek, R. Rola, and T. Trojanowski, "Size and location correlations with higher rupture risk of intracranial aneurysms," *Journal of Clinical Neuroscience*, vol. 48, pp. 181–184, 2018, ISSN: 15322653.

[185] Q. T. Nguyen, Y. Hwang, A. C. Chen, S. Varghese, and R. L. Sah, "Cartilage-like mechanical properties of poly (ethylene glycol)-diacrylate hydrogels," *Biomaterials*, vol. 33, no. 28, pp. 6682–6690, 2012, ISSN: 01429612.

[186] J. J. Roberts, A. Earnshaw, V. L. Ferguson, and S. J. Bryant, "Comparative study of the viscoelastic mechanical behavior of agarose and poly(ethylene glycol) hydrogels," *Journal of Biomedical Materials Research - Part B Applied Biomaterials*, vol. 99 B, no. 1, pp. 158–169, 2011, ISSN: 15524973.

[187] A. Khoushabi, A. Schmocker, D. Pioletti, C. Moser, C. Schizas, J. Månson, and P. Bourban, "Photo-polymerization, swelling and mechanical properties of cellulose fibre reinforced poly(ethylene glycol) hydrogels," *Composites Science and Technology*, vol. 119, pp. 93–99, 2015, ISSN: 02663538.

[188] D. L. Kurdikar and N. A. Peppas, "A kinetic study of diacrylate photopolymerizations," *Polymer*, vol. 35, no. 5, 1994.

[189] D. A. Rennerfeldt, A. N. Renth, Z. Talata, S. H. Gehrke, and M. S. Detamore, "Tuning mechanical performance of poly(ethylene glycol) and agarose interpenetrating network hydrogels for cartilage tissue engineering," *Biomaterials*, vol. 34, no. 33, pp. 8241–8257, 2013, ISSN: 01429612.

[190] A. Khoushabi, C. Wyss, B. Caglar, D. Pioletti, and P.-E. Bourban, "Tailoring swelling to control softening mechanisms during cyclic loading of PEG/cellulose hydrogel composites," *Composites Science and Technology*, vol. 168, pp. 88–95, 2018, ISSN: 02663538.

[191] C. B. Stanley and H. H. Strey, "Measuring osmotic pressure of poly(ethylene glycol) solutions by sedimentation equilibrium ultracentrifugation," *Macromolecules*, vol. 36, no. 18, pp. 6888–6893, 2003, ISSN: 00249297.

[192] M. Waqas, M. Mokin, J. Lim, K. Vakharia, M. E. Springer, K. M. Meess, R. W. Ducharme, C. N. Ionita, S. V. S. Nagesh, L. C. Gutierrez, K. V. Snyder, J. M. Davies, E. I. Levy, and A. H. Siddiqui, "Design and Physical Properties of 3-Dimensional Printed Models Used for Neurointervention: A Systematic Review of the Literature," *Neurosurgery*, vol. 0, no. 0, pp. 1–9, 2020, ISSN: 0148-396X.

[193] I. O. Torres and N. De Luccia, "A simulator for training in endovascular aneurysm repair: The use of three dimensional printers," *European Journal of Vascular and Endovascular Surgery*, vol. 54, no. 2, pp. 247–253, 2017, ISSN: 15322165.

[194] K. Baráth, F. Cassot, D. A. Rüfenacht, and J. H. D. Fasel, "Anatomically shaped internal carotid artery aneurysm in vitro model for flow analysis to evaluate stent effect.," *AJNR. American journal of neuroradiology*, vol. 25, no. 10, pp. 1750–1759, 2004, ISSN: 0195-6108.

[195] Y. Liu, Q. Gao, S. Du, Z. Chen, J. Fu, B. Chen, Z. Liu, and Y. He, "Fabrication of cerebral aneurysm simulator with a desktop 3D printer," *Scientific Reports*, vol. 7, no. 1, p. 44 301, 2017, ISSN: 2045-2322.

[196] J. Chueh, A. Wakhloo, and M. Gounis, "Neurovascular Modeling: Small-Batch Manufacturing of Silicone Vascular Replicas," *American Journal of Neuroradiology*, vol. 30, no. 6, pp. 1159–1164, 2009, ISSN: 0195-6108.

[197] N. Kaneko, T. Mashiko, T. Ohnishi, M. Ohta, K. Namba, E. Watanabe, and K. Kawai, "Manufacture of patient-specific vascular replicas for endovascular simulation using fast, low-cost method," *Scientific Reports*, vol. 6, no. July, pp. 1–7, 2016, ISSN: 20452322.

[198] M. Palanca, G. Tozzi, and L. Cristofolini, "The use of digital image correlation in the biomechanical area : a review," *International Biomechanics*, vol. 5432, pp. 1–21, 2016.

[199] K Genovese, M. J. Collins, Y. U. Lee, and J. D. Humphrey, "Regional Finite Strains in an Angiotensin-II Induced Mouse Model of Dissecting Abdominal Aortic Aneurysms," *Cardiovascular Eng Technol*, vol. 3, no. 2, pp. 194–202, 2012.

[200] J. Rodrigues, Raquel O. and Pinho, Diana and Bento, David and Lima, Rui and Ribeiro, "Wall expansion assessment of an intracranial aneurysm modelby a 3D Digital Image Correlation System," *Measurement*, vol. 88, pp. 262–270, 2016.

[201] V. Vijayakumar and J. S. Jayakumar, "Fluid–Structure Interaction Simulation: Effect of Endovascular Coiling in Cerebral Aneurysms Considering Anisotropically Deformable Walls," in *Advances in Fluid and Thermal Engineering*, 2019, pp. 435–443.

[202] D. Dai, Y.-H. Ding, I. Rezek, D. F. Kallmes, and R. Kadirvel, "Characterizing patterns of endothelialization following coil embolization: a whole-mount, dual immunostaining approach," *Journal of NeuroInterventional Surgery*, vol. 8, no. 4, pp. 402–406, 2016, ISSN: 1759-8478.

[203] R. Bai, J. Yang, and Z. Suo, "Fatigue of hydrogels," *European Journal of Mechanics, A/Solids*, vol. 74, no. December 2018, pp. 337–370, 2019, ISSN: 09977538.

[204] V. N. Yamaki, N. M. Cancelliere, P. Nicholson, M. Rodrigues, I. Radovanovic, M. Sungur, T. Krings, and V. M. Pereira, "Biomodex patient-specific brain aneurysm models : the value of simulation for first in-human experiences using new devices and robotics," *J. NeuroIntervent. Surg.*, pp. 1–7, 2020.

[205] M. Mokin, M. Waqas, S. V. S. Nagesh, N. V. Karkhanis, E. I. Levy, C. N. Ionita, and A. H. Siddiqui, "Assessment of distal access catheter performance during neuroendovascular procedures: Measuring force in three-dimensional patient specific phantoms," *Journal of NeuroInterventional Surgery*, vol. 11, no. 6, pp. 619–623, 2019, ISSN: 17598486.

[206] N. M. Cancelliere, P. Nicholson, I. Radovanovic, K. M. Mendes, E. Orru, T. Krings, and V. M. Pereira, "Comparison of intra-aneurysmal flow modification using optical flow imaging to evaluate the performance of Evolve and Pipeline flow diverting stents," *Journal of NeuroInterventional Surgery*, pp. 1–4, 2020, ISSN: 17598486.

[207] K. Makino, R. Idenuma, T. Murakami, and H. Ohshima, "Design of a rate- and time-programming drug release device using a hydrogel: Pulsatile drug release from κ-carrageenan hydrogel device by surface erosion of the hydrogel," *Colloids and Surfaces B: Biointerfaces*, vol. 20, no. 4, pp. 355–359, 2001, ISSN: 09277765.

[208] P. S. Gade, K. Lee, B. N. Pfaff, Y. Wang, and A. M. Robertson, "Degradation and erosion mechanisms of bioresorbable porous acellular vascular grafts: An in vitro investigation," *Journal of the Royal Society Interface*, vol. 14, no. 132, 2017, ISSN: 17425662.

[209] H. Omidian, J. G. Rocca, and K. Park, "Advances in superporous hydrogels," *Journal of Controlled Release*, vol. 102, no. 1, pp. 3–12, 2005, ISSN: 01683659.

[210] F. Zhao, X. Qin, and S. Feng, "Preparation of microgel/sodium alginate composite granular hydrogels and their Cu2+ adsorption properties," *RSC Advances*, vol. 6, no. 102, pp. 100 511–100 518, 2016, ISSN: 20462069.

[211] A. Dalmoro, A. A. Barba, M. Grassi, G. Grassi, and G. Lamberti, "In situ coronary stent paving by Pluronic F127-alginate gel blends: Formulation and erosion tests," *Journal of Biomedical Materials Research Part B: Applied Biomaterials*, vol. 104, no. 5, pp. 1013–1022, 2016, ISSN: 15524973.

[212] A. Bar, E. Ruvinov, and S. Cohen, "Live imaging flow bioreactor for the simulation of articular cartilage regeneration after treatment with bioactive hydrogel," *Biotechnology and Bioengineering*, vol. 115, no. 9, pp. 2205–2216, 2018, ISSN: 10970290.

[213] Health Quality Ontario, *Coil embolization for intracranial aneurysms: an evidence-based analysis.* 1. 2006, vol. 6, pp. 1–114, ISBN: 1424903351.

[214] A. F. Hulsbergen, L. Mirzaei, A. T. van der Boog, T. R. Smith, I. S. Muskens, M. L. Broekman, R. A. Mekary, and W. A. Moojen, "Long-Term Durability of Open Surgical versus Endovascular Repair of Intracranial Aneurysms: A Systematic Review and Meta-Analysis," *World Neurosurgery*, vol. 132, e820–e833, 2019, ISSN: 18788750.

[215] T. R. Smith, D. J. Cote, H. H. Dasenbrock, Y. J. Hamade, S. G. Zammar, N. E. El Tecle, H. H. Batjer, and B. R. Bendok, "Comparison of the Efficacy and Safety of Endovascular Coiling Versus Microsurgical Clipping for Unruptured Middle Cerebral Artery Aneurysms: A Systematic Review and Meta-Analysis," *World Neurosurgery*, vol. 84, no. 4, pp. 942–953, 2015, ISSN: 18788750.

[216] K. Ravindran, M. Salem, A. Alturki, A. Thomas, C. Ogilvy, and J. Moore, "Endothelialization following Flow Diversion for Intracranial Aneurysms: A Systematic Review," *American Journal of Neuroradiology*, vol. 40, no. 2, pp. 295–301, 2019, ISSN: 0195-6108.

[217] M. Abdihalim, M. Watanabe, S. A. Chaudhry, B. Jagadeesan, M. F. K. Suri, and A. I. Qureshi, "Are Coil Compaction and Aneurysmal Growth Two Distinct Etiologies Leading to Recurrence Following Endovascular Treatment of Intracranial Aneurysm?" *Journal of Neuroimaging*, vol. 24, no. 2, pp. 171–175, 2014, ISSN: 10512284.

[218] R. Tulamo, J. Frosen, J. Hernesniemi, and M. Niemela, "Inflammatory changes in the aneurysm wall: a review," *Journal of NeuroInterventional Surgery*, vol. 2, no. 2, pp. 120–130, 2010, ISSN: 1759-8478.

[219] S. Marbacher, M. Niemelä, J. Hernesniemi, and J. Frösén, "Recurrence of endovascularly and microsurgically treated intracranial aneurysms—review of the putative role of aneurysm wall biology," *Neurosurgical Review*, vol. 42, no. 1, pp. 49–58, 2019, ISSN: 0344-5607.

[220] *Onyx Liquid Embolic System Onyx HD-500*.

[221] Y. Zhang, J. Yu, K. Ren, J. Zuo, J. Ding, and X. Chen, "Thermosensitive Hydrogels as Scaffolds for Cartilage Tissue Engineering," *Biomacromolecules*, vol. 20, no. 4, pp. 1478–1492, 2019, ISSN: 1525-7797.

[222] S. Li, S. Dong, W. Xu, S. Tu, L. Yan, C. Zhao, J. Ding, and X. Chen, "Antibacterial Hydrogels," *Advanced Science*, vol. 5, no. 5, p. 1 700 527, 2018, ISSN: 21983844.

[223] T. Dimatteo, Robert and Darling, Nicole J. and Segura, "In situ forming injectable hydrogels for drug delivery and wound repair," *Advanced Drug Delivery Reviews*, vol. 127, pp. 167–184, 2018.

[224] X. Shi, H. Gao, F. Dai, X. Feng, and W. Liu, "A thermoresponsive supramolecular copolymer hydrogel for the embolization of kidney arteries," *Biomaterials Science*, vol. 4, no. 11, pp. 1673–1681, 2016, ISSN: 2047-4830.

[225] H. Zhao, C. Zheng, G. Feng, Y. Zhao, H. Liang, H. Wu, G. Zhou, B. Liang, Y. Wang, and X. Xia, "Temperature-Sensitive poly(N -Isopropylacrylamide-Co-Butyl Methylacrylate) Nanogel as an Embolic Agent: Distribution, Durability of Vascular Occlusion, and Inflammatory Reactions in the Renal Artery of Rabbits," *American Journal of Neuroradiology*, vol. 34, no. 1, pp. 169–176, 2013, ISSN: 0195-6108.

[226] L. Weng, N. Rostambeigi, N. D. Zantek, P. Rostamzadeh, M. Bravo, J. Carey, and J. Golzarian, "An in situ forming biodegradable hydrogel-based embolic agent for interventional therapies," *Acta Biomaterialia*, vol. 9, no. 9, pp. 8182–8191, 2013, ISSN: 17427061.

[227] F. Zhou, L. Chen, Q. An, L. Chen, Y. Wen, F. Fang, W. Zhu, and T. Yi, "Novel Hydrogel Material as a Potential Embolic Agent in Embolization Treatments," *Scientific Reports*, vol. 6, no. 1, p. 32 145, 2016, ISSN: 2045-2322.

[228] S. Doran, O. S. Taskin, M. A. Tasdelen, and Y. Yağci, "Controlled Photopolymerization and Novel Architectures," in *Dyes and Chromophores in Polymer Science*, Hoboken, NJ, USA: John Wiley Sons, Inc., 2015, pp. 81–121.

[229] N. E. Fedorovich, M. H. Oudshoorn, D. van Geemen, W. E. Hennink, J. Alblas, and W. J. A. Dhert, "The effect of photopolymerization on stem cells embedded in hydrogels.," *Biomaterials*, vol. 30, no. 3, pp. 344–53, 2009, ISSN: 1878-5905.

[230] R. P. Sinha and D. P. Häder, "UV-induced DNA damage and repair: a review.," *Photochemical photobiological sciences : Official journal of the European Photochemistry Association and the European Society for Photobiology*, vol. 1, no. 4, pp. 225–36, 2002, ISSN: 1474-905X.

[231] A. Schmocker, A. Khoushabi, C. Schizas, P.-E. Bourban, D. P. Pioletti, and C. Moser, "Photopolymerizable hydrogels for implants: Monte-Carlo modeling and experimental in vitro validation," *Journal of Biomedical Optics*, vol. 19, no. 3, p. 035 004, 2014, ISSN: 1083-3668.

[232] F. Bonneville, N. Sourour, and A. Biondi, "Intracranial Aneurysms: an Overview," *Neuroimaging Clinics of North America*, vol. 16, no. 3, pp. 371–382, 2006, ISSN: 10525149.

[233] D. R. Enzmann, M. R. Ross, and M. P. Marks, "Blood Flow in Major Cerebral Arteries Measured by Phase-Contrast Cine MR," *American Journal of Neuroradiology*, vol. 15, pp. 123–129, 1994.

[234] W. L. Lim, Y. T. Chew, T. C. Chew, and H. T. Low, "Pulsatile flow studies of a porcine bioprosthetic aortic valve in vitro: PIV measurements and shear-induced blood damage.," *Journal of biomechanics*, vol. 34, no. 11, pp. 1417–27, 2001, ISSN: 0021-9290.

[235] D. Vollherbst, C. Sommer, C. Ulfert, J. Pfaff, M. Bendszus, and M. Möhlenbruch, "Liquid Embolic Agents for Endovascular Embolization: Evaluation of an Established (Onyx) and a Novel (PHIL) Embolic Agent in an In Vitro AVM Model," *American Journal of Neuroradiology*, vol. 38, no. 7, pp. 1377–1382, 2017, ISSN: 0195-6108.

[236] R. K. Avery, H. Albadawi, M. Akbari, Y. S. Zhang, M. J. Duggan, D. V. Sahani, B. D. Olsen, A. Khademhosseini, and R. Oklu, "An injectable shear-thinning biomaterial for endovascular embolization," *Science Translational Medicine*, vol. 8, no. 365, 365ra156–365ra156, 2016, ISSN: 1946-6234.

[237] K. Lei, Q. Ma, L. Yu, and J. Ding, "Functional biomedical hydrogels for in vivo imaging," *Journal of Materials Chemistry B*, vol. 4, no. 48, pp. 7793–7812, 2016, ISSN: 2050-750X.

[238] I. Saatci, H. S. Cekirge, E. F. M. Ciceri, M. E. Mawad, A. G. Pamuk, and A. Besim, "CT and MR imaging findings and their implications in the follow-up of patients with intracranial aneurysms treated with endosaccular occlusion with onyx.," *AJNR. American journal of neuroradiology*, vol. 24, no. 4, pp. 567–78, 2003, ISSN: 0195-6108.

[239] J. J. Connors, D. Sacks, A. J. Furlan, W. R. Selman, E. J. Russell, P. E. Stieg, and M. N. Hadley, "Training, competency, and credentialing standards for diagnostic cervicocerebral angiography, carotid stenting, and cerebrovascular intervention: A Joint Statement from the American Academy of Neurology, the American Association of Neurological Surgeons," *Neurology*, vol. 64, no. 2, pp. 190–198, 2005, ISSN: 0028-3878.

[240] Z. Wang, H. Kumar, Z. Tian, X. Jin, J. F. Holzman, F. Menard, and K. Kim, "Visible Light Photoinitiation of Cell-Adhesive Gelatin Methacryloyl Hydrogels for Stereolithography 3D Bioprinting," *ACS Applied Materials Interfaces*, vol. 10, no. 32, pp. 26 859–26 869, 2018, ISSN: 1944-8244.

[241] A. Schmocker, C. Schizas, P.-e. Bourban, D. P. Pioletti, and C. Moser, "Miniature probe for the delivery and monitoring of a photopolymerizable material," *Journal of Biomedical Optics*, 2015.

[242] S. Paramasivam, G. Baltsavias, E. Psatha, G. Matis, and A. Valavanis, "Silicone models as basic training and research aid in endovascular neurointervention—a single-center experience and review of the literature," *Neurosurgical Review*, vol. 37, no. 2, pp. 331–337, 2014, ISSN: 0344-5607.

[243] A. Martins Lima, M. E. Bragina, O. Burri, J. Bortoli Chapalay, F. P. Costa-Fraga, M. Chambon, R. A. Fraga-Silva, and N. Stergiopulos, "An optimized and validated 384-well plate assay to test platelet function in a high-throughput screening format," *Platelets*, vol. 30, no. 5, pp. 563–571, 2019, ISSN: 0953-7104.

[244] N. C. Santos, J. Figueira-Coelho, J. Martins-Silva, and C. Saldanha, "Multidisciplinary utilization of dimethyl sulfoxide: pharmacological, cellular, and molecular aspects," *Biochemical Pharmacology*, vol. 65, no. 7, pp. 1035–1041, 2003, ISSN: 00062952.

[245] S. J. Bryant, C. R. Nuttelman, and K. S. Anseth, "Cytocompatibility of UV and visible light photoinitiating systems on cultured NIH/3T3 fibroblasts in vitro," *Journal of Biomaterials Science, Polymer Edition*, vol. 11, no. 5, pp. 439–457, 2000, ISSN: 15685624.

[246] A. Sabnis, M. Rahimi, C. Chapman, and K. T. Nguyen, "Cytocompatibility studies of an in situ photopolymerized thermoresponsive hydrogel nanoparticle system using human aortic smooth muscle cells," *Journal of Biomedical Materials Research Part A*, vol. 91A, no. 1, pp. 52–59, 2009, ISSN: 15493296.

[247] S. Zhang, Y. L. Cui, M. Y. Diao, D. C. Chen, and Z. F. Lin, "Use of platelet indices for determining illness severity and predicting prognosis in critically ill patients," *Chinese Medical Journal*, vol. 128, no. 15, pp. 2012–2018, 2015, ISSN: 03666999.

[248] M. R. McGill, "The past and present of serum aminotransferases and the future of liver injury biomarkers.," *EXCLI journal*, vol. 15, pp. 817–828, 2016, ISSN: 1611-2156.

[249] K. Kashani, W. Cheungpasitporn, and C. Ronco, "Biomarkers of acute kidney injury: The pathway from discovery to clinical adoption," *Clinical Chemistry and Laboratory Medicine*, vol. 55, no. 8, pp. 1074–1089, 2017, ISSN: 14374331.

[250] R Nirogi, V. Goyal, S. Jana, S. Pandey, and A Gothi, "What Suits Best for Organ Weight Analysis : Review of Relationship Between Organ Weight and Body / Brain Weight for Rodent Toxicity Studies," *Int. J. Pharmaceutical Sciences and Research*, vol. 5, no. 4, pp. 1525–1532, 2014.

[251] S. Johannsmeier, M. T. T. Nguyen, R. Hohndorf, G. Dräger, D. Heinemann, T. Ripken, and A. Heisterkamp, "PEGDMA Hydrogels for Cell Adhesion and Optical Waveguiding," *ACS Applied Bio Materials*, vol. 3, no. 10, pp. 7011–7020, 2020, ISSN: 25766422.

[252] S. Jeon, J. Lee, J. Andrade, and P. De Gennes, "Protein—surface interactions in the presence of polyethylene oxide," *Journal of Colloid and Interface Science*, vol. 142, no. 1, pp. 149–158, 1991, ISSN: 00219797.

[253] S. Nagaoka, Y. Mori, H. Takiuchi, K. Yokota, H. Tanzawa, and S. Nishiumi, "Interaction Between Blood Components and Hydrogels With Poly(Oxyethylene) Chains," in *Polymers as Biomaterials*, Boston, MA: Springer US, 1984, pp. 361–374.

[254] W. Brinjikji, Y. H. Ding, D. F. Kallmes, and R. Kadirvel, "From bench to bedside: utility of the rabbit elastase aneurysm model in preclinical studies of intracranial aneurysm treatment," *Journal of NeuroInterventional Surgery*, vol. 8, no. 5, pp. 521–525, 2016, ISSN: 1759-8478.

[255] W. Brinjikji, D. F. Kallmes, and R. Kadirvel, "Mechanisms of healing in coiled intracranial aneurysms: A review of the literature," *American Journal of Neuroradiology*, vol. 36, no. 7, pp. 1216–1222, 2015, ISSN: 1936959X.

[256] V. W. van Hinsbergh, "The endothelium: vascular control of haemostasis," *European Journal of Obstetrics and Gynecology and Reproductive Biology*, vol. 95, no. 2, pp. 198–201, 2001, ISSN: 03012115.

[257] V. W. van Hinsbergh, "Endothelium - Role in regulation of coagulation and inflammation," *Seminars in Immunopathology*, vol. 34, no. 1, pp. 93–106, 2012, ISSN: 18632297.

[258] P. F. Sánchez, E. M. Brey, and J. C. Briceño, "Endothelialization mechanisms in vascular grafts," *Journal of Tissue Engineering and Regenerative Medicine*, vol. 12, no. 11, pp. 2164–2178, 2018, ISSN: 19327005.

[259] A. J. Melchiorri, N. Hibino, and J. P. Fisher, "Strategies and techniques to enhance the in situ endothelialization of small-diameter biodegradable polymeric vascular grafts," *Tissue Engineering - Part B: Reviews*, vol. 19, no. 4, pp. 292–307, 2013, ISSN: 19373368.

[260] T. Liu, S. Liu, K. Zhang, J. Chen, and N. Huang, "Endothelialization of implanted cardiovascular biomaterial surfaces: The development from in vitro to in vivo," *Journal of Biomedical Materials Research - Part A*, vol. 102, no. 10, pp. 3754–3772, 2014, ISSN: 15524965.

[261] S. Mantha, S. Pillai, P. Khayambashi, A. Upadhyay, and Y. Zhang, "Smart Hydrogels in Tissue Engineering and," *Materials*, vol. 12, no. 3323, p. 33, 2019.

[262] M. Gomez-Florit, A. Pardo, R. M. Domingues, A. L. Graça, P. S. Babo, R. L. Reis, and M. E. Gomes, "Natural-Based Hydrogels for Tissue Engineering Applications," *Molecules (Basel, Switzerland)*, vol. 25, no. 24, pp. 1–29, 2020, ISSN: 14203049.

[263] M. Sun, X. Sun, Z. Wang, S. Guo, G. Yu, and H. Yang, "Synthesis and properties of gelatin methacryloyl (GelMA) hydrogels and their recent applications in load-bearing tissue," *Polymers*, vol. 10, no. 11, 2018, ISSN: 20734360.

[264] K. Yue, G. T.-d. Santiago, A. Tamayol, N. Annabi, A. Khademhosseini, W. Hospital, and S. Arabia, "Synthesis, properties, and biomedical applications of gelatin methacryloyl (GelMA) hydrogels," *Biomaterials*, vol. 73, no. 3, pp. 254–271, 2016, ISSN: 1878-5905.

[265] A. I. Van Den Bulcke, B. Bogdanov, N. De Rooze, E. H. Schacht, M. Cornelissen, and H. Berghmans, "Structural and rheological properties of methacrylamide modified gelatin hydrogels," *Biomacromolecules*, vol. 1, no. 1, pp. 31–38, 2000, ISSN: 15257797.

[266] C. R. Nuttelman, M. C. Tripodi, and K. S. Anseth, "Synthetic hydrogel niches that promote hMSC viability," *Matrix Biology*, vol. 24, no. 3, pp. 208–218, 2005, ISSN: 0945053X.

[267] X. Zhao, Q. Lang, L. Yildirimer, Z. Y. Lin, W. Cui, N. Annabi, K. W. Ng, M. R. Dokmeci, A. M. Ghaemmaghami, and A. Khademhosseini, "Photocrosslinkable Gelatin Hydrogel for Epidermal Tissue Engineering," *Advanced Healthcare Materials*, vol. 5, no. 1, pp. 108–118, 2016, ISSN: 21922659.

[268] S. L. Bellis, "Advantages of RGD peptides for directing cell association with biomaterials," *Biomaterials*, vol. 32, no. 18, pp. 4205–4210, 2011, ISSN: 01429612.

[269] T. Kadohama, K. Nishimura, Y. Hoshino, T. Sasajima, and B. E. Sumpio, "Effects of different types of fluid shear stress on endothelial cell proliferation and survival," *Journal of Cellular Physiology*, vol. 212, no. 1, pp. 244–251, 2007, ISSN: 00219541.

[270] Y. S. J. Li, J. H. Haga, and S. Chien, "Molecular basis of the effects of shear stress on vascular endothelial cells," *Journal of Biomechanics*, vol. 38, no. 10, pp. 1949–1971, 2005, ISSN: 00219290.

[271] F. W. Charbonier, M. Zamani, and N. F. Huang, "Endothelial Cell Mechanotransduction in the Dynamic Vascular Environment," *Advanced Biosystems*, vol. 3, no. 2, p. 1 800 252, 2019, ISSN: 23667478.

[272] C. Souilhol, J. Serbanovic-Canic, M. Fragiadaki, T. J. Chico, V. Ridger, H. Roddie, and P. C. Evans, "Endothelial responses to shear stress in atherosclerosis: a novel role for developmental genes," *Nature Reviews Cardiology*, vol. 17, no. 1, pp. 52–63, 2020, ISSN: 17595010.

[273] R. S. Reneman, T. Arts, and A. P. Hoeks, "Wall Shear Stress – an Important Determinant of Endothelial Cell Function and Structure – in the Arterial System in vivo," *Journal of Vascular Research*, vol. 43, no. 3, pp. 251–269, 2006, ISSN: 1018-1172.

[274] X. Xie, F. Wang, L. Zhu, H. Yang, D. Pan, Y. Liu, X. Qu, Y. Gu, X. Li, and S. Chen, "Low shear stress induces endothelial cell apoptosis and monocyte adhesion by upregulating PECAM-1 expression," *Molecular Medicine Reports*, 2020, ISSN: 1791-2997.

[275] E. VanBavel, "Effects of shear stress on endothelial cells: Possible relevance for ultrasound applications," *Progress in Biophysics and Molecular Biology*, vol. 93, no. 1-3, pp. 374–383, 2007, ISSN: 00796107.

[276] S. Kim, C. C. Pan, and Y. P. Yang, "Development of a Dual Hydrogel Model System for Vascularization," *Macromolecular Bioscience*, vol. 20, no. 10, pp. 1–12, 2020, ISSN: 16165195.

[277] W. Schuurman, P. A. Levett, M. W. Pot, P. R. van Weeren, W. J. Dhert, D. W. Hutmacher, F. P. Melchels, T. J. Klein, and J. Malda, "Gelatin-methacrylamide hydrogels as potential biomaterials for fabrication of tissue-engineered cartilage constructs," *Macromolecular Bioscience*, vol. 13, no. 5, pp. 551–561, 2013, ISSN: 16165187.

[278] J. J. Liao, D. W. Smith, S. Miramini, N. Thibbotuwawa, B. S. Gardiner, and L. Zhang, "The investigation of fluid flow in cartilage contact gap," *Journal of the Mechanical Behavior of Biomedical Materials*, vol. 95, no. December 2018, pp. 153–164, 2019, ISSN: 18780180.

[279] J. Margolis, "Initiation of blood coagulation by glass and related surfaces," *The Journal of Physiology*, vol. 137, no. 1, pp. 95–109, 1957, ISSN: 00223751.

[280] D. C. Leslie, A. Waterhouse, J. B. Berthet, T. M. Valentin, A. L. Watters, A. Jain, P. Kim, B. D. Hatton, A. Nedder, K. Donovan, E. H. Super, C. Howell, C. P. Johnson, T. L. Vu, D. E. Bolgen, S. Rifai, A. R. Hansen, M. Aizenberg, M. Super, J. Aizenberg, and D. E. Ingber, "A bioinspired omniphobic surface coating on medical devices prevents thrombosis and biofouling," *Nature Biotechnology*, vol. 32, no. 11, pp. 1134–1140, 2014, ISSN: 15461696.

[281] S. Logunov, E. Fewkes, P. Shustack, and F. Wagner, "Light diffusing optical fiber for Illumination," *Optics InfoBase Conference Papers*, pp. 4–6, 2013, ISSN: 21622701.

[282] N. Bosschaart, G. J. Edelman, M. C. Aalders, T. G. Van Leeuwen, and D. J. Faber, "A literature review and novel theoretical approach on the optical properties of whole blood," *Lasers in Medical Science*, vol. 29, no. 2, pp. 453–479, 2014, ISSN: 1435604X.

Oriane POUPART

R&D Biomedical Engineer

+41 76 212 89 98
oriane.poupart@gmail.com
1007 Lausanne

8 January 1994
French (Swiss B Permit)

A biomedical engineer with strong expertise in developing novel biomaterials. Proven ability to manage projects in a multidisciplinary environment.

Work experience

03.2017-04.2021 **PhD researcher, Laboratory of Biomechanical Orthopedics, Ecole Polytechnique Fédérale de Lausanne (EPFL), Lausanne**
Development of in situ photopolymerizable hydrogels to treat intracranial aneurysms:
Multidisciplinary applied project – material characterization, mechanical testing, biology assays and prototyping – in collaboration with engineers, researchers and clinicians.
Scientific publications writing, courses teaching and students mentoring.

04.2016-01.2017 **Research assistant**, Laboratory of Biomechanical Orthopedics, EPFL
Development of photopolymerizable bone cements for vertebroplasty
Co-author of a **Patent** (PCT/IB2017/057124)
First prize of master thesis received from Ecole Centrale Marseille

02-08.2015 **Research intern, Wellman Center for Photomedicine, Harvard-affiliated Massachusetts General Hospital, Boston (USA)**
Development of a position localization system for an endomicroscopy capsule for quantitative diagnosis of diseases of the upper gastrointestinal tract

07-08.2014 **Technical intern, Cristal Laser**, Messein (France)
Inventory and reorganization of the stock and participation in the various stages of manufacturing crystals

Education

2017-2021 **PhD in Biomedical Engineering**, Laboratory of Biomechanical Orthopedics, Ecole Polytechnique Fédérale de Lausanne (EPFL), Lausanne

2013-2016 **Master of Engineering in Mechanics of Materials and Structures,** Ecole Centrale Marseille Graduate Engineering School, France, GPA: 3.94/4

2015-2016 **Master of Science in Bioengineering in Tissues and Implants**, Aix-Marseille University, France, with merit

2011-2013 2-year intensive undergraduate course in mathematics, physics and chemistry for competitive entrance to French graduate engineering schools, Lycée Henri Poincaré, Nancy, France

Skills

Languages
- French: Native, C2
- English: Fluent, C1
- Italian: Intermediate, A2

Computer
- MS Office, LaTeX
- SolidWorks, CATIA
- Abaqus, Comsol
- Matlab
- Adobe Illustrator

Technical
- Mechanical testing (testing machine, rheology, photo-rheology)
- Cell culture and cell viability assays
- Microfluidics
- 3D printing

Activities and Interests

Passionate by sport: athletics (10 years of practice), cycling (Etape du Tour 2019), modern-jazz dance, bouldering, hiking, skiing

Peer reviewed publications

O. Poupart et al. - Pulsatile flow-induced fatigue-resistant photopolymerizable hydrogels for the treatment of intracranial aneurysms - *Frontiers in Bioengineering and Biotechnology* (2021).

O. Poupart et al. - *In vitro* Implementation of Photopolymerizable Hydrogels as a Potential Treatment of Intracranial Aneurysms - *Frontiers in Bioengineering and Biotechnology* (2020).

Conferences & Seminars

Tissue Engineering and Regenerative Medicine International Society, 2019, Rhodes (Greece)
"Swelling of hydrogels for intracranial aneurysms treatment" (Oral Presentation)

La folle Journée de l'Anévrisme, 2018, Nantes (France)
"Luminoseal: a photosensitive hydrogel-based technology to treat cerebral aneurysms" (Oral Presentation)

Swiss-Japanese Symposium on NanoBioEngineering and Medicine, 2018, Lausanne (Switzerland)
"Dual cross-linked PMBV/AWP hydrogels" (Poster Presentation)

EPFL SV PhD retreat, 2018, Ovronnaz (Switzerland)
"Stability characterization of hydrogel for cerebral aneurysms treatment" (Poster Presentation - Award for Best Poster)

International Neurovascular Exploratory Workshop (iNew), 2018, Zurich (Switzerland)

European Society of Biomechanics (ESB), 2017, Seville (Spain)
“Photopolymerizable bone cements for vertebroplasty” (Oral Presentation)

Tissue Engineering and Regenerative Medicine International Society, 2017, Davos (Switzerland)

SPIE BiOS, 2016, San Francisco (USA)
“Development of a position localization system for an endomicroscopy capsule for quantitative diagnosis of diseases of the upper gastrointestinal tract” (Poster presentation)

Patents

Photopolymerizable bone filler material, PCT/IB2017/057124, A. Schmocker, O. Poupart and D.P. Pioletti.